Sinehbaghizadeh, S., Saptoro, A., Amjad-Iranagh, S., Naeiji, P., Tiong, A. N. T., Mohammadi, A. H. (2023): A comprehensive review on molecular dynamics simulation studies of phenomena and characteristics associated with clathrate hydrates. - Fuel, 338, 127201.

https://doi.org/10.1016/j.fuel.2022.127201

A comprehensive review on molecular dynamics simulation studies of phenomena and characteristics associated with clathrate hydrates

Saeid Sinehbaghizadeh [a], Agus Saptoro [a*], Sepideh Amjad-Iranagh [b], Parisa Naeiji [c], Angnes Ngieng Tze Tiong [a], Amir H. Mohammadi [d*]

[a] Department of Chemical and Energy Engineering, Curtin University Malaysia, CDT 250 Miri, Sarawak 98009, Malaysia

[b] Department of Materials and Metallurgical Engineering, Amirkabir University of Technology, Tehran, 15875-4313, Iran

[c] GFZ German Research Centre for Geosciences, Telegrafenberg, 14473 Potsdam, Germany

[d] Discipline of Chemical Engineering, School of Engineering, University of KwaZulu-Natal, Howard College Campus, King George V Avenue, Durban 4041, South Africa

* Corresponding authors, E-mail addresses:

Agus Saptoro, agus.saptoro@curtin.edu.my

Amir H. Mohammadi, amir_h_mohammadi@yahoo.com

Abstract

Clathrate hydrates or gas hydrates have received worldwide attention due to their potential to be utilized in various sustainable technologies. The hydrate-based industrial applications as well as developing green technologies or safely extracting natural gases stored in the nature require profound comprehension of the phenomena associated with gas hydrates. On the flip side, identifying the characteristics of different hydrate formers and the effects of a wide range of introduced additives to these technologies is the critical

objective, so that needs to be deeply investigated at both macroscopic and microscopic scales. The expensive experiments and limited availability of facilities at the nanoscale encourage researchers to apply novel computational methods and simulation approaches. For three decades, molecular dynamics (MD) simulations in the field of gas hydrates have been widely used to mathematically analyse the physical movements of molecules and the evolution of atomic positions in time. In this work, the mechanisms involved in the pure, binary, and mixed gas hydrates, and the impressions of promoters/ inhibitors/minerals on gas hydrates were briefly reviewed. Also, the phenomena and properties associated with gas hydrates such as nucleation, growth, stability, dissociation, cage occupancy, storage capacity, morphology analysis, guest role, thermo-physical and mechanical properties, and dynamical and vibrational behaviour of gas hydrates were reviewed. This work aims to provide readers with an extensive overview of MD simulations of gas hydrates to stimulate further research on this riveting field.

Keywords: Clathrate Hydrate; Gas Hydrate; Promoters/ Inhibitors; Molecular Dynamics Simulation; Gas Hydrates Characteristics; Gas Hydrates Microscopic Phenomena

Contents

1 Introduction

Gas hydrates are ice-like compounds that can be inherently formed under certain thermodynamic conditions within a gas/water mixture where hydrogen-bonded water molecules create a crystalline lattice around the gas molecules. Clathrate hydrates are categorized into three types of structures I, II, and H. Gas species are known as small guests with molecular diameters between 0.4-0.55 nm are able to form structure I; components like hydrocarbons with larger sizes mostly between 0.6-0.7 nm can generate structure II of clathrate hydrate; while for the formation of structure H, simultaneous presence of both small guests and large molecular guests (LMGs) normally liquid hydrocarbons with a molecular diameter of 0.75-0.9 nm are needed [1]. Aside from the clathrate hydrates, there are some substances such as tetra-alkylammonium salts/halides e.g. tetra-nbutylammonium bromide (TBAB), with which the guest gases like CH_4, CO_2, N_2, H_2, etc. can generate semiclathrate hydrates [2,3]. Due to the innovative applications of hydrates, they can be at the centre of research within sustainable chemistry. The early era of hydrate explorations was dominated by pipeline blockage and flow assurance, however, the idea of using this phenomenon for sustainable development, supporting the economy, and make to a cleaner atmosphere has recently received widespread attention. So that the processes such as hydrate-based CO_2 capture and sequestration, gas storage and transport, secondary refrigeration, water desalination, gas separation, and energy recovery have been the upsurge of research in this field. Figure 1 shows some suggested industrial applications of hydrate-based methods. The scope of these technologies in the context of a new master plan with concerted collaborative endeavour between various disciplines e.g. engineering, energy, chemistry, and physics have recently been developed.

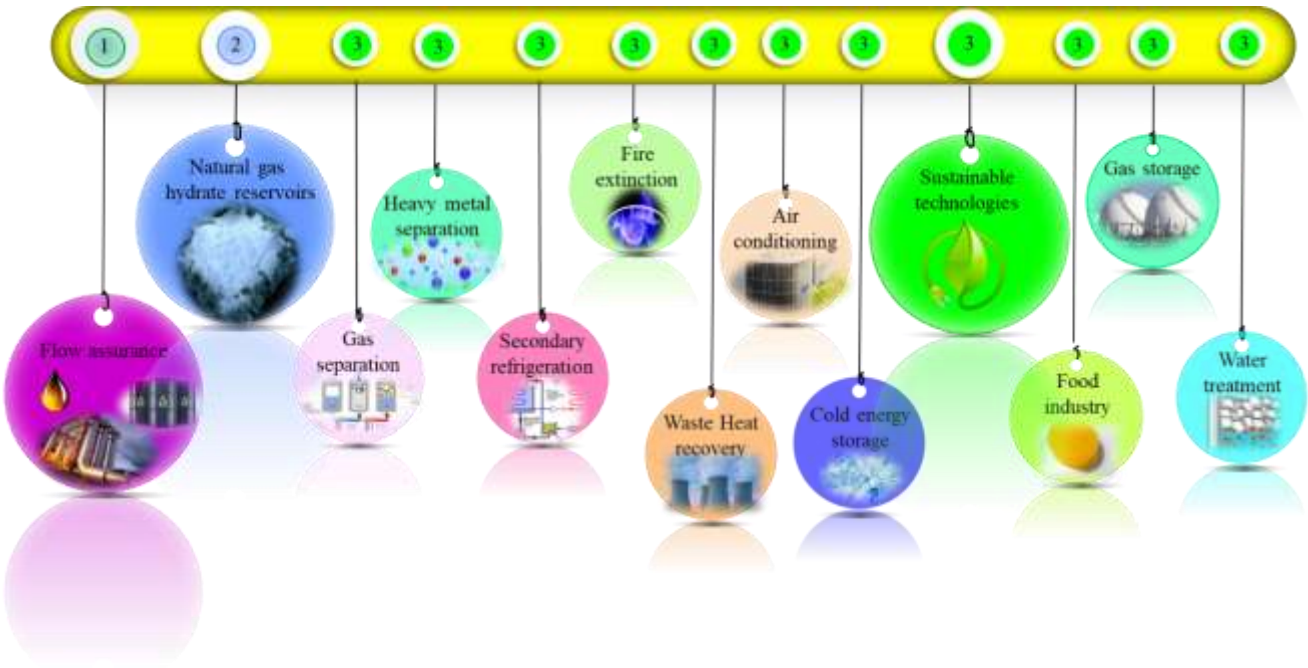

Figure 1: Gas hydrate industrial applications.

Recent experimental results have revealed the variety of properties associated with hydrate-based technologies. Although such investigations can cover the required scientific data and reveal the mechanisms at macroscopic and mesoscopic levels, the microscopic mechanisms and molecular characteristics of these systems cannot mostly be explored in the laboratory. In addition, investigating under the harsh operating pressure-temperature conditions may be the other limitation. In this regard, the utilization of molecular dynamics simulations would be the desirable option by which the vast majority of such characteristics can be probed. These new computational techniques may respond to many questionable issues in the engineering processes involved. The number of reviews on the computational studies of gas hydrates is not substantial. Liang and Kusalik provided an overview of explorations of gas hydrate crystal growth [4]. English and MacElroy conducted a review on thermodynamics, equilibrium properties, thermal conductivity, nucleation, growth, dissociation, electromagnetic fields, energy storage, and CO_2 sequestration [5]. Also, English and Waldron discussed the prospects and challenges of external

electric fields in molecular simulations [6]. Ripmeester and Alavi overviewed the nucleation, decomposition, and memory effect of clathrate hydrates [7]. Somewhat more recently, Alavi and Ripmeester conducted a review focusing on computational studies of H_2 storage in clathrate hydrate phases [8]. Recently, we reviewed the new research findings of CO_2 clathrate hydrates which have been reviled from the molecular dynamics (MD) simulations [9]. Nonetheless, there is still a lack of comprehensive review discussion in the literature on the investigated gas hydrates from the molecular perspective which can be useful for further progress in hydrate-based industrial applications. Therefore, in this work, the phenomena and characteristics of all clathrates (sI, sII, and sH) and semiclathrate hydrates at the molecular level ranging from pure, binary, mixed hydrate systems, and gas hydrates in the presence of promoters, inhibitors, and minerals will be reviewed. Hence the following sections are organized to review the performed MD investigations of various gas hydrate systems (in section 2); explored hydrate phenomena and properties at microscopic scale (in section 3); and the proportions of conducted MD studies of gas hydrates and the future research suggestions (in section 4).

2 Molecular dynamics (MD) simulation theory

Due to the power in calculating the motion and equilibrium of each molecule or atom, molecular dynamics (MD) simulations in diverse fields of science and engineering have received worldwide attention. The knowledge concerning the structural as well as dynamic properties of substances in either gas, liquid, and solid states can be achieved by MD simulations at molecular or atomic scales [10]. The common applications of MD are either to provide explanations by determining the mechanisms involved or to predict the properties of materials. In classical MD, to predict the energies of molecules and equation of motions at thermodynamic conditions, the laws of mechanics are applied. The positions and velocities in molecular systems are dependent on P-T condition and the chemical structure of the simulated system. Empirical interatomic potentials including a long-range Coulombic force and short-range repulsive/ attractive force are usually used to describe the atomic interactions. Generally, two approaches can be

used to conduct the MD simulations; the first is the non-equilibrium mode in which the system away from the equilibrium is stimulated and the system response is followed while in the equilibrium model, the macroscopic property of interest during the simulation is calculated from the time average of that property [11–13]. The theories, approaches, and outputs of MD simulations are displayed in Figure 2.

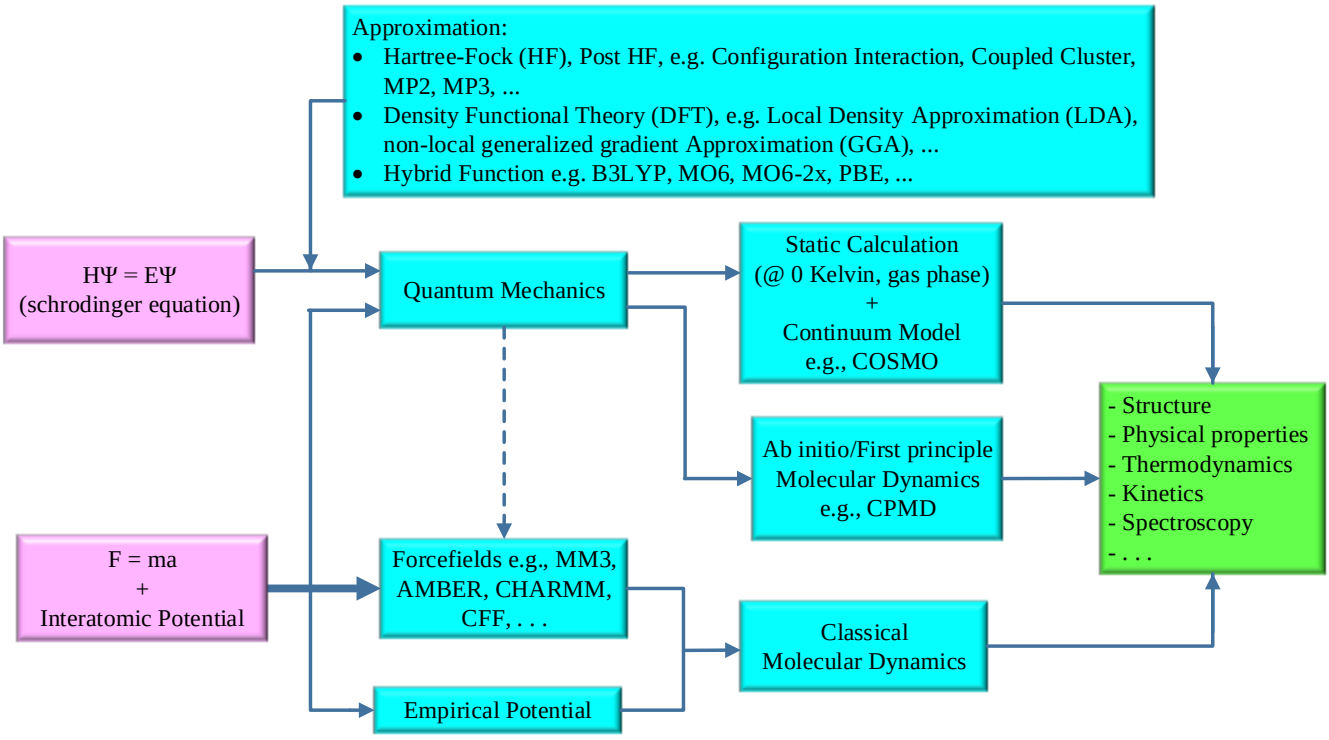

Figure 2: The theories, approaches, and outputs of molecular simulations.

As exhibited, solving the Schrödinger equation is the basis of the calculations of quantum mechanics; more details of this equation have been given elsewhere [14]. Density functional theory (DFT) is an exact theorem that was developed in the physics community. This method carries out energy calculations and electronic structure using the approximation of Kohn−Sham [15] which can be employed for many practical calculations. Besides, DFT can be combined with the HF method which is known as a Hybrid function [16–18]. Worth highlighting that, against semi-empirical methods, *ab initio* calculations can determine atomic interactions accurately in which the calculations are based on principles of quantum

mechanics. However, limitations to treating nanoscale and macroscale decisions are substantial. Many properties that are of critical importance to process performance cannot yet be integrated into process design and computer-aided molecular problems. In this context, the interplay between process design and the design of materials and molecules has been discussed elsewhere [19]. Using MD analysis, many different questions about the molecular mechanisms of phase separation, crystal growth, surface absorption, etc. can be addressed. In this regard, the combination of Monte Carlo and MD can also be employed [20–29]. It should be pointed out that Monte Carlo simulations can be regarded as classical mechanics methods.

2.1 MD Simulations of Gas Hydrate systems

Various aspects of gas hydrates through MD approaches e.g. Free-energy methods, classical MD, potential models, massively parallel MD, DFT, and *ab initio* calculations have been evaluated. It is conceivable that these studies can be rewarding for either hydrate-based gas separation or other utilization approaches of gas hydrates. The phenomena and properties associated with hydrates explored by applying MDs are shown in Figure 3. Generally, the workflow of MD simulations consists of three steps: pre-processing, MD simulations, and post-processing. The first step includes the preparation of simulation box setup and initial configuration, adjustments of the force field (FF) for each molecule, and energy minimization of the system. To provide the initial hydrate structure, the X-ray diffraction analysis for the initial positions of water molecules in the hydrate structure has been reported [30]. However, the coordinates of water molecules and cages for sI, sII, and sH clathrate hydrates specified using TIP4P potential are presented elsewhere [31]. These water molecular orientations of guest-free cages were determined based on a net-zero dipole moment as well as the lowest potential energy. The next step is a production run in which the system is equilibrated under specific thermodynamic ensembles to obtain the desired results. The final step is analysing the parameters along which the properties or phenomena can

be evaluated. To study the intermolecular behaviours, properties, phenomena, and microscopic mechanisms, there are many analysis parameters (target parameters) to employ. Figure 3 exhibits the list of these parameters along with MD steps and employed software in gas hydrate field.

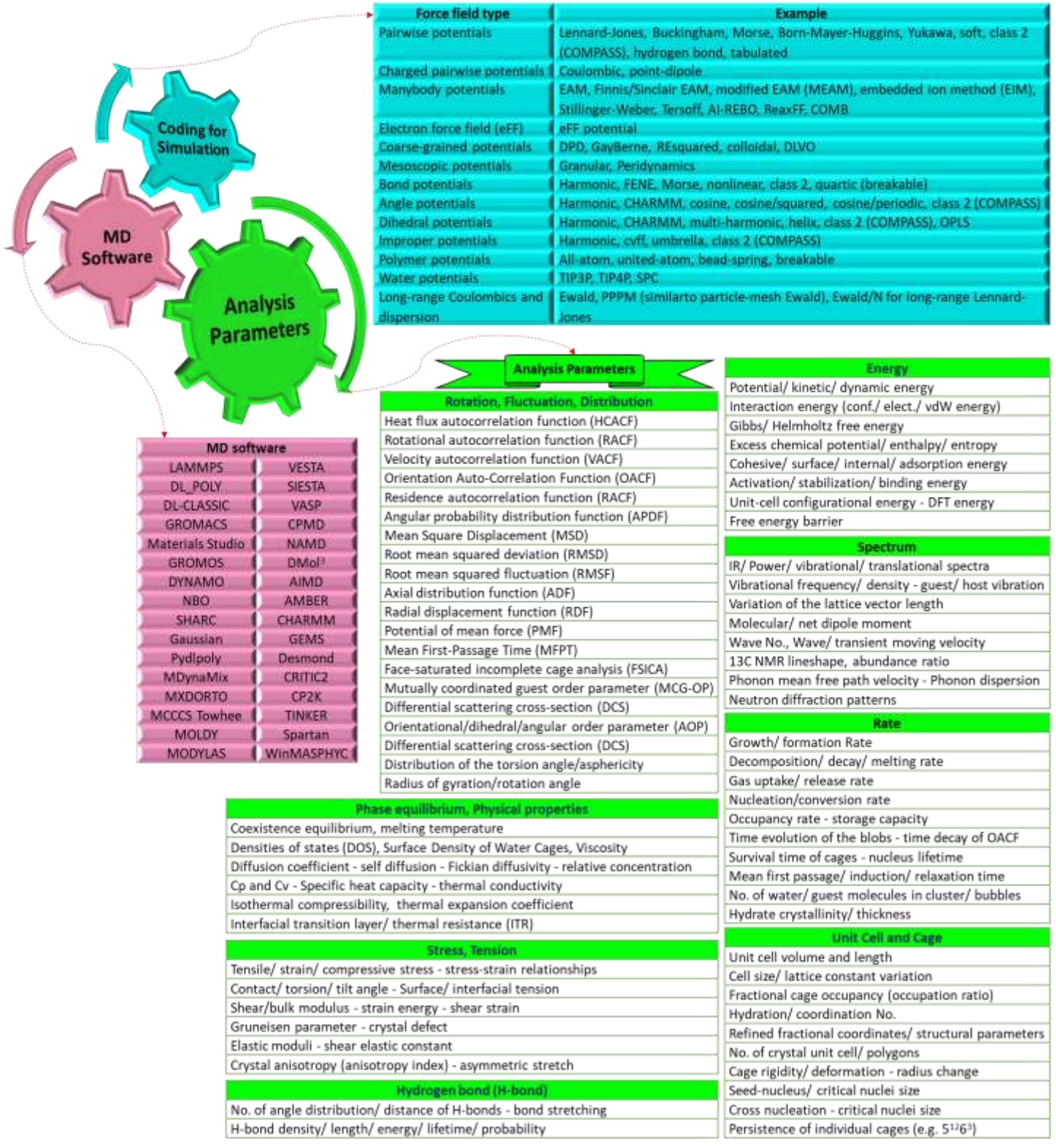

Figure 3: Molecular simulation steps, analysis parameters, and employed software to study gas hydrate systems.

The classical mechanic's methods can be developed based on intermolecular and intramolecular interactions described by empirical potential energy parameters which are the so-called force field (FF). As a fundamental issue underlying all atomistic simulations, Force-field development has drawn considerable attention. A few examples of developed general force fields are MM3, MM4, Dreiding, SHARP, VALBON, UFF, CFF93, AMBER, CHARMM, OPLS, and MMFF. The FFs shown in Figure 3 are also the set of corresponding parameters for a single molecule and the specific force functions for inter/intra-molecular forces. Over decades, several force fields for classical MD simulations have been developed. Therefore, a wide variety of potential models for components has been proposed. As an example, water models to study the characteristics of gas hydrates are: SPC [32–37], SPC/E [38–43], F-SPC [44], SPC/Fw [45,46], TIPS2 [47], TIP3P [48], TIP4P [4,49–59], TIP4P/2005 [60–64], TIP4P-Ew [22,26,65], TIP4P/Ice [27,66–78], TIP4P-FQ [44,79,80], TIP4P/F [81], TIP5P [82,83]; polarizable force fields: AMOEBA [84], COS [85], COS/G2 [86], Stillinger-Weber (SW) model [87–89], mW model [90–96], and KKY potential [97].

These potential approaches can simply be applied to water molecules as employed in many studies due to their computational efficiencies, however, their performances for different systems and operating conditions are dissimilar. For instance, notwithstanding the SPCE/OPLS-UA model that indicated no CH_4 hydrate formation at 230-260 K and 30 MPa, the formation of CH_4 hydrate using the SPC/TSE model was observed [98]. To analyse the accuracy of the coarse-grained mW model, it was compared with TIP4P+OPLS-AA and SPC+OPLS-UA CH_4 models at 250 K and 6 MPa. Based on the results, the mW model was found to be more accurate at recreating structural properties but it has a limitation in identifying small details in the RDFs. This is so that, the utilization of the coarse-grained model depends on what phenomenon is of interest [99]. The coarse-grained method to determine the surface tension at the interface of CH_4 and water, melting temperature, and the hydration number of sI and sII clathrate

hydrate may estimate the CH_4 and water diffusivity, however, it overrates the mobility of guests in solution. Also, it was revealed that the density temperature evolution depends on the ability of a water model in reproducing the solubility of hydrophobic molecules [100].

By comparing CH_4 Hydrate properties using polarizable AMOEBA and COS/G2 force fields with TIP4P and TIP4P-FQ models, it was clarified that AMOEBA and COS/G2 models are better at reproducing the experimental data than TIP4P and TIP4P-FQ models that do not explicitly account for polarization [84]. To simulate the hydrate properties of full occupied CH_4 hydrate at low-temperature ranges, the performance of TIP4P-FQ intramolecular was found to be higher than the other four-site potential models [50,51]. Also, the TIP4P-FQ model outperforms F-SPC, TIP4P, SPC, and SPC/E force fields in predicting the experimental velocity spectrum [44]. Previously, using rigid/non-polarizable SPC/E, TIP4P-Ew, and the rigid/polarizable TIP4P-FQ potentials, thermal conductivity, and diffusivity of CH_4 hydrate were evaluated. Although the predicted thermal expansion using polarizable force fields and isothermal compressibility in comparison with experiments were in agreement, the deviations are substantial at very low temperatures [85]. MD simulations of Metastable sI and sII hydrates showed that in describing the liberational region of the spectra, the polarizable force-fields outperform non-polarisable models [101]. Also, to describe differences in the spectroscopy of clathrate hydrates, a combination of anharmonic bond potentials and accurate molecular electrostatics can be applied [102]. The thermal conductivities estimated from MD simulations were found to be independent of pressure. In addition, with decreasing cage occupancy, the simulations predicted a slight increase in thermal conductivity [80]. The three coexistence phases (H-L_W-V) of CO_2 hydrate by examining the performance of TIP4P/Ice, TIP4P/2005, MSM, EPM2, TraPPE, and ZD molecular models showed that the combination of TraPPE and TIP4P/Ice potential models gives a striking accuracy to predict the experiments of CO_2 phase equilibrium up to 200 MPa [103]. Also, TIP4P/Ice and mW models can more

accurately reproduce the three-phase coexistence than SPC, SPC/E, TIP4P/2005, and TIP4P force fields [39]. Previously, heat capacity, thermal expansion coefficient, and compressibility of CH_4+CO_2 hydrate using TIP5P, TIP4P, TIP3P, TIP4P2005, TIP4PIce, TIP4PEw, SPC/E for water, DACNIS-UA, TKMAA, OPLS-UA for CH_4, and rigid three-site TraPPE, EPM2, EPM potentials for CO_2 were simulated. Using the combination of TraPPE CO_2 rigid potential, DACNIS united-atom CH_4 potential, and TIP4P/2005 water models, the most accurate results compared to experimental values were obtained [48].

The assumptions of the vdWP theory using MD analysis determined that changes in the configurational energy by the nonplanar TIP5P model are higher than the planar SPC [83]. The selected potential model can also affect the estimation of hydrate fractional occupancies. For instance, by employing Gubbins (MG) and OPLS potential models, the accommodation of 2 and 5 CH_4 molecules in large cages of sH hydrate at 300 K and 2 GPa were estimated respectively [104]. Recently, it was shown that the stability of CO_2 hydrate is quite relevant to the water molecular interactions in which the order of different FF for this hydrate stability would be TIP4P/Ice > TIP4P/2005 > SPC/E > SPC/Fw [105]. Simulations displayed that the type of water force field quantitatively affects the estimated hydrogen bonding but does not affect the qualitative trends. Also, a stronger electrostatic interaction with the guests and neighbour water molecules was observed for TIP4P/ice potential compared to the SPC/E model [106]. Simulation of the CH_4 hydrate in conditions of oceanic sediments showed that the SPC/E water model requires a shorter simulation time than the TIP4P model [41]. However, the impacts of potential models on CH_4 hydrate dissociation conditions in the other research were found to be negligible. [107]. Although the deviation of MD predictions by TIP4P/Ice and OPLS-UA force fields was approximately 3 K below the experimental values, calculated CH_4 solubility was found in good agreement with continuum scale models [108]. According to an evaluation of the accuracy of TIP4P/Ice, GAFF, and OPLS-AA force fields in predicting the phase equilibrium and enthalpy of TBAB semiclathrate at various temperatures,

it was concluded that compared to the experimental data, the OPLS-AA outperforms the GAFF. Also, TIP4P/Ice model can more accurately describe the interactions of water molecules in TBAB semiclathrate (type B) [109]. MD analysis of hydrogen bonding and guest conformation of 1-propanol hydrate showed that a larger value of the dihedral angle obtained from the single crystal XRD measurement than the value predicted by the MD simulation might be related to the approximate nature of the intramolecular dihedral potential in the force fields [110]. It should be noted that for intermolecular separations higher than 50% of the unit cell length, Lennard-Jones interactions can assume to be zero [35]. Table S1 presents the list of force fields for hydrate formers and promoter/ inhibitor additives employed in different gas hydrate simulations.

Generally, the gas hydrates based on hydrate formers and additives which contribute into the solid phase and solution phase can be classified into pure, binary, and mixed gas hydrates, and the impressions of promoters/ inhibitors/ minerals on gas hydrates. The MD simulations of these hydrate systems are briefly reviewed in the following sub-sections.

2.2 Pure gas hydrates

Many MD studies have focused on determining the crystallization/ dissociation mechanisms and contributing factors that govern the nucleation, dissociation rate, guest-host interactions, molecular mobility, cage occupancy, and cage preference. In this context, it was reported that at the same thermodynamic conditions, dissimilar cage preferences and occupancy of CH_4 and C_2H_6 may result from their differences in size and shape [111]. MD simulations confirmed that the two-steps dissociation model which was introduced by Sloan [1] is reliable for the mechanism of hydrate dissociation [82] in which the dissociation rate directly depends on the fractional occupancy [112]. Also, expanding the water-hydrate interfacial contact area and higher initial temperature can effectively promote hydrate decomposition [113]. It was proved that the thermal-driven breakup of CH_4 hydrate is controlled by the

diffusion of CH_4 molecules from the hydrate surface to the liquid phase; additionally, break-up for empty hydrate was determined about an order of magnitude faster than filled clathrate hydrate [79]. Also, CH_4 in the gas-like fluid transforms from high-density to low-density while reversely occurs for dissolved water in an ice-like phase. This phenomenon is more dominant at an upper melting temperature [40]. Monitoring hydrate dissociations confirmed the formation of nano-bubbles when the mole fraction of dissolved CH_4 in the water phase is at least 0.044 [72]. MD simulations also revealed an approximately similar growth mechanism for CO_2 and CH_4 hydrates [114]; water molecules that are adsorbed and tend to complement the open large cavities induce the rearrangements at the surface of CH_4 clathrate hydrate [97]. Also, the nucleus size and relative positions of the guest molecules have bearing on the control of hydrate nucleation [77]. During the induction times, the formation of structural defects within hydrate lattices can also be observed [64]. The MSD analysis elucidated the anomalous diffusion and anisotropic characteristics of the H_2 guest molecule [115]. Based on MD findings of thermal expansion, the unit cell volume is significantly dependent on temperature. Also, to analyse the self-preservation mechanism of gas hydrates which takes place at the interface, MD simulations have exhibited that the formation of a layer of solid-like water increases the resistance of mass transfer against guest diffusion from hydrate, consequently, inhibiting further dissociation [55]. MD is also highly useful for investigations at equilibrium conditions that cannot be determined by experiments. For instance, analysing H_2 hydrate properties at vigorously high pressure or low temperature (e.g. above several GPa or near 0 Kelvin) cannot be performed by the use of X-ray diffraction patterns but MD verified the existence of different possible structures like (sT′ and C0-II) at such harsh conditions [116]. In a way of more accurate modelling, select force fields respective to guests and simulation techniques are highly crucial. Also, between different ensembles, the sequence of accurate clathrate nucleation was found to be NPT > NVT > NVE; however, the crystallinity sequence is exactly reversed [117]. According to the decomposition

of CO_2 and CH_4 hydrates at180-280 K, it was concluded that hydrate stability using isochoric conditions is lower than that in isobaric conditions [118]. Although remarkable advances in macroscopic measurements have been accomplished, MD simulations as a powerful technique can provide insights into the fundamental mechanisms of gas hydrates at molecular and atomistic levels. In this regard, computational studies of pure gas hydrates would be a reasonable alternative.

2.3 Binary and mixed gas hydrates

To reveal the interfacial behaviors and characteristics of the mixed gas hydrates which play a central role in developing hydrate applications, investigating molecular interactions can aid in accurately determining the characteristics of their processes. Bearing in mind that a fundamental understanding of different aspects of mixed gas hydrates will be critical for many applications e.g. flow assurance, gas storage, and transportation and MD probes can support the macroscopic experimental studies. MD simulations showed the guest-guest interactions which were ignored as the assumption of vdWP theory can contribute to the Helmholtz free energy and subsequently some deviation in predicting hydrate equilibrium conditions [83]. It was also found that the mass transfer, memory effect, and guest molecule chemical potentials are the main controllers of mixed CO_2+CH_4 hydrate in the replacement phenomenon [119]. This phenomenon without structural change occurs first after partial melting of CH_4 hydrate surface and followed by partial collapses of large cages at the interface and entering CO_2 molecules into them [120]. Worth highlighting that at the macro level, the free water was identified as a significant feature during the replacement [121], however, hydrate growth may become a quasi-static equilibrium at the hydrate-liquid interface rather than in the free gas [122]. Interfacial characteristics of brine water and CO_2+CH_4 mixture indicated that the degree of IFT reduction consistent with experimental evidence is directly proportional to the CO_2 concentration [123]. MD simulations can also contribute to molecular level explorations at the early stages of hydrate nucleation and the roles of mixed guest molecules in such

phenomena. Cage composition details for CH_4+C_2H_6 and CH_4+C_3H_8 hydrate systems indicated that increasing CH_4 composition greatly reduces the appearance of other complete cages whereas grows the formation of standard cages of sI and sII hydrates (i.e., 5^{12}, $5^{12}6^2$, and $5^{12}6^4$ cages). This suggests that the more stable hydrate nuclei should be obtained with an increasing CH_4 percentage. Dissimilar to those mixed systems, C_2H_6+C_3H_8 hydrate exhibited that growing C_3H_8 percentage decreases the formation of sI large cages ($5^{12}6^2$), however, promotes the appearance of sII large cages ($5^{12}6^4$). The results of the average composition of cages over the final 30 ns of nucleating trajectories for the aforesaid mixed hydrates are shown in Figure 4 [124].

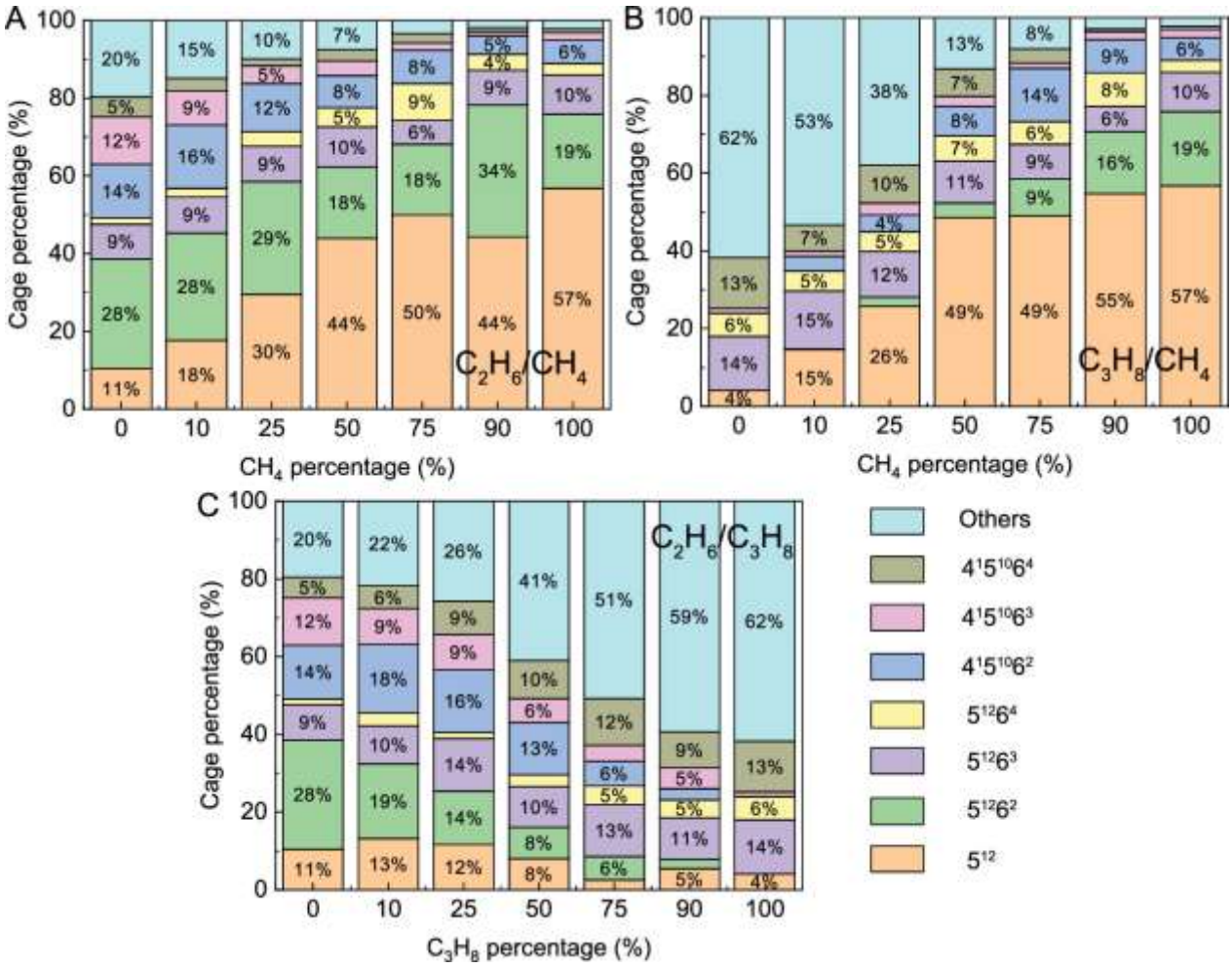

Figure 4: Average composition of cages in (A) C_2H_6+CH_4, (B) C_3H_8+CH_4, and (C) C_2H_6+C_3H_8 mixed hydrates with varying compositions [124].

The number of complete cages during hydrate nucleation in the CH_4+H_2S nano-bubble system revealed that forming a nucleus is normally associated with first the emergence of 5^{12} and then $5^{12}6^2$ cages, followed by both $4^15^{10}6^2$ and $5^{12}6^3$ cages almost simultaneously. Entropy can also play a critical role in the appearance of specific cage types. For instance, since 5^{12} cages are highly symmetric than $4^15^{10}6^m$ and $5^{12}6^n$ cages, they have higher degeneracy and are structurally more consistent with the aqueous phase, resulting in smaller entropic penalty linked with their generation. However, space-filling structures require the appearance of additional cages. Besides, the earlier formation of $5^{12}6^2$ cages because of having higher symmetry than $4^15^{10}6^2$ cages and fewer water molecules than $5^{12}6^3$ cavities is expected to be entropically favorable [125]. For the sake of a weak H_2S-H_2O hydrogen bond, the presence of H_2S in mixed hydrates stabilizes crystal defects in the crystal lattice. These H-bonds are transient with H_2S which typically behaves as the hydrogen bond donor [126].

2.4 Gas hydrates in the presence of promoters

For energy storage and transportation purposes, perhaps CH_4 and H_2 are the most potent candidate. To date, a number of materials/ techniques have been suggested, and a hydrate-based methodology would be the proper option. Since pure H_2 hydrate requires uneconomic conditions, the presence of additives as promoters such as TBAB [127], THF [128], or SF_6 [129] have been suggested. Given that identifying the key controllers of the kinetics and thermodynamics of gas hydrates in contact with promoters for the suggested hydrate-based applications is particularly critical. As a direct and valuable method, MD investigations have manifested various aspects of microscopic contributors. For example, recent MD simulation results of CO_2 double and mixed hydrates showed that the type of large molecular guests in

the large cages plays a major role in the stabilization of the clathrate network. In addition, among different types of sII thermodynamic promoters, cyclopentane, and cyclohexane in comparison with greenhouse F-gases (F-promoters) seem to be more susceptible to maintaining the stability of CO_2 clathrate hydrate [130]. Gas hydrates can also be useful for gas storage aims, however, the common challenge associated with this is to balance the trade-off between thermodynamic efficiency and H_2 storage capacity. Raman spectroscopic measurements revealed that if sII SF_6 hydrate is exposed to H_2 molecules in the vapor phase, as time proceeds, the H_2 concentration in hydrate will hit a peak and then reduce before reaching a stable value [129]. Although this phenomenon cannot be fully explained through spectroscopy experiments, its dynamic process was recently explored through MD simulations in which every large cavity was initially co-occupied by both SF_6 and H_2 molecules. It was observed that by the end of the simulation time as is shown in Figure 5 (left), the neighbouring small cavity became partially broken, and then the H_2 molecule penetrated them. The red structure shows the initially occupied large cage, and the cyan structure is a partially broken small cage containing an H_2 molecule that diffused into it. Also, as Figure 5 (right) shows, over enough time, the periodic clathrate turned into an amorphous structure and H_2 molecules escaped from their original cavities, gathered, and formed clusters which imply that the large cage co-occupancy of SF_6 and H_2 molecules could not be the stable configuration. Besides, infiltrating into small and large cages are two main patterns of H_2 diffusion as displayed in Figure 5 (right). The partially broken hydrogen bond ring coloured in green shows the opening through which the H_2 molecule can move. Although occupancy of large cages by H_2 molecules (once they are filled with SF_6) approaches zero, H_2 molecules have sufficient space to pass through the hexagonal ring without any cage breaking.

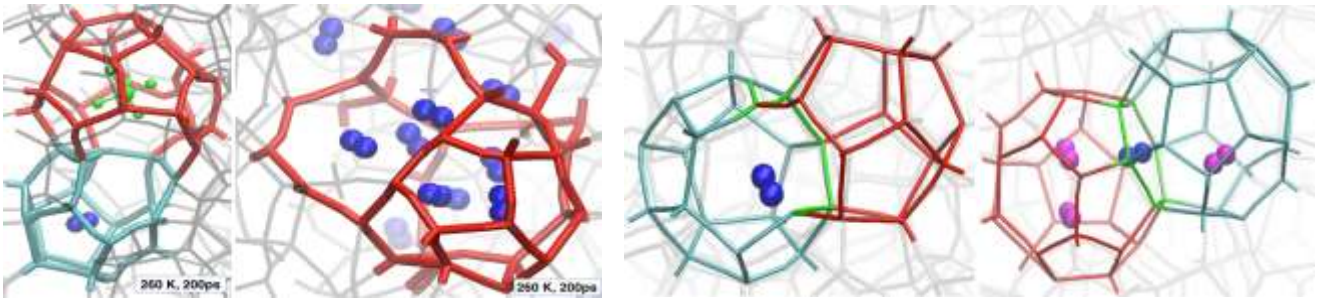

Figure 5: (Left) H_2 penetration into neighboring small cavities. (Right) A cluster of H_2 molecules in the bulk system; diffusion of H_2 molecules from one small cage to another (left) and from one large cage to another (right) [131]. (atoms of H_2 and SF_6 are in blue and green color respectively)

Also, the penetration processes in two special structures of H_2 hydrate (C_0 and sT') determined that dissimilar to the sT' structure, the number of jumps of H_2 molecules among neighbouring channels in the C_0 structure is noticeable. However, due to the growth of H_2 jumps, with changing temperature from 140 to 260 K, a little acceleration of diffusion can be observed [115]. Generally, pressure and temperature have a critical impact on the growth mechanism, cage occupancy, and storage capacity of H_2+THF hydrate. At 50 MPa and 250 K, the H_2+THF hydrate growth rate can be 3.6 times higher than the pure THF hydrate which implies the kinetics promotion role of H_2 molecules. The occupancy of small cages can be enhanced by the presence of H_2 molecules while a faster rate of growth can facilitate the formation of H_2-filled large cages. However, there is a striking resemblance between the growth behaviour of H_2+THF and pure THF hydrates which indicates that THF is the major controller of the H_2+THF hydrate growth [132]. Recent MD investigations showed that the addition of THF+DMSO can help CO_2 molecules diffuse into the CH_4 hydrate more readily that either the case with no additive or utilization of a single THF [133]. It was also manifested that in line with experimental results [134], CO_2 behaviors in the presence of SDS due to very strong distortion of SDS are quite dissimilar to CH4 interactions with SDS. Both SDS apolar and polar ends lose its shape once it faces CO_2 molecules which becomes SDS incapable to exert any substantial driving activity to promote CO_2 hydrate formation [135]. The exclusion

of SDS and methylene blue (MB) organic molecules from hydrate structure during CO_2 hydrate growth indicated that these molecules do not contribute to the crystalline structure [136]. However, the promotion effects of these molecules are different. For example, the urea surfaces make this molecule operate as a catalyst for the formation of CO_2 hydrate layers [137]. The role of urea in the growth process was found to be an increase in mass transport and catalysation of forming cages at the solid-liquid interface [138]. Recent MD findings for the solution phase including urea and Cu, Fe, Ag metal particles revealed that the mixture of Cu, Fe, and urea (without the inclusion of Ag) possesses desirable promotion effect on the CO_2 clathrate hydrate growth rate [139]. The impact of surfactant at near ambient conditions highlighted that the guest molecules can get absorbed into the aggregates during the aggregation process which provides structural flexibility and enhances the aggregation kinetics [140]. In addition, creating hydrate memory effect by organic molecules (e.g. lecithin) may help hydrate be dissociated more slowly when they are adsorbed on the hydrate surface through their hydrocarbon chains crossing and narrowing the available space for water movement and hydrate [141]. Simulating the marine hydrates in contact with protein also confirmed the role of microorganisms in accelerating marine hydrate formation via an approximation mechanism of enzymatic catalysis [142]. CO_2 hydrate growth in the presence of metal particles showed that the increase of the concentration of the metal particles can accelerate CO_2 hydrate formation but inhibit when their mass fractions were too high which is caused by strong Brownian motion in the solution [143]. The performance of combined promoters may also be more efficient. For instance, the extent of CH_4 in the hydrate phase can be increased due to the addition of both DMSO and THF. The ratio of CH_4 to CO_2 in the existence of THF and THF+DMSO were 1.06 and 1.34 respectively [133]. A combination of absolute thermodynamic and MD modelling for CO_2 interactions used to analyse its consequences for hydrate formation revealed that the generate hydrate nearest to the hematite surface

possesses lower chemical potential, therefore, it would be thermodynamically favoured to adsorb on hematite [144].

2.5 Structure-H of gas hydrates

MD research can be advantageous for determining the micro-scale properties of sH hydrates toward upgrading the hydrate stability and its performances for storage aims. The correlation between the molecular reactivity and stability of H_2+LMGs sH hydrates through analyzing chemical potential and electrophilicity index, electronegativity, and cohesive energy showed that higher hydrate stability corresponds to the larger value of these parameters [145–149]. Studying the stability and chemical activity of 16 promoters on H_2 sH hydrates at 230-270 K highlights that by utilizing alkane components with several heavy atoms less than 7, better stability for H_2 sH hydrates can be obtained. Moreover, small cavities have a higher hydrogen-trapping ability than medium ones [150]. Hence, the role of LMGs in sH hydrate nucleation/ formation mechanisms, as well as molecular-level factors were found to be unequivocally unique. More recently, it was revealed that compared to a pure CH_4 hydrate, 2,2-dimethylbutane (DMB) promotes the formation of CH_4 hydrate by at least 5 times faster than its absence. More specifically, the hydration shell of DMB behaves as a heterogeneous nucleation site for hydrate formation. This occurs due to the longer residence time of water molecules in the first hydration shell. Indeed, the greater the structural order, the slower the dynamics of DMB relative to that of CH_4 [151]. Figure 6 shows the number of complete cages, the time evolution of the potential energy, and the representative trajectory of CH_4+DMB sH hydrate nucleation. As exhibited, from 200-230 ns a sharp increase in the number of CH_4 associated with DMB confirmed the first persistent complete cage of the largest cluster. After that more cages were observed to form near the DMB but at 400 ns, the DMB started to create the hydration shell of CH_4+DMB sH hydrate. In this Figure, carbons and hydrogens of DMB are shown in cyan and purple, the water and CH_4 molecules are represented as blue and orange spheres,

red-dashed lines and red tubes denote the first hydration shells of the associated CH_4 molecules and the cages in the largest cluster. Gray lines, green and cyan spheres are also the liquid water, DMB, and CH_4 molecules respectively.

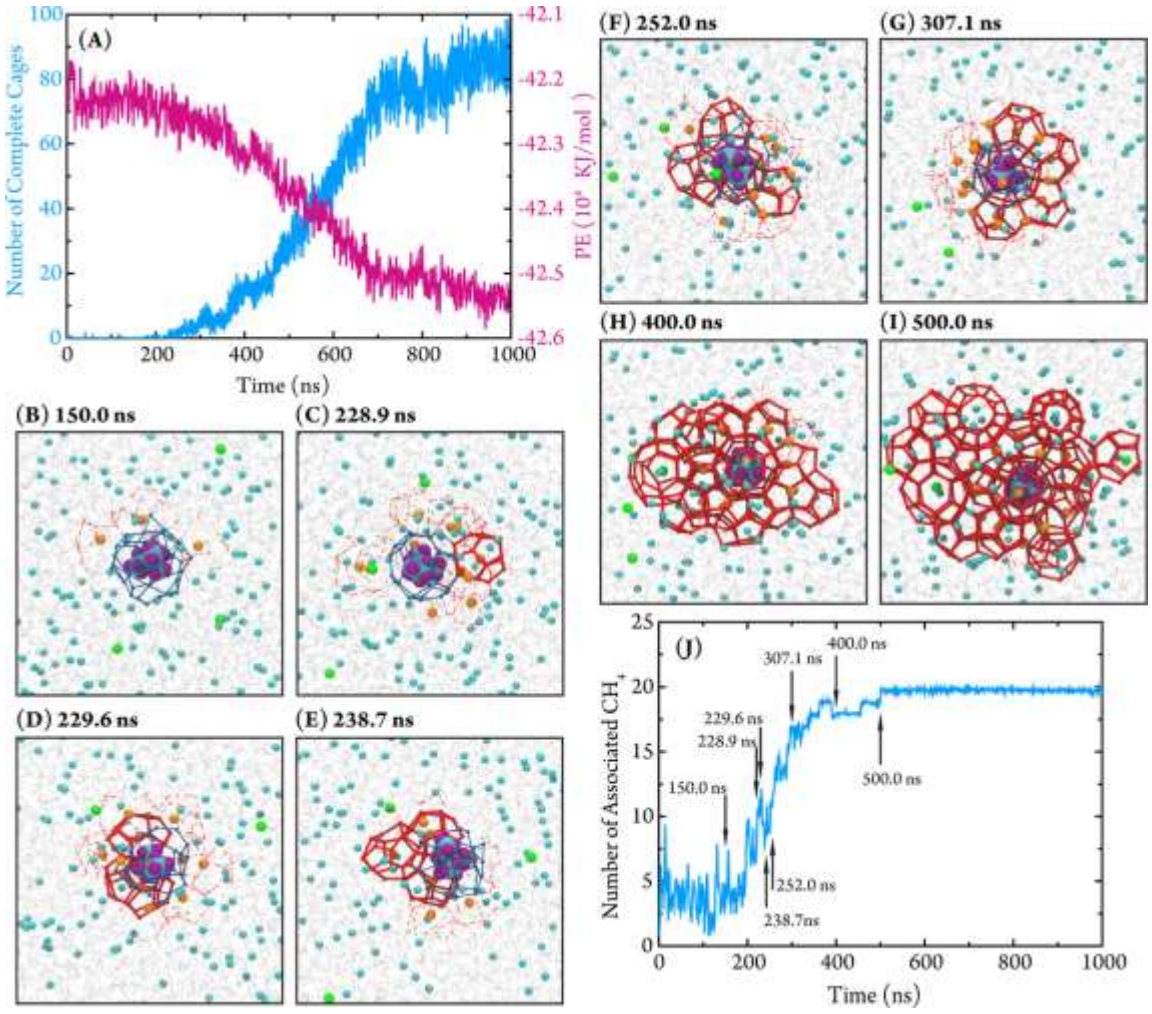

Figure 6: Time evolution of the potential energy, the number of complete cages, and cluster evolution from the trajectory of CH_4+DMB sH hydrate nucleation [151].

Recently, several studies have focused on understanding the effect of guest size and the structural anisotropy which defines the directional dependency of sH hydrate properties [152–154]. In this respect, sH hydrate elastic constants indicated that the type of the LMGs is the main contributor to sH hydrate elastic properties in which LMGs in the large cage of sH hydrate were found to increase its rigidity as

well as resistance to shear deformations. Based on DFT calculations, hexagonal sH hydrate compared to hexagonal ice (Ih) possesses higher resistance and stiffness to principal strains [155,156]. To describe the stiffness of materials, calculated values of Young's modulus as one of the key mechanical properties also demonstrated more resistance of filled sH hydrates to elastic deformation than empty structure. However, compared to sI CH_4 hydrate, sH has lower resistance to shear deformations [157,158]. These differences can be linked to the relatively isotropic sI and sII gas hydrates as compared to the anisotropic characteristics of sH and the role of LMGs. Also, the stability of the overall structure strongly depends on both types of guest molecules (CH_4 and LMGs) [159]. MD investigation focusing on the impact of guest size and conformation on the structure and stability of sH hydrates showed that tilt angle in the cages, structural flexibility, and guest molecule size are identified as key parameters of stability of sH hydrates. Generally, in large cages, molecules with shorter lengths have larger tilt angles. Additionally, the width dimension of the LMG may affect the tilt angle. [153]. Also, the sensitivity of cell parameters and thermodynamic properties of sH hydrates to the temperature is higher than pressure [160]. Structural characterization of sH hydrates (Ar/ CH_4/ N_2/ Xe + neohexene) at the atomistic level and 0 K revealed that in distinction to nearly isotropic clathrate hydrates, anisotropy is a distinguishing feature of sH hydrate. This structure was found to be more resistive to uniform compression and denser as well as having an isothermal bulk modulus in which the type of help gas plays a crucial role [161]. By analysing the free-energy difference to evaluate the thermodynamic stability conditions of sH hydrates, a strong relationship between the σ parameter of Lennard-Jones and free energy was certified. However, using this method, the highest stable structure for sH hydrate cannot be precisely specified [162].

2.6 Gas hydrates in the presence of inhibitors

Safety and economic concerns caused by pipeline plugging have driven the exploration for finding efficient inhibitors that help to prevent the crystallization of clathrate hydrates. Molecular insights into

the decomposition process of gas hydrates under the influence of inhibitors can aid flow assurance experts to find cost-effective and eco-friendly inhibition compounds. In this regard, different MD studies of gas hydrates in the presence of thermodynamic or kinetic organic/ inorganic or mixed inhibitors have been conducted. Also, MD simulations can aid to comprehend the factors that play a pivotal role in controlling thermodynamics and adsorption of kinetic inhibitors of gas hydrates. The interactions between hydrate, water, and inhibitor molecules, cohesion and adhesion of hydrate particles, mobility, binding free energy at interfaces, etc., can be accurately analysed via MD [163]. Evidence suggests hydrate in brine solutions requires a lower dosage of anti-agglomerants (AAs) which keep hydrate particles dispersed in fluids and prevent aggregation [164,165]. In this context, MD simulations showed that salt does not change notably the binding configurations. The free energy of binding with the increase of NaCl concentration from 0 to 10% becomes more negative which can be attributed to the two individual phenomena. The increase of salt content in the aqueous solution decreases the AA solubility, as a result, AA tends to move into the interfacial region. Additionally, an excess of chloride anions near the hydrate surface establishes a negatively charged interfacial layer which disrupts the network of hydrogen bonding close to the hydrate interface [166]. The influence of surfactants on the clathrate wettability indicated that they can bind to both water-clathrate and oil-clathrate interfaces which promote the nucleation for the former and prevent their coalescence with water droplets as well as an agglomeration of clathrate particles through altering the clathrate wettability from water-wet to oil-wet for the latter [167]. It was determined that the contact angle of a water droplet at a dodecane-clathrate interface (Figure 7a) can be $\theta=34 \pm 2°$ and clathrate covered with a monolayer made of intercalated dodecane and dodecanol or with a pure dodecanol monolayer (Figure 7b) at the dodecane-clathrate interface can be the same which is consistent with the water wetting angles more than 150° reported in experiments. Also, Figure 7c shows that being exposed to vapor instead of alkane, the contact angle of dodecanol-covered clathrate can be decreased from 180°

to 88 ± 2°. This indicates that the van der Waals interactions among alkane and water stabilize the water droplet higher than vapor acts. For a water droplet, even-if surfactants partially cover the clathrate surface, high contact angles will be obtained. Concur with the experiments, the existence of a surfactant monolayer at the oil-clathrate interface by changing the hydrophobicity of the hydrate surface alters the wettability of the clathrate surface to oil-wet as is shown in Figure 7d. Hence as MD simulations show, the coalescence of a bare water droplet cannot be made by the surfactants but the kinetic barrier by their presence will be increased [167]. MD also determined that although the inhibition effect of light oil (toluene, and iron) on the CH_4 hydrate growth can be observed, the presence of asphaltenes enhances the hydrate growth rate [168]. Investigation of the surfactant layer impacts at the water-oil-clathrate interface on the melting temperature of sII and sI clarified that the factors which contribute to preventing the clathrate agglomeration are the density of the interfacial layer, the length of molecules of surfactant, and the binding affinity and intensity of surfactant molecules to the surface of the clathrate hydrates [167].

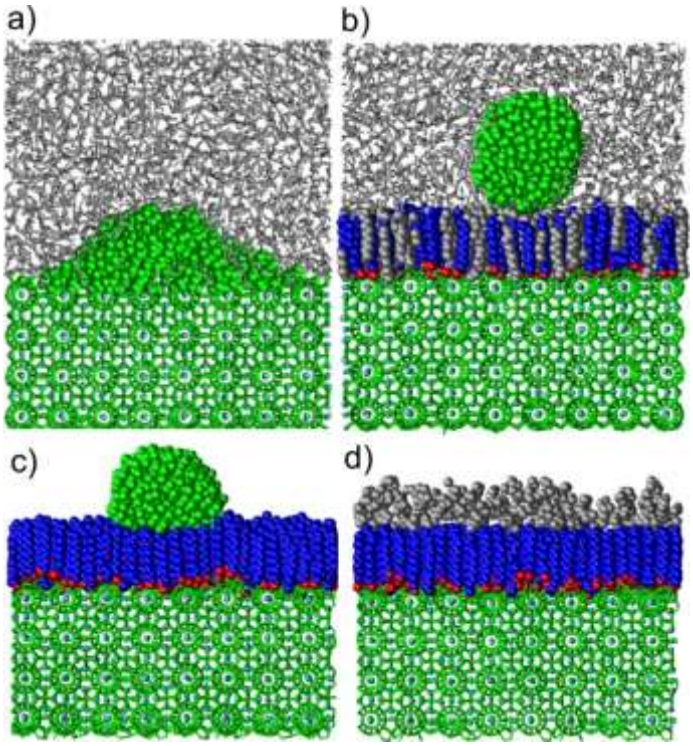

Figure 7: The change of clathrate surface from water-wet to oil-wet by surfactants. (a) Water wets the bare hydrate surface, forming a nonwetting droplet on the surfactant-covered clathrate surface. (b) The clathrate surface is covered with the dodecane-dodecanol interfacial film which repels the water droplet in the alkane oil and behaves as a super-hydrophobic surface. (c) water at the vapor-clathrate interface in the existence of a dodecanol monolayer possesses a less contact angle compared to oil. (d) Dodecane fully wets the clathrate surface [167].

MD also reveals that the inhibition mechanism of organic and inorganic inhibitors is not identical. As an example, in the initial stage, the CH_4 hydrate dissociation rate in the NaCl and methanol solutions are slower and faster than that in pure water respectively. However, in the final stage, the NaCl solution finishes the dissociation process earlier than that in pure water. Indeed, methanol in contact with CH_4 hydrate lowers the free energy of supersaturation and facilitates the CH_4 bubble formation but NaCl due to the strengthening of the hydrophobic interactions can boost the bubble formation more conveniently than pure water [169]. Examining the effect of salt NaCl on the aggregation of CH_4+C_3H_8 hydrates showed that with increasing NaCl concentration in solution, the solubility of the Anti-agglomerate in the aqueous solution decreases, and the binding free energy becomes more negative [166]. Previously, the structural effect of TBAPS kinetic inhibitor on the interface of CH_4+C_3H_8 hydrate was also confirmed, however, the sulfonate group and the hydrophobic end of the molecule make it act as a bi-functional additive [170]. CH_4 hydrate formation with kinetic inhibitor indicated that the surface of the crystals can be blocked by hydrophobic inhibitors at the initial stage while hydrophilic ones impose the inhibition effects by disrupting the water structural network [171]. By making a comparison between CH_4 hydrate in the absence and presence of 5% of methanol, it can be implied that although the existence of methanol reduces the equilibrium stability conditions of CH_4 hydrate, it can simultaneously boost the diffusion of CH_4 molecules at the interface by at least 40% [172]. CH_4 hydrate in the presence of antifreeze proteins (AFPs) showed that the structural aspects of the protein and hydrate surface can contribute to the binding. Also, nonbinding sites are not required for the operation of the protein as a hydrate inhibitor [173]. In

addition, simulations of hydrate growth of CH_4 in the existence of type I and III antifreeze proteins (AFPs) determined that a type I AFP binding on the hydrate surface can be stabilized by the formation of hydrogen bonds between water molecules and anchoring pendant groups [174]. Moreover, the exchange of hydroxyl groups and amide by mutagenesis may change the hydrogen bonding capability and the side chain shape which implies that the hydrogen bonds are not directly responsible for the activity of AFP III antifreeze [175]. MD simulations revealed that inhibitor molecules e.g. PEO/ PVP/ PVCap/ VIMA that have been found to exhibit more inhibition strength experimentally also possess higher free energies of binding [176]. Investigation of the mechanism of CH_4 hydrate growth with combined ethylene oxide (EO) and PVCap showed that the amide H-bonds do not contribute to the adsorption, however, dissimilar to antifreeze proteins, PVCap adsorbs on various crystallographic planes of clathrate hydrates [177]. Analysing the effects of amino acids (glycine/ alanine/ serine/ proline) on CH_4 hydrate formation at 250 K and 15 MPa revealed that among the simulated amino acids, serine has the highest inhibition influence on the hydrate growth whereas alanine and proline have the lowest. Besides, the more the concentration, the less the hydrate growth rate. H-bonds between water molecules and amino acids can mostly damage the cavities [178]. Also, CH_4 hydrate in the presence of 8 different oligomer inhibitors (PVPs/ amino acids) highlighted that except for asparagine, other inhibitors are absorbed into the interface of CH_4-water and suppress the growth of nanoclusters [179]. According to the results of CH_4 hydrate formation with PVP/ PVCap/ PDMAEMA, it was indicated that PVP increases the induction time for the formation of the first hydrate nuclei. Also, the synergistic impact of PVP and PVCap were found to be more efficient than PVCap alone [180] but the existence of PMAEMA reduced the temperature at which sustained hydrate growth can be observed. Hydrate content and the number of H-bonds also can be decreased by increasing the temperature [181]. A molecular study of CH_4/ C_3H_8 hydrate + PVP/ PVCap determined that PVCap kinetically outperforms PVP and such kinetic inhibitors without coming into direct contact

with hydrate surfaces can trigger the dissolution of the hydrate [182]. The properties of kinetic hydrate inhibitors (KHIs) on CH_4 hydrate growth at 260 K and 80 MPa showed that during the adsorption process, the heterocyclic ring of PVCaps intensively tends to approach the interface of hydrate-liquid [183]. By conducting molecular insights into the kinetic inhibitor adsorption on the surface of CH_4 hydrate, although the contribution of the adsorption affinity of hydrogen bonding between water molecules and the amide group of the inhibitor was not observed, a monomer of the KHI (PVCap) was found to be vigorously adsorbed on the surface of CH_4 hydrate [184]. GNs in the aqueous phase can also form H-bonds with water at the hydrate surface which reduces the water activity to obstruct hydrate growth [185].

2.7 Gas hydrates in the presence of minerals

For gas hydrates in marine sediments, the zone hydrate formation is an area of sedimentary rock or unconsolidated clay saturated with gas and water in which clay minerals include common constituents of various grain particles in gas hydrate-bearing sediments such as chlorite, kaolinite, illite, montmorillonite, etc. [186,187]. The intercalation of CO_2 in minerals within brine aquifers mainly causes significant alteration in the spacing between the mineral layers [188]. The interactions among surrounding sediment grains and hydrates determine the physical properties of the hydrate-sediment matrix. It has been experimentally uncovered that the appearance of the solid surfaces could notably influence hydrate formation [189]. In some studies due to the reduced water activity in confined space, the stronger inhibition compared to the promotion effects has been reported [190,191]. In contrast, experiments revealed CH_4 hydrate formation for conditions milder than that required in the bulk can be promoted by the confinement effects of porous materials [192–195]. Due to the experimental challenges associated with quantifying hydrate nucleation and growth, MD simulations were recently applied for examining the CH_4 hydrate in hydroxylated silica pores. Based on the results, at relatively milder conditions (at simulation pressures below 10 MPa), confinement impacts can surprisingly induce CH_4 hydrate growth.

In fact, at constant temperature and in the bulk system, the external pressure governs CH_4 hydrate growth whereas in the confinement zone and at pressures less than the minimum expected experimental CH_4 hydrate phase equilibria, it grows regardless of the applied external pressure. Figure 8 displays the initial configuration and lateral growth of the hydrate slab at the water-hydrate interface in which complete cages adjacent to the silica surfaces were replaced by a thin water layer [196]. The formation of a convex-shaped CH_4 slab in the first 1 μs is followed by spontaneous lateral hydrate growth for the sake of CH_4 nanobubble formation over 6 μs.

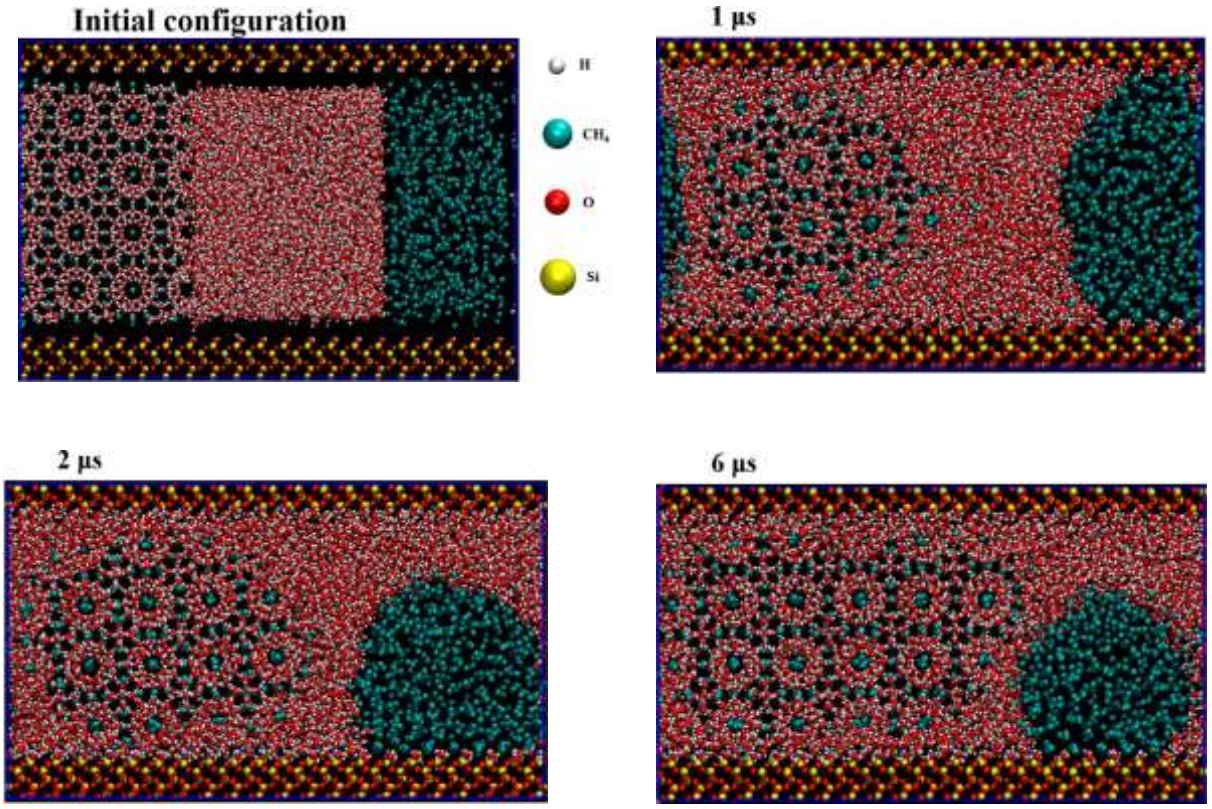

Figure 8: The initial configuration; (1μs) The transition of CH_4 slab into a convex-shaped CH_4 bubble, (2μs) a hemisphere CH_4 nanobubble formation, (6μs) The final snapshot of the simulation. [196].

Compared to pure water, bentonite can enhance the hydrate formation of a gas mixture rather than pure CH_4. However, by applying MD simulations and neutron scattering experiments, it was found that hydrate

formation is insensitive to the addition of impurity particles. Although mineral particles cannot be the most source of heterogeneous nucleation sites, they may do so indirectly if they have a notable impact on gas uptake into solution [197]. Somewhat more recently, MD manifested that kaolinite and illite minerals do not greatly influence the CO_2 hydrate phase equilibrium whereas montmorillonite owing to its interlayer cations can shift the equilibrium curve toward lower stability conditions [198]. Besides, the montmorillonite surface by providing nucleation sites can enhance CH_4 hydrate nucleation in which the montmorillonite interlayer produces stable CH_4 hydrate with H_2O and a basal montmorillonite d-spacing of 24 Å [199]. Also, the increase of basal d-spacing may improve the diffusion coefficients for guest molecules [200]. Since experimental techniques are associated with some limitations of the spatial and temporal resolution to obtain direct evidence of the gas hydrate nucleation and growth behaviour in contact with minerals, MD simulations have therefore emerged as a useful technique for such discoveries. Simulations of the hydrated silica-water interface (CH_4+CO_2+SiO_2) and the contact angle determined that the density of water in the layers far from the surface is less than the layers adjacent to the silica. Similarly, at the interfaces of liquid and silica, the concentrations of the gases are more than regions in the gas phase [201]. Evaluations of the reaction rate of CO_2 hydrate with Na_2CO_3 showed that the carbonation of the Na_2CO_3 is not mainly affected by the kinetics of the reaction at the surface. In addition, the reaction rate of Na_2CO_3 is considerably less than K_2CO_3 [202]. Under an external electric field, the migration of NaCl solution in the calcium silicate hydrate (C–S–H) nanochannel showed that bond stability can be weakened by an external electric field. Additionally, the diffusion coefficient of ions confined in pores is around three orders of magnitude less than the mobility of ions in the bulk solution [203]. It was also reported that the cosine oscillation electric field can induce and play positive roles in both dissociation and growth of CH_4 hydrate [71].

2.8 Semi-clathrate gas hydrates

Aqueous solutions of semiclathrate hydrate formers would be an option for hydrate-based gas separation or cold storage aims. The ionic clathrate hydrates can form from ionic guests such as (TBAB) which have two distinct types of D cages occupied by gas species e.g., CO_2, N_2, and CH_4 [204–208]. Although the cage occupancy and anisotropic angular distribution of D_A and D_B cavities are dissimilar, they have nearly equal volumes. In this regard, MD simulations revealed that CO2 and CH4 molecules prefer to occupy the elongated D_A cavity and the regular quasi-spherical D_B cavity respectively. Although semiclathrate hydrate properties e.g. density, enthalpy, and equilibrium formation conditions have been successfully predicted by the MD approach, the number of such investigations is quite a few. By analyzing the rotation angle, for CO_2 molecules in two cavities at 100-250 K and the lattice structure of CO_2+TBAB, it was revealed that the lattice vibrations of bromide and tetra-n-butylammonium groups about their equilibrium positions are small and they are kept in place by electrostatic and van der Waals interactions with the neighbouring water molecules [209]. With the utilization of crystal XRD and MD simulations, CH_4 trapped in the two dodecahedral cavities of TBAB semiclathrate hydrate reported that cage occupancies for CO_2 and CH_4 can be 0.87 and 0.17 in D_A and 0.49 and 0.99 in D_B respectively. [208].

3 Hydrate phenomena and properties

Alongside the abovementioned MD simulations of gas hydrate systems, the other characteristics such as structural, energetic, mechanical, physicochemical properties, and dynamical behaviour of gas hydrates have always been the subject of MD investigations. As exhibited in Figure 9, there are different gas hydrate characteristics and phenomena which can be investigated through MD methods at the molecular level. In this section, the MD simulations of phenomena and properties of gas clathrate hydrates such as those indicated in Figure 9 are reviewed.

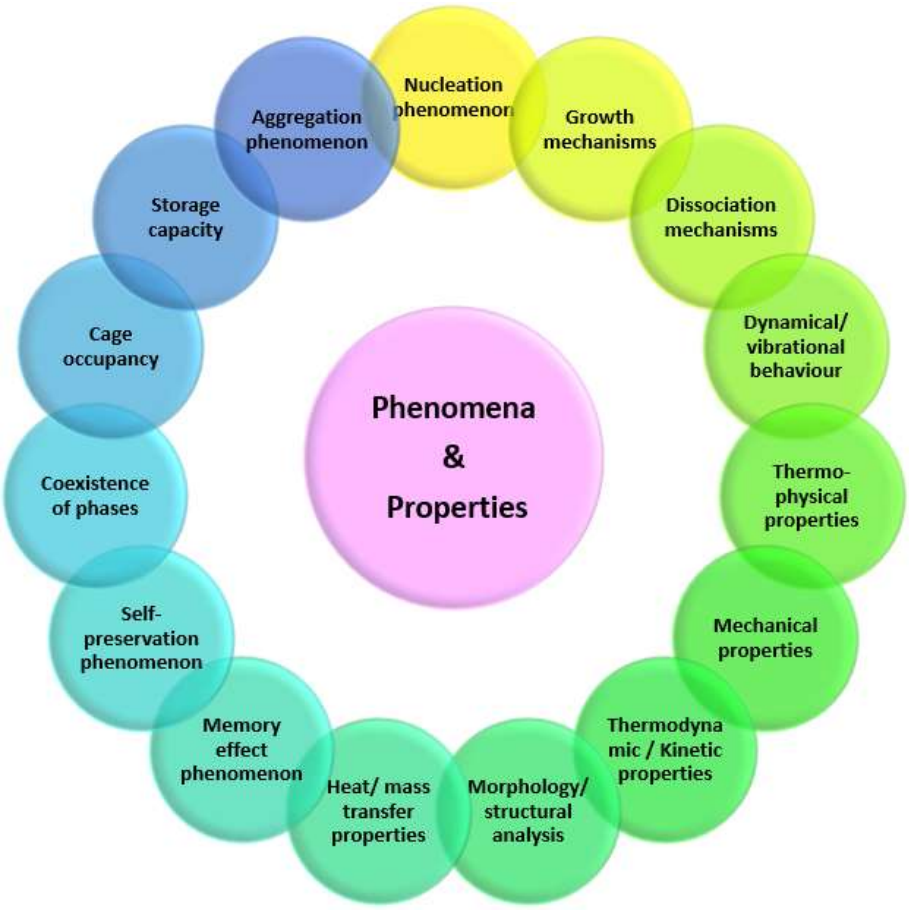

Figure 9: Studied phenomena and properties of hydrates via MD simulations.

To study the aforementioned phenomena/ properties of gas hydrates, there are several terms such as the dimension of the simulation box, type of ensemble in the final/ production phase of simulations, and simulation time MD simulations that need to be properly selected. For example, to obtain a high-ordered hydrate, an NPT ensemble and to observe a critical nucleus as large as possible, an NVE ensemble would be more proper to implement respectively [117]. The nucleation of H_2S hydrate under constant energy conditions (NVE) showed that in the early stages of the nucleation, unlike NPT or NVT which ignored the heat generated by hydrate formation, the NVE simulations can closely mimic experimental conditions [210]. After conducting the simulations, the final step will be the calculations of analysis parameters.

Table 1 summarizes some examples of MD simulations studied on different gas clathrate hydrate systems.

Table 1: Molecular simulation studies on different hydrate systems.

System	Investigated phenomenon/ properties	Analysis parameters	P (MPa)	T (K)	Hydrate supercell/ Simulation box (nm^3)	Production run time (ns)	Ref.
CO_2	Relationship between hydrate occupancy and dissociation	▪Density ▪Energy ▪Release rate ▪Dissociation of empty/ filled cages ▪Interface velocity	3	270-290	4×4×4 (10.8×4.8×4.8)	50 ns in *NPT*	[112]
	NEMD, EMD simulations of the thermal-driven breakup of hydrate	▪Fluctuations autocorrelation function (ACF) ▪No. of hydrate-like CO_2 molecules	20	260-320	4×4×4 (9.6×4.8×4.8)	10 ns in *NPT*	[211]
	Three coexistence phases	▪Cage occupancy ▪P-T prediction ▪potential energy ▪Density ▪Cross interaction parameters	2-500	260-295	2×2×2 (2.4×2.4×7.2)	400 ns in *NPT*	[103]
	Homogeneous nucleation mechanism	▪No. of cages ▪Growth rate ▪Nucleus size ▪Mutually coordinated guest (MCG)	50	250-273	(4.8×4.8×4.8)	1 μs in *NPT*	[212]
CH_4	Surface tension at the interface of CH_4, water, hydrate	▪Density ▪Enthalpy ▪Interaction parameters	10	300	4×4×4 (9.6×4.8×4.8)	800 ns in *NPT*	[100]

	▪RDF					
Cross-nucleation and equilibrium conditions of the empty and filled lattice	▪No. of cages ▪Surface density of cages ▪Persistence of individual $5^{12}6^3$ cages	10	240-320	6×6×6 (14.4×7.2×7.2)	400 ns in *NPT*	[93]
Self-preservation mechanism	▪Density ▪Melting rate ▪Time evolution of total energy	1-20	200-275	4×4×4 (9.6×4.8×4.8)	100 ns in *NVT/E*	[55]
Relationship between grain size, mechanical instability, and fracture behavior	▪Cohesive energy distributions ▪Stress-strain relationships	10-50	203-283	8×8×8	10 ns in modified *NPT*	[73]
Mechanical properties of monocrystalline hydrate, Young's modulus, and strain rate	▪Tensile stress ▪Compressive stress	10	203-283	8×8×8 (9.6×9.6×9.6)	1 ns in modified *NPT*	[89]
Interfacial free energy, and stress at the crystal-liquid interface	▪Density ▪Potential energy ▪Interfacial tension ▪Excess enthalpy/ entropy ▪RDF	30	271	4×4×10 (4.8×4.8×20.0)	20 ns in NP_NAT*	[46]
Hydrate growth based on non-equilibrium thermodynamics	▪Potential energy ▪No. of guest molecules ▪RDF ▪hydrate growth rate	5-25	240-270	3×3×3 (3.6×3.6×11.0)	10 ns in *NPT*	[213]
Mechanical failure of monocrystalline hydrate	▪Tensile stress	10-20	120-325	4×4×12	100 ns in *NPT*	[91]
Clathrate hydrate nucleation in the presence of a growing ice front	▪Density ▪Interfacial transition layer ▪Potential energy	500	250-270	8×8×8 (9.1×10.6×36.0)	10 ns in *NPH*	[214]

		▪Competing growth					
	Thermo-physical properties of hydrate using AIMD simulations	▪Thermal expansion ▪Compressibility ▪Total energy ▪Heat capacity ▪Elastic moduli	1-400	210-323	1×1×1	63 ps in *NVT*	[215]
H_2	Special structures of H_2 hydrate (C_0 and sT')	▪MSD	200-1000	140-260	-	15 ns in *NPT*	[115]
	Vibrational properties, and structural changes	▪Enthalpy ▪Lattice constant ▪P-T prediction ▪Density ▪RDF	3-100 GPa	300	-	15 ps in *NVT*	[216]
	Inter-cage hopping in II clathrate hydrate	▪Diffusion coefficient ▪Activation energy ▪Cage occupancy ▪Inter-cage hopping	150	80-240 K	2×2×2 (3.4×3.4×3.4)	50 ns in *NVT*	[217]
H_2/ deuterium (D_2)	Molecular scape from hydrate phase	▪No. of guests ▪Activation energy ▪Cage occupancy ▪Binding free energy	200	150-180	2×2×2 (3.4×3.4×3.4)	1 μs in *NPT*	[218]
H_2S	Rapid nucleation of hydrate	▪Order parameter ▪Nucleation rate	50	230-265	3×3×6	80 ns in *NVE*	[210]
C_2H_6/ C_3H_8	Decomposition and encapsulation energies	▪RDF ▪Dissociation Enthalpy	0.1	273	3×3×3 (sI) 2×2×2 (sII)	1 ns in *NPT*	[219]
CO_2+CH_4	Replacement phenomenon	▪Cage-guest Distance Coordination number	3.2-6.0	260-280	2×2×4	5 ns in *NPT*	[120]
	Replacement and co-growth of CO_2 and CH_4 hydrates	▪No. of adsorbed guests ▪Cage composition ▪No. of cages	2-10	250-275	3×3×3	1 μs in *NPT*	[220]

	Heat capacity, thermal expansion coefficient, and compressibility	▪Lattice parameter ▪Density ▪Compressibility ▪Thermal expansion ▪Specific heat capacity	10-100	271	3×3×3 (3.6×3.6×3.6)	3 ns in *NPT*	[48]
CH_4+CO_2 +N_2	Effect of N_2 on the process of CO_2/CH_4 replacement	▪No. of guest molecules in phases ▪No. of rings ▪Density	6	280	3×2×2 (6.5×2.4×2.4)	2 μs in *NPT*	[221]
CH_4+C_2H_6+ C_3H_8	Interfacial tension and behavior of mixed hydrocarbons and water	▪Density ▪Angular distribution ▪Interfacial tension ▪No. of adsorbed molecules	10-20	275-298	(3.2×3.2×10)	5 ns in *NVT*	[222]
CH_4+SDS+ CAPB	Impact of surfactant on hydrate formation	▪No. of guest and host molecules ▪Distribution of asphericity, acylindricity ▪ACF	0.1-5	275-298	-	3 μs in *NPT*	[140]
H_2 + LMGS	Storage capacity of sH hydrate	▪Order parameter ▪Potential energy ▪Density ▪No. of guests ▪Storage capacity	70-110	230-260	(5.0×4.2×3.0)	2.3 μs in *NPT*	[223]
HFC-41/ CH_4+ pinacolone	Anisotropic expansion of the sH hydrate lattice	▪Lattice constant ▪RDF ▪MSD ▪OACF	0.1	90-180	3×3×3	25 ps in *NPT*	[224]
CH_4+NaCl/ KCl/ $CaCl_2$	Hydrate dissociation, kinetic energy, and transport parameters	▪RDF ▪MSD ▪Diffusion coefficient ▪potential energy	-	273	2×2×3	600 ps in *NVT*	[225]

CH_4+Ethanol+ 1-Propanol/ 2-Propanol	Hydrate growth in the presence of inhibitors	▪Order parameter ▪Gas uptake ▪RDF	0.1	100-250	2×2×2	500 ps in *NPT*	[226]
CH_4+ Antifreeze proteins (AFPs)	Hydrate growth in the existence of antifreeze proteins	▪RMSD ▪RMSF ▪No. of H-bond ▪Order parameter	15	250	7×3×2 (8.4×3.6×9.8)	30 ns in *NPT*	[174]
CH_4+ SiO_2	Thermal conductivity of hydrate in porous media	▪Thermal conductivity ▪Potential energy	1	253-273	2×2×3	1 ns in *NVE*	[227]
CH_4 +clay/ kaolinite/ silica nanoparticles	Effects of impurity nanoparticles on hydrate nucleation	▪Density ▪Adsorption energy	18	278-298	-	100 ns in *NPT*	[197]
CH_4+ Na-MMT + fatty acids	Formation and dissociation of hydrate in porous media	▪Order parameter ▪No. of H-bond ▪No. of cages ▪RDF ▪Diffusion coefficient	50	250-303	10×6×1	3 μs in *NPT*	[228]

*: isothermal−isobaric−isointerface area (NP_NAT) ensemble

3.1 Hydrate nucleation and growth

Understanding the phenomena of clathrate hydrates can promote hydrate-based applications [229]. A good illustration of this is a large number of discussions of the hydrate nucleation phenomena [230,231]. Generally, order parameters to analyse and trace the hydrate nucleation are utilized. Analyzing 7 classes of order parameters with a total of 33 individual variants for the nucleation mechanism of hydrate of THF as a water-soluble guest determined that the approximations of order parameters that provide the transition state (TS) and reaction coordinate, based upon water structure are more appropriate than those which are based on guest structure [232]. Also, it was reported that survival probability and mean first-passage time (MFPT) methods can accurately calculate both the CH_4 hydrate nucleation rate and critical

nucleus size [70]. Using a coarse-grained method for self-assembled monolayers (SAMs), the impacts of hydrophobic and hydrophilic surfaces on THF hydrate nucleation showed that with a homogeneous mechanism in CH_3-SAM and OH-SAM, the nucleation rate in OH-SAM due to its higher bulk guest concentration can be faster [233]. To study the structure of clathrate-ice interfaces, conducting four different clathrate and ice nucleation methods revealed that the interfacial transition layer between clathrate and ice is always disordered and could assist in the heterogeneous nucleation of clathrates from ice [214]. A combination method of coarse-grained mW model and the forward flux sampling (FFS) showed that in the vicinity of the water-CH_4 interface, hydrate nucleation occurs and then the transition from amorphous to a crystalline structure accelerates its rate [90]. Compelling evidence suggested that hydrates can nucleate through multiple pathways in which direct formation to the globally stable crystalline phase is one of them [234]. The face-saturated incomplete cage analysis (FSICA) method can also be used to identify all possible face-saturated cage compositions in a system [37]. Via examining mutually coordinated guest order parameter (MCG-OP), it was found that both host and guest structuring are crucial to accurately describe the hydrate nucleation [67]. Since MCG-OP considers the effects of both guest and solvent molecules, it can be compatible with defective or hitherto undetected cavity types [235].

Figure 10 displays a crystallization pathway of clathrate hydrates. As is shown, the crystallization mechanism can be divided into three consecutive stages. The fist step starts with the generation of blobs and the half-cages in which solvent-separated guest molecules and dilute solution are in equilibrium. The next steps are the organization of clathrate cages leading to the amorphous structure and finally the formation of amorphous maturation [236]. Previously, the nucleation mechanisms of sI and sII clathrate hydrate were also investigated by employing the coarse-grained model which demonstrated that the current process occurs first for the small cages followed by large ones [236].

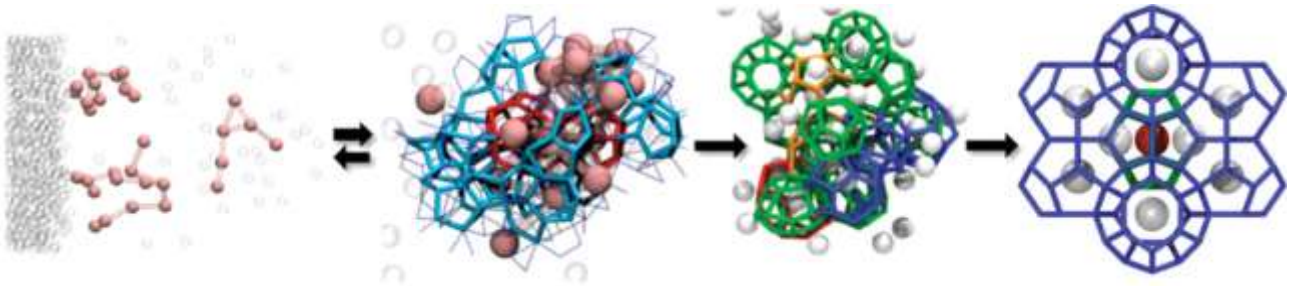

Figure 10: Multi-step blob mechanism of clathrate hydrate crystallization pathway [236].

The nucleation path in the other study was found to occur in four stages: an increase in the concentration of solvated CH_4 via diffusion, formation of an unstructured cluster, a decrease in water content of the nucleus, and finally reordering process of solvated CH_4, and water molecules (consistent with the blob hypothesis) [96]. Hence, the hydrate growth rate was found to be due to CH_4 solubility and diffusivity in a liquid phase and CH_4 adsorption by incomplete water cages at the solid-liquid interface [66,237]. The effect of hydroxylated silica on CO_2 kinetic hydrate formation revealed that the process of CO_2 hydrate nucleation takes place in 3 stages: the formation of an ice-like layer; intermediate structure and motif layer; and finally, the nucleation seeds can form [238]. With the use of massively parallel molecular dynamics for the formation of CH_4 hydrate, two distinct steps were recognized for this process: first, the concentration of solvated CH_4 clusters increases through penetration from the water-CH_4 interface. Then, consistent with the blob hypothesis, the process of re-ordering solvated water and CH_4 molecules takes place [94]. To probe hydrate nucleation using forward and backward flux sampling it was demonstrated that the half-cage order parameter describes well the reaction coordinates of hydrate nucleation. Results also suggested that besides the two-step-like mechanism, there exist multiple active transition pathways for hydrate nucleation [95]. Hence, the clathrate nucleation of hydrophobic guests comparable to CO_2 and CH_4 has suggested that destabilizing the formation of blobs could be a good strategy to apply for the presentation of the nucleation stage [239]. By conducting a two-step method for clathrate structural recognition to identify the nuclei and analyze the relative position of cages, it was observed that 80% of

the enclathrated CH_4 molecules at the transition state are contained in sII clathrate-like crystallite. To determine the relative propensity to form sI versus sII motifs, dissipation of the nucleation energy is also essential [240]. It was revealed that CH_4 subcritical clusters can be formed at the initial stage but a higher time is required to aggregate and give the hydrate nucleus which indicates that the aggregation stage is a vital controller of hydrate nucleation [241]. MD simulations also showed the phenomenological similarities between crystallization and protein folding processes [125]. Moreover, high-level kinetic similarities between pure and corresponding mixed hydrate cannot be a reliable basis for predicting the composition of early-stage mixed hydrate nuclei [242]. Somewhat recently, the rugged funnel-shaped potential-energy landscapes and the consistency of structural biased dynamics associated with hydrate nucleation were also studied [125,243]. For the heterogeneous nucleation process, a three-step such as induce, promote, and nucleate mechanisms was suggested to occur. The heterogeneous nucleation of CH_4 hydrate from an aqueous CH_4 solution can be facilitated by the interface of hexagonal ice [244]. Nucleation of gas hydrate with high CH_4 super-saturation without necessarily allowing enough time for the structure to anneal may enable water cavities to form more quickly [36]. Nucleation of CH_4 hydrate indicated that the stability of the initial formation of sII in comparison with sI would be higher [245]. In addition, the equilibrium conditions of the empty and filled lattice of sI and sII CH_4 hydrates showed that the cross-nucleation from sI to sII or vice versa needs the formation of $5^{12}6^3$ which is not native to both structures but plays a crucial role [93]. Previously, homogeneous and heterogeneous nucleation of CH_4 hydrate using the six-site model for water molecules were analysed that indicated at the early stage of hydrate formation as amorphous intermediate hydrate structures, a set of seven cage types (5^{12}, $5^{12}6^2$, $5^{12}6^3$, $5^{12}6^4$, $4^15^{10}6^2$, $4^15^{10}6^3$, $4^15^{10}6^4$) can be formed in the nucleated solids [78]. Probing the C_2H_6 hydrate nucleation showed that the full cavity most likely to form first is $4^15^{10}6^2$ which then transforms into both 5^{12} and $5^{12}6^2$ cavities [111].

Explorations of CO_2+CH_4 hydrate nucleation highlighted that stability of CH_4+CO_2 nanobubbles in the water phase and the nucleation rate may be affected by the difference in hydrophobicity between CO_2 and CH_4 molecules. In addition, the temporary formation of metastable cages such as $4^1 5^{10} 6^2$, $4^1 5^{10} 6^3$, and $4^1 5^{10} 6^4$ was verified [246].

The role of operating conditions is also determinative. The melting temperature and clathrate growth at 260 K specified that a 37% decrease in the rate of CO_2 hydrate growth with increasing pressure from 3 to 100 MPa can be observed while the pressure increase can facilitate the growth rate of CH_4 hydrate [114]. In addition, increasing the pressure is less effective than lowering the temperature in promoting hydrate nucleation because the latter induces more water cages to form while the former makes them less prevalent [62]. Additionally, the crystalline structure may grow faster once the sub-cooling is reduced. Also, at moderate temperatures, transient coexistence of crystalline sI and sII may take place [68].

Homogeneous nucleation mechanism of CO_2 hydrate through transition path sampling at 260-273 K revealed that amorphous structures with $4^1 5^{10} 6^2$ cages at low temperature are predominantly formed which is the most abundant, however, increasing temperature above 265 K can change the $4^1 5^{10} 6^2$ to $5^{12} 6^2$ cages and help the formation of sI crystalline [212]. In addition, during the nucleation stage, $4^1 5^{10} 6^2$ cavities were found to be the most popular type in the amorphous [247]. By simulating the amorphization of THF hydrate from 1.1 to 1.2 GPa and amorphous densification between 130 K and 170 K, it was found that repulsive interactions between guest and water molecules result in holding a cage structure around the guest [248]. Exploration of the amorphous CO_2 hydrate in a water-CO_2-silica three-phase system revealed that the nucleation and growth of the nucleus occur mostly near the three-phase contact line. Also, the SiO_2 surfaces act as a stabilizer to prolong the lifetime of hydrate cavities. For large cavities, the translational formation of the cage is formed before the rotational structure. However, these occur at

the same time for small cavities [249]. Simulation for sI and sII empty hydrate lattices at 150-50 MPa to evaluate their meta-stability, and growth mechanism revealed that the empty lattice of sII hydrate can be stable at 275 K and 130 MPa. In addition, the empty sI lattice can nucleate guest-free sII with superior stability. Also, more stability of empty lattice of water clathrates than ice at < 130 MPa and higher stability than liquid at < 275 K and negative pressure were confirmed [250]. Based on H_2+CH_4 hydrate simulations, the fastest growth rate can be observed at 250 K and 50 MPa. Additionally, at the constant temperature, the more the pressure results in the higher the crystal growth. Also, the temperature above 240 K is directly and inversely proportional to cage occupancies of CH_4 and H_2 molecules respectively [251]. The growth rate and storage capacity of sII H_2+THF double hydrate at 230-250 K and 10-110 MPa specified that the growth rate of the THF hydrate at 250 K and 50 MPa can be enhanced by the existence of H_2 but THF molecules are the main controller of the growth process. Moreover, the increase of pressure leads to the multi-occupancy of large cages, e.g. triple H_2 molecules can occupy the cages [132]. By analyzing CO_2 storage capacity at 289 K and 2.5 MPa, it was confirmed that, unlike pure CO_2 hydrate, CO_2+THF hydrate can be fully stable as displayed in Figure 11. Furthermore, the growth evolution showed that THF significantly boosts CO_2 diffusion at the hydrate-liquid interface [252].

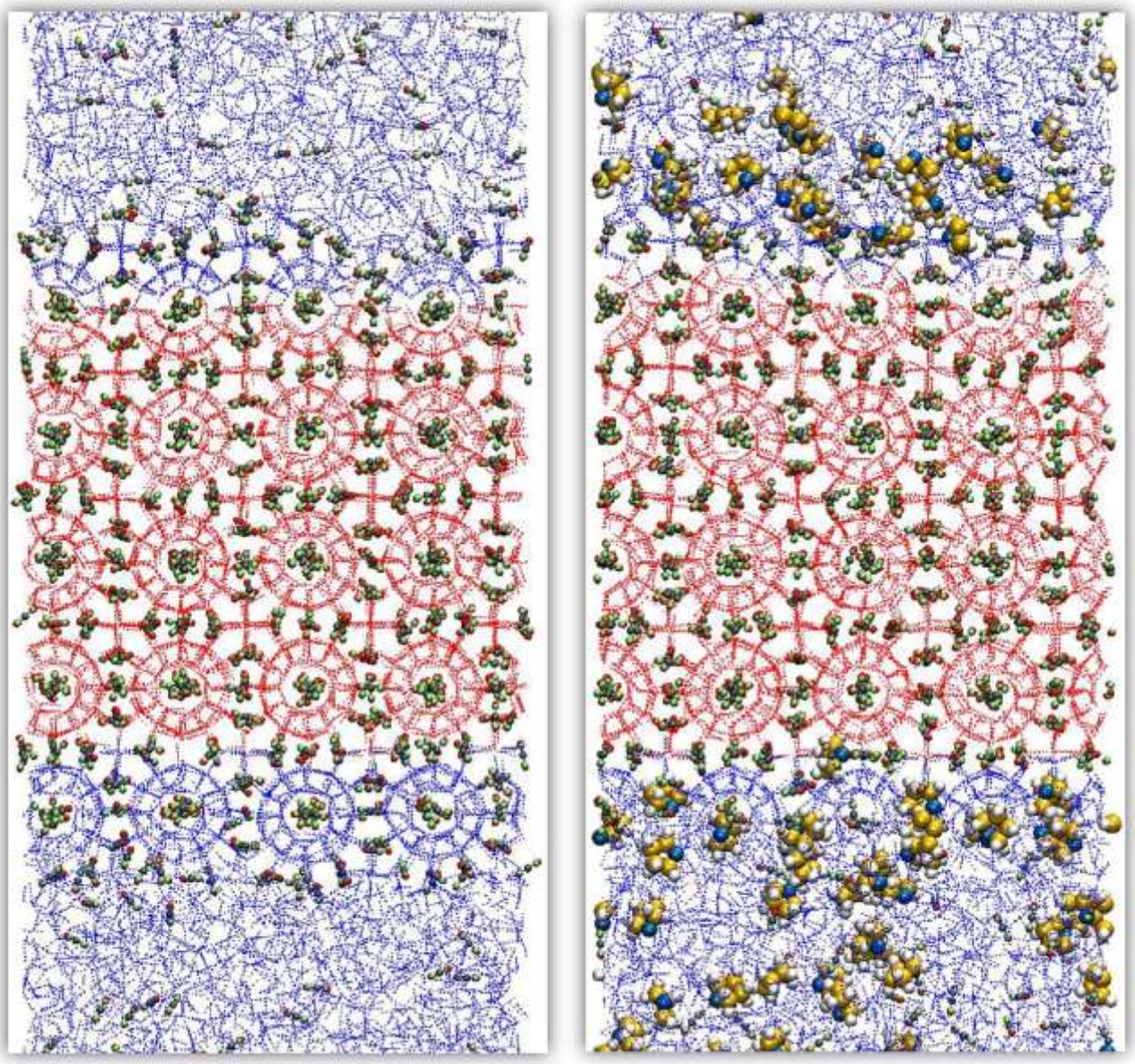

Figure 11: Final trajectories of the hydrate systems including CO_2 (left), and CO_2+THF (right) in the aqueous phase [252].

Interestingly, investigation of CH_4 hydrates in the presence of cyclic organic compounds (COC) such as cyclohexane, cyclobutanone, and tetrahydropyran revealed that replacing COC molecules with CH_4 results in reducing the unit cell stability. Also, the interface of heterogeneous crystal growth of CH_4 hydrate indicated a strong affinity for CH_4 molecules. In addition, the growth rate for hydrate crystals

was found to be four times higher than ice [253]. Analyzing the impact of high solvated CH_4 concentration on the nucleation of CH_4 hydrate revealed that a very rapid increase of nucleation rate with solvated CH_4 concentration can be observed which proved that even beyond bulk super-saturation, CH_4 molar fraction is a key that triggers the homogeneous nucleation of clathrate [88]. Analysing the solid-liquid water transition in the presence of a low concentration of CH_4 molecules as a hydrophobic guest determined that hydrate growth is dependent on the rate of empty growth lattice and filling of the cages by guest diffusion. Hence, CH_4-encaged molecules may act as a catalyst [32,254]. Commonly, thermodynamic properties of CH_4 hydrate such as entropy, enthalpy, and kinetic energy during the process of hydrate formation are in accordance with the organized water molecules in the crystal [255]. Based on the non-equilibrium thermodynamics it was also certified that the process of clathrate growth starts by dissolving CH_4 molecules to the interface and then arranging water molecules [213]. MD simulations for spontaneous nucleation and growth of CH_4 hydrate showed that without an energetically unfavourable interface, uncommon $5^{12}6^3$ cavities facilitate the structural coexistence of two dominant hydrate types (sI and sII) [77]. Also, a simulation of the effect of CH_4 adsorption on the lifetime of a dodecahedral water cluster (DWC) showed that the adsorbed CH_4 molecules can prolong the DWC lifetime, thereby being more adapted for the DWC [256]. The DWC itself vigorously adsorbs CH_4 molecules. As an inherent driving force, shell radii between 6.2 and 8.8 Å is the strong net attraction in DWC which may control the hydrate formation [257]. It was revealed that the stability of the hydrate nucleus on the surface deems to be dependent on the affinity for guest molecules. Decomposition of the hydrate nucleus can also be induced by a strong affinity for guest molecules. [258]. The controllers of cross-nucleation between 4 recognized polymorphs of Frank-Kasper clathrate specified that the sequence of intrinsic growth rate between crystalline polymorphs is sII > TS > HS-I > sI. Among non-identical polymorphs, the formation of an interfacial transition layer mostly prevents cross-nucleation to the quicker growing polymorph.

However, an increase in super-cooling overcomes this barrier [259]. The simulations of hydrate nucleation at a CH_4-water Interface indicated that although the nucleated structure was incompatible with the two most common bulk crystal structures, it contains structural elements of both of them [36]. For metastable sI and sII polymorphs of empty hydrate lattices, it was found that the detailed shape of the liberational spectra, and the differences between clathrate spectra and the ice, arise from dynamical correlations between each molecule and its local area [260]. Previously, super-saturation, dynamic and thermodynamic properties of hydrate nuclei were studied using a coarse-grained mW model. It was found that under realistic conditions of formation in industry and nature, homogeneous nucleation of clathrate hydrates does not contribute to their crystallization [92]. The convergence of the nucleation rate is also dependent on the spatial distribution of the spontaneously formed hydrate seeds [90]. Probing the effects of ice on CH_4 hydrate nucleation showed that items such as high CH_4 concentration near the ice surface, H-bond between the ice surface and hydrate lattices, absorption of released heat from hydrate formation by ice, and finally the preference of cages to occur in the vicinity of ice surface rather than in bulk solution can promote the nucleation of CH_4 hydrate [261]. Also, in the direction of fluid−fluid (water-C_3H_8) phase separation, high-density fluctuations may promote hydrate nucleation [262]. Investigation of the crystal growth of water-soluble hydrate formers showed that the growth rate of THF hydrate is an order of magnitude less than that of EO and H_2S hydrates. However, the surface trapping effect which leads to the slow growth rate of THF hydrate was not observed for EO hydrate [263]. It should be noted that the growth behaviour and induction time for the gas mixture or in the presence of additives are dissimilar. The sequence of induction time for pure guest hydrate nucleation at a fixed solution composition and the temperature was found to be $C_2H_6 < C_3H_8 < CH_4 < H_2S$. Additionally, there is a strong nonlinear correlation between induction time and guest composition of mixed hydrates [124,264]. The effect of single-walled carbon nanotubes (SWCNTs) on selective separation as well as capturing CO_2 molecules

from the mixture of CO_2+H_2 exhibited that Quasi-one-dimensional (Q1D) hydrates can be an eligible approach aiming at H_2 purification from syngas which may offer a safe and clean way to store a large-quantity of H_2 [265,266]. It was found that CH_4+THF mixed hydrate has a lower induction time than both pure CH_4 and THF hydrates. Also, at the initial stage of crystal growth, 5^{12}, $5^{12}6^2$, $5^{12}6^3$, and $5^{12}6^4$ cages were observed but in the later stages, a possibility of structural change from sI or sII was confirmed [267]. Insights into the effects of hydrophobic solid surfaces on the formation of gas hydrate determined that at hydrophobic surfaces, the tendency of getting more local ordering of water and interfacial gas enrichment (IGE) gives rise to the promotion of hydrate formation [65]. According to MD simulations to investigate the formation of hydrate at the gas-liquid-metal interface, it was found that the metal surface remarkably accelerates the water conversion to hydrate by facilitating the dissolution of CH_4 in THF solution. Increasing the liquid-gas interface curvature can result in a decrease in the energy barrier by 15% [268]. Based on the influence of amino acids on CH_4 hydrate growth at 10 MPa and 270 K, the presence of L-histidine in the system was found to markedly boosts CH_4 hydrate growth kinetics [269]. Also, analyzing the possible formation of CH_4 clathrate attributed to the capability of single SDS (form dimer to solvation sphere) revealed that the folding of SDS in water solutions is the crucial dynamical step to create incipient small cages when the SDS micelle cannot be formed [270]. The presence of hydrophobic nanoparticles can also influence CH_4 hydrate crystallization. With the addition of nanoparticles, a trend of hydrate nucleation on the side of the aqueous phase occurs but crystallization on the solid substrate may not be observed [271]. It was found that nanoparticles can facilitate CO_2 dissolution by improving the CO_2 migration from the bulk of the solution to the interfaces, however, it may physically block the CO_2 migration at high concentrations [272]. The spatial distributions and orientations of sH hydrates of CH_4 + TBME/ NH/ MCH showed that dissimilar to TBME, the hydrophobic interaction of MCH and NH with water restricts the host-guest contact, leading to lower initial kinetics of hydrate formation. The attraction

between water and MTBE may also perturb the formation of a hydrate cavity and curb the CH_4 occupancy [273]. The effects of 2,2-Dimethylbutane (DMB) on nucleation of CH_4 hydrate proved that DMB serves as a nucleation site that promotes the formation of CH_4 hydrate so that the presence of a pretty larger hydrocarbon in low concentration notably affects hydrate nucleation [151]. The influence of electrolyte solutions (MgCl2/NaCl) on hydrate formation of CO_2 in terms of ions mobility, density profile, and cage content is also unique. Although the inhibition behaviour of $MgCl_2$ and NaCl on CO_2 hydrate growth can be observed, the inhibition effects of $MgCl_2$ compared to NaCl are higher [274]. This may be attributed to their inhibition mechanisms at the initial stages. The kinetic structure and thermodynamic properties of CH_4 hydrate from the aqueous phase in the existence of NaCl solution revealed that the hydrate growth rate with the addition of 2 mole% NaCl can be decreased by 30% to 50%. Also, the presence of ions affects the CH_4 cage occupancy [275]. According to the Hofmeister series, the influence of non-ionic and ionic salts (NaCl/ NH4Cl/ guanidinium chloride (GdmCl)/ methanol) on the growth of CH_4 hydrate was explored. At low concentrations e.g. 1 wt.%, the promoting effect of a few monovalent salts was the highest for GdmCl while at high concentrations e.g. 10 wt.%, methanol showed the slowest hydrate formation kinetics [276]. The growth of CH_4 Hydrate with ethanol+1-propanol/ 2-propanol confirmed that the kinetics of hydrate formation for pure water is faster than the existence of inhibitors [277,278]. CH_4 hydrate growth +Na-MMT+ leonardite humic acid (LHA) showed that at a high concentration of LHA when the self-aggregation takes place, LHA acts as kinetic inhibition for the hydrate formation on clay minerals [279]. To explore the nucleation of CH_4 in the presence of two different kinetic inhibitors, it was revealed that the inhibition impact of KHIs (PVP-A/ PVP) on CH_4 hydrate at great sub-cooling decreases significantly and unexpected promotion behaviour can be observed. Under such conditions, KHIs decrease the mass transfer resistance, leading to the nucleation of CH_4 hydrate [280]. According to the simulation results of CH_4 hydrate in contact with seawater (water with 3.5 wt% NaCl), the inhibition

effects of electrolyte ions on nucleation, and orientation of water molecules were certified. Also, ions facilitate the mass transfer of CH_4 but suppress simultaneously the penetration of guest molecules [281]. The investigation of CO_2 hydrate near silica surfaces revealed that the nucleation of CO_2 hydrate tends to occur on relatively less hydrophilic surfaces more easily. Also, the structuring of molecules induced by amorphous solid surfaces is less ordered than that by crystalline surfaces at the initial hydrate growth [282]. The CH_4 hydrate sandwiched by hydroxylated silica nanopores showed that the growth of CH_4 hydrate in the pore centre is more than on the surfaces where a thin film of water exists. In addition, at pressures lower than that required for the growth of CH_4 clathrate in the bulk, CH_4 hydrate forms in the nano-pores [196]. The simulation of CH_4 hydrate nucleation between hydrophobic graphite and hydrophilic silica surfaces also showed that due to the adsorption of CH_4 molecules by graphite surface to form a nanobubble and induce hydrate-like water ordering by graphite near the surface, hydrate nucleation does not occur. In contrast, silanol groups on silica form strong H-bonds which can stabilize the incipient hydrate and facilitate the formation of CH_4 hydrate [283]. Also, the effects of impurity nanoparticles (clay/ kaolinite/ silica nanoparticles) on CH_4 hydrate nucleation highlighted that in a similar fashion to heterogeneous ice nucleation, impurity particles for water-soluble guest molecules act as a promoter but CH_4 hydrate formation is mostly insensitive to the existence of impurity particles [197]. CH_4 hydrate nucleation in the presence of porous sediments showed that the dissolved CH_4 molecules migrate to the clay surface where hydroxylated edge sites of clay can facilitate the hydrate nucleation [284]. However, the external surface of clay mineral effects on CH_4 hydrate formation demonstrated that unlike the neutral-charge layer, CH_4 hydrate nucleation for clay minerals with a negatively charged layer can occur in the bulk-like region but away from the clay mineral surfaces (water-mineral interface) [285]. According to the simulations of the influence of silica and clay nanoparticles on CH_4 hydrate formation, notwithstanding the hydrate nucleation of hydrophilic molecules like CO_2 and THF which can be

promoted by adding impurity particles, the nucleation of CH_4 hydrate is not sensitive to these materials [286]. The impact of organo-minerals such as adsorbed zwitterionic glycine on the sodium montmorillonite surface (Na-MMT) during CO_2 hydrate nucleation showed that employing organo-mineral complexes increases the interface area of mineral and water to accelerate the nucleation and crystal growth stages of CO_2 hydrate [287].

3.2 Hydrate stability and dissociation

To use the hydrate applications, comprehending hydrate stability and dissociation mechanisms would be the critical objective. Previous MD studies of the relationship between hydrate occupancy and dissociation rate and interface velocity showed that identical total occupancy may result in different dissociation behaviour [112]. Also, for pressure ranges up to 500 MPa it was demonstrated that decay temperature is directly dependent on the cage occupancy [60]. MD simulation of the hydrate cluster dissociation elucidated that the kinetics of atomic dissolution is 5 times faster than crystal hydrate dissolution [42]. Additionally, the kinetic rate of hydrate dissociation was found to be remarkably higher than that in the hydrate formation [288]. Generally, smaller guest molecules than CH_4 may have the earlier hydrate dissociation. However, quick decomposition can be observed for those molecules larger than the cage diameter of sI hydrate [289]. According to the MD results of non-equilibrium adiabatic CH_4 hydrate dissociation, releasing large amounts of CH_4 near a surface increases the formation of bubbles and subsequently the rate of mass transfer [43]. MD also suggests that the dissociation process may occur in four successive stages in which the dissociation process equally undergoes small cages first and next to large cavities [290]. The first step of dissociation is the diffusive behaviour of water and cell size increase which leads to fracture of the cages. This is mainly followed by the escape of guest molecules from broken hydrate cages and then aggregating together [82]. Although the resistance of heat and mass transfer during the dissociation increases, it mostly reduces the rate of CH_4 hydrate decomposition [113].

Dissociation of partially occupied hydrates is somewhat faster than those of fully occupied hydrates [291]. Also, during the initial homogeneous stages of melting gas hydrate, the aggregation and migration of CH_4 molecules are critical [64] and until the threshold of bubble formation, hydrate exists as a metastable superheated solid [63]. Simulations of gas hydrate dissociation in sediments determined that the dissociation occurs layer by layer in a shrinking core manner. In addition, the released CH_4 molecules aggregate and subsequently evolve into nanobubbles [292]. Relative to the case where the hydrate is in contact with silica, the presence of a water layer between the silica surface and the hydrate phase increases the hydrate stability [293].

The Non-equilibrium MD (NEMD) simulations methodology to study the acoustic-propagation properties of CH_4 clathrate hydrate, and reproduce the P-wave and S-wave velocities in the elastic-response regime of sI and sII CH_4 hydrate can be accurately employed [53]. NEMD simulations for CH_4 clathrate hydrate dissociation indicated that the dissociation rate of hydrate surrounded by (50% CH_4+50% H_2O) and 100% CH_4 are nearly 30% and 55% lower than 100% pure water [79]. Analyzing thermal-driven CH_4 hydrate breakup at the water-hydrate interface proved that before the threshold of hydrate dissociation, the fluctuation-dissipation theory is valid and can properly describe the nature of the non-equilibrium [45]. NEMD and EMD simulations of the thermal-driven breakup of CO_2 hydrate at 300 K to 320 K demonstrated that Onsager's hypothesis (about the composition-dependence of corresponding decomposition rates above the melting points) is applicable for an initial period of hydrate dissociation [211]. Also, fluctuation-dissipation at the interface plays a critical role [294]. Thermal-driven break-up of C_3H_8 hydrate interfaced with liquid water also specified that the Arrhenius equation can predict the dissociation rate of C_3H_8 hydrate satisfactorily [295]. According to the dissociation of H_2+C_3H_8 hydrate by NEMD and EMD simulations using pairwise potentials, it was found that different surface-cavity terminations lead to substantial differences in initial break-up rates [296]. NEMD

simulations in a range of externally applied electromagnetic fields showed that below a certain intensity threshold, electromagnetic fields cannot bring about structural distortion or dissociation effect on bulk clathrate [297]. However, once a CH_4 molecule escapes from a distorted cavity, it is not possible to re-enter them even in the absence of static fields [298]. In the presence and absence of an electric field, release and uptake of sII neon hydrate showed that activation energies for uptake and release of neon in the absence of an electric field were 14.9 and 16.4 kJ/mol which indicated a good agreement with the experimental measurements, however, the release value in the existence of an electric field was declined to 6.5 kJ/mol [299]. By simulating the role of the magnetic field on the formation of CH_4 hydrate in the existence of micro-organisms (proteins), some evidence of oriented magnetic fields on the hydrate-formation kinetics by a prototypical aromatic peptide was confirmed [300]. Based on exploring the dissociation of N_2 hydrate within SWCNT and under the axial electric field, the electric field was found to change the orientations of water dipoles which results in altering the diffusion coefficient and hydrogen-bonding network of the water molecules [301]. Figure 12 shows the NEMD simulation of C_3H_8 hydrate in contact with liquid under the electric field. Analysis of this system revealed that an electric field under 0.7 V nm^{-1} does not lead to dissociation of pre-existing bulk clathrates but field strengths more than that result in significant differences in the initial dissociation rates. In addition, the dissociation rates were observed to be strongly dependent on temperature [302]. It was also revealed that lower frequency and higher intensity may facilitate C_3H_8 hydrate dissociation [303]. Based on the results of an external electric field to simulate the dissociation of CH_4 hydrate using the non-polarizable models, the presence of an electric field leads to the formation of an ice Ih-type structure while in continuous simulation without the external field, the ice-like structures become disordered. This may result in the separated gas and liquid phases [76].

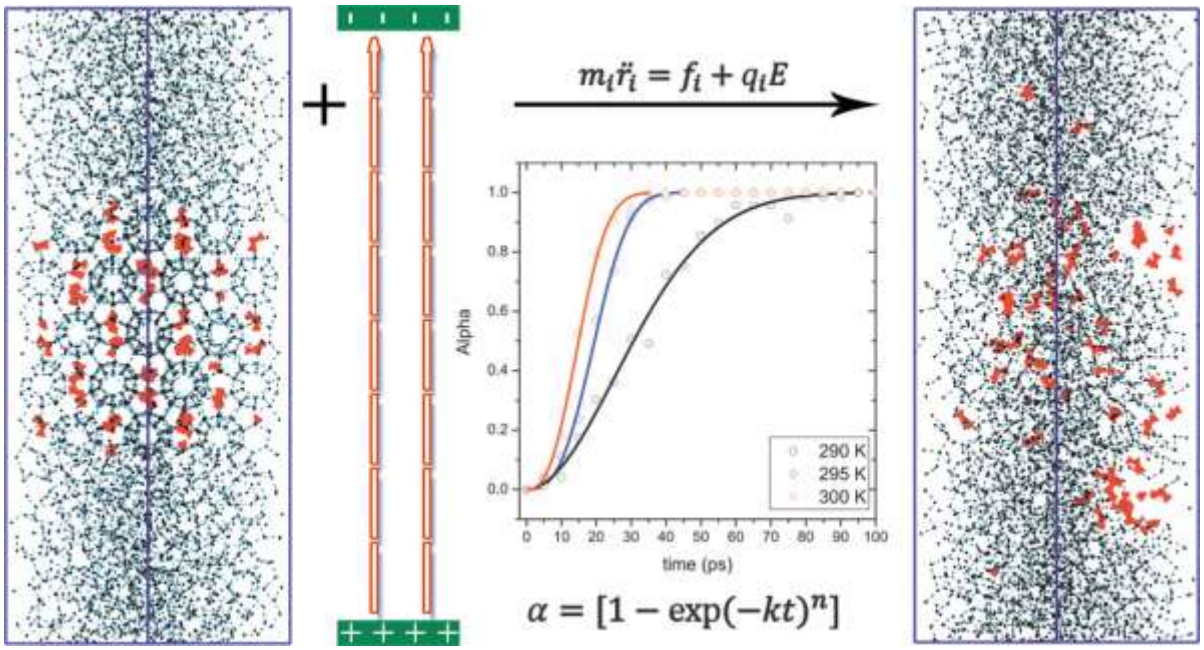

Figure 12: NEMD of both electric field-driven breakup of planar C_3H_8 hydrate interfaces with liquid water in electric field intensity [302].

Based on MD monitoring of the evolution of the CH_4 hydrate dissociation in the inclusion of two water reservoirs, it was found that the released CH_4 molecules at the initial steps reach the gas phase so that increase the gas pressure on the hydrate phase. As the hydrate dissociates, CH_4 molecules aggregate and form nano-bubbles [304]. Moreover, the slow diffusion of CH_4 molecules out of the liquid phase results in the agglomeration of CH_4 molecules and forms quasi-spherical bubbles with a radius of 11 Å [72]. Concerning the simulation of CO_2 and CH_4 bubble formation during the dissociation, it was found that when the CH_4 and CO_2 molecules occupy the small and large cages respectively, the most stable structure can be attained. In addition, the size of formed bubbles during the dissociation for each guest molecule is most likely dependent on solubility conditions of CH_4 and CO_2 in water [305]. The impact of the grain boundary structures on CO_2 hydrate at 220-310 K revealed that the stability of CO_2 hydrate somewhat above the bulk melting temperature can remain stable which confirms the relevance of thermal stability of polycrystalline hydrate to the guest's type and the grain boundaries [306]. Simulating the

decomposition and encapsulation energies of sI and sII highlighted that the encapsulation energies of guests may stabilize the cavities of sI and sII hydrate but the larger molecules give higher encapsulation energies [219].

The process and behaviour of hydrate dissociation are vigorously relevant to the encaged guest type. By analyzing the diffusion barriers, it was found that the residence of specific cavities and the overall occupancy markedly affect the dissociation of CO_2 hydrate. Moreover, unlike CH_4 and CO_2 molecules, small guests e.g. H_2 molecules due to the little penetration barrier can diffuse into the liquid phase during the early stages of the breakup of cavities [307]. MD simulations of H_2+THF hydrate during decomposition revealed that the encaged THF molecules in large cavities increase the resistance of the diffusion behaviour of H_2 molecules, however, THF serves as a strong stabilizer [308]. According to the NH_3 hydrate MD analysis, this molecule within temperatures up to 240 K gives more stable host-guest configurations than CH_4 [309]. The dissociation conditions and structural change of krypton in the existence of large molecular guests showed that the cell size of krypton increases with increasing temperature which results in clathrate distortion, small bubble formation, and krypton aggregation in the aqueous phase [310].

By evaluating CH_4 hydrate dissociation, kinetic energy, and transport parameters with the utilization of inorganic salts, it was revealed that under the same concentration, the sequence of ion's coordination number (CN) is $Na^+ > Ca^{2+} > K^+$ while $CaCl_2$ > KCl > NaCl is the order of diffusion coefficients [225]. It was also shown that the generation of CH_4 bubbles in dense NaCl solutions near the hydrate interface accelerates the CH_4 hydrate dissociation [311]. However, methanol and NaCl through dissimilar mechanisms facilitate the formation of bubbles. In addition, the ions in the solution enhance the hydrophobic interactions and cause non-uniform distribution of dissolved CH_4 molecules [169]. With respect to the MD results of the effects of alcohols on the decomposition of CH_4 hydrate, it was found

that the chain length and the hydrogen number of alcohols are inversely and directly proportional to the CH_4 hydrate decomposition respectively [312]. MD investigation of CH_4 hydrate decomposition with the addition of methanol indicated that up to 10 MPa and temperatures above 280 K, the effect of pressure would not be tangible. However, the combination of increasing temperature, reducing pressure, and the addition of methanol notably increase the rate of hydrate dissociation [313]. The inhibition capability of alcohols on gas hydrates was found to be disparate [314]. By probing the C_3H_8 hydrate dissociation mechanism with methanol it was found that the hydroxyl and methyl groups of methanol create H-bonds with water molecules that destroy the original H-bonds of water molecules in the hydrate. Also, engaging methanol molecules in small cages may enhance C_3H_8 diffusion behaviours and shorten the decomposition time of C_3H_8 hydrate [315].

3.3 Hydrate cage occupancy and storage capacity

The fraction of gas adsorption into the cages is of great importance for hydrate-based gas separation and gas storage. Results of cage rigidity and the maximum/ optimum cage occupancy for various types of cages using quantum calculations (MP2, M05-2X, and DFT-D) revealed that the maximum and the optimum number of CO_2 molecules that can occupy the cavities are: one and one for small cages (5^{12}) of all clathrate hydrates, two and one for sI large cages ($5^{12}6^2$), two and two for sII large cages ($5^{12}6^4$), two and one for sH medium cages ($4^35^66^3$) and seven and five for sH large cages ($5^{12}6^8$) [316]. Intermolecular potentials using *ab initio* quantum mechanical to determine the reference energy/ chemical potential of sI CO_2 hydrate indicated that the filled fraction for small and large cavities can be around 32%~51% and 98% respectively [317]. Interestingly, by decreasing the fractional cage occupancy from 95% to 85%, the decomposition rate was found to be increased by 30% [318]. However, the size of guest molecules not only affects the fractional occupancy but also changes the unit cell value [61].

Based on free-energy barriers and profiles of H_2 hydrate, the energy barriers dramatically decline with increasing the occupancy of small cages by H_2 molecules [319]. In addition, the free-energy barriers for H_2 molecules from 1 to 5 molecules per large cavity showed a linear decrease for 1 to 3 molecules but become larger for 4 molecules [320,321]. MD simulations indicated that for pressures above 400 MPa, a small number of the large cavities can fill with five H_2 molecules [322]. However, the maximum cage occupancies of H_2 molecules in sI and sII large cages ($5^{12}6^4$ and $5^{12}6^2$) and small cages (5^{12}) were determined as eight, six, and two while in the optimum case were two, two, and one [323]. Also, the negative interaction energy of sI H_2 hydrate up to 50% large cage occupancy revealed that H_2 hydrate at 150 K and 10 MPa can be metastable which would be competent for H_2 storage [324]. MD simulations for sH hydrate storage capacity highlighted that the optimum number of guest molecules in the large cavity for CH_4, C_2H_6, C_3H_8, n-butane, and n-pentane were determined at 4, 3, 2, 2, 1 respectively [325]. In addition, hydrate systems with small empty cages would have higher stability than that with large empty cages. Also, hydrate stability in small cages was found to be less sensitive to CO_2 molecules compared to CH_4 [326]. Somewhat more recently, the effect of cage occupancy, pressure, and the temperature was investigated to reveal the thermos-physical properties of CH_4 hydrate in the existence of methanol. Cage stability is directly dependent on temperature and inversely proportional to the pressure and cage occupancy. Studying 100% to 75% fractional occupancy at a certain condition indicated that the lower the cage occupancy, the higher the diffusion coefficient [327]. According to MD analysis, the rate of fractional occupancy in the small cavities of sI hydrate at the pressure ranges below 1 MPa was found to be insignificant but gradually increases with elevating the pressure [328]. Recently, the intra-cage behaviour of guest molecules in doubly occupied large cavities of sII hydrates at 100 K was probed by AIMD simulations in which the qualitative consistency of tetrahedral sites with the neutron scattering classical diffusion findings was confirmed [329].

MD investigation of the occupancy and growth of binary H_2+THF clathrate hydrate at 50 MPa and 304-333 K determined that with increasing the super-cooling, more large cages can be filled with H_2 molecules but it does not affect the small cavities [330]. Investigation of the structural stability of sII H_2 hydrate determined that the increasing temperature reduces the optimum occupancy of large cages [331]. Previously, migration of H-radicals and energy barriers calculated at the MP2 level showed that the compatible calculated H-radical migration rates with the actual migration rates [332]. According to the diffusive properties of inter-cage H_2 migration in H_2 and H_2+THF hydrates at 5 MPa and 200-260 K it was found that H_2 migration does not occur. Also, the diffusivities of H_2 in H_2+THF hydrate are an order of magnitude lower than that of pure H_2 hydrate [333]. Dynamical cage behaviour and H_2 migration in both H_2 and H_2+THF hydrates at 200-250 K showed that cage hopping events can be facilitated by temporary openings of small-cage faces with the reformation and relaxation of stabilizing H-bonds [334]. Also, the inter-cage hopping in sII clathrate hydrate showed that although the small cavities remained with only one guest molecule, the large cage occupancy with two and three H_2 molecules appeared to be the most stable. The activation energy for guest diffusion was found to be the lowest and the highest for the 4 and 1 occupancy models respectively [217]. Figure 13 exhibits the hopping and exchange for CH_4 molecules between the bubble and large cages. As is shown, initially 2 CH_4 molecules occupied cages A and C. Then, the guest molecules hop into the neighbour cages (e.g. cage B). However, the exchange of CH_4 molecules between the bubble and the $5^{12}6^3$ cavities is different. During guest hopping between the hydrate cage and bubble, a water molecule in the $5^{12}6^3$ cavities was replaced by another water molecule. In addition, the diffusion rate during the hopping process of CH_4 hydrate growth was estimated to be in the order of 10^{-9} to 10^{-8} m^2/s, which is 3~4 order of magnitude faster than that during hopping between one-occupied and empty hydrate cages [335].

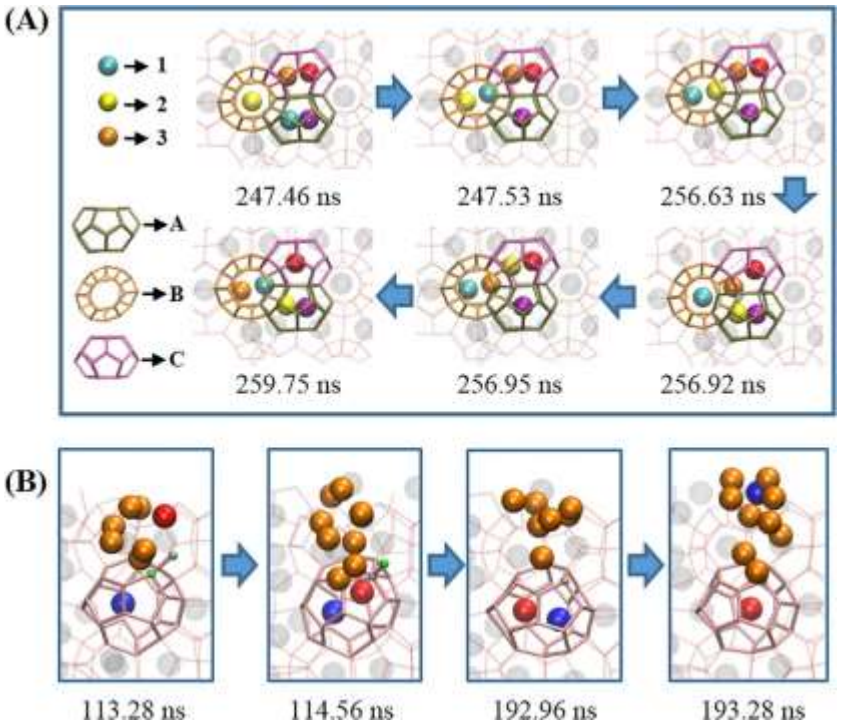

Figure 13: The hopping of CH_4 molecules: (A), the hopping and replacement for CH_4 molecules between three large cages; (B), the exchange of CH_4 molecules between the bubble and large cage [335].

MD analysis of H_2+SF_6 hydrate revealed that SF_6 molecules inhibit the diffusion of H_2 molecules and tend to occupy close to 100% of large cages [131]. Newly, the storage capacity of H_2 in the H_2+THF and H_2+MCH hydrates as a function of temperature and pressure was evaluated. Also, the small cage occupancy is directly proportional to the thermal expansion coefficient and unit cell volume [336]. It was revealed that the cage occupancy is directly and inversely proportional to the pressure and temperature respectively. H_2 storage capacity (wt.%) can be reduced by increasing the molecular weight of the promoter [337]. NEMD simulations to study the H_2 storage in C_3H_8 hydrate revealed that the diffusion coefficient at 273 K is approximately 1.5 times higher than that at 260 K. Based on the experimental and theoretical estimations, H_2 content in C_3H_8 hydrate can be stored by 1.04 wt% and 1.13 wt% respectively [338]. It was estimated that for the pressure ranges over 270 MPa, double occupancy prevails with the

single occupancy of Argon molecules in large cages [339]. MD also specified that under moderate conditions, no double occupancy occurred for the small sI, sII, sH, or medium sH cages but multiple occupancies for the large cages can be observed [340]. Previously, based on MD and vdW-P theory, simulations were performed to study the CH_4 content and occupancy in various hydrates. It was proved that multi CH_4 occupancies in large cages of sH hydrate are intensively dependent on pressure and temperature. Based on MD analysis of the storage capacity of H_2+THF sII hydrate and H_2+MCP sH hydrate at 274K and up to 500 MPa, it was estimated that large cages at high pressure can be filled with up to 8 H_2 molecules whereas small and medium cages can be occupied by just a single molecule. Moreover, the capacity of pure H_2, double sII, and sH hydrates were estimated at 3.6 wt %, 1.05 wt%, and 1.4 wt% respectively [341]. To determine H_2 storage in sH hydrate at 230-260 K and 70-110 MPa, MD simulations determined that the pressure effects at 250-260 K on the H_2 storage capacity are not substantial, however, temperatures below 240 K can at least double the storage capacity of H_2 molecules. Also, the main diffusion barriers are found to be the presence of small cages on the boundary layer and the scape of H_2 molecules due to the low kinetic energy [223]. Simulations of the CO_2 storage in sH hydrate at 100 K and ambient pressure, 273 K and 10 MPa, and also 300 K and 500 MPa revealed that although a single CO_2 molecule occupies the small and medium cages, occupancy of 5 and 3 molecules in large cages at the low and high temperatures are the most favoured [342]. Cage occupancy of double hydrates is also found to be slightly dependent on the type of large guests. For example, by simulating CO_4 and different large guests, it was determined that the most and least CH_4 storage capacity can be 11.9% and 9.6% for tetrahydropyran and cyclohexane respectively [343]. However, conducting simulations on the dependency of small guest cage occupancy and LMGs showed no relevance between CH_4 occupancy in small cages and the LMGs but the stability of sH CH_4 hydrate requires more than 40% cage occupancies of small and medium cavities by encaged molecules [344]. MD simulations of the sH

H_2+MTBE hydrate at 10-200 MPa revealed that the configurational energy of the unit cell increases when MTBE molecules are replaced by H_2 molecules in the large cavities. Also, the volume and energy of the clathrate at the lower temperature are not sensitive to the number of H_2 guests in the large cavities [345]. In addition, hydrate guest occupancies in interstitial sites using DFT and MD simulations showed that by occupying interstitial sites, H_2 can be incorporated within H_2+ tert-butylamine hydrate crystal structures [346]. Also, CH_4 may be able to replace MTBE in large cavities. In the absence of large guests, theoretically pure CH_4 hydrate requires a pressure higher than 0.5 GPa to form sH clathrate [347]. The simulated double hydrates of CH_4 and LMGs at 278 K and up to 1 GPa to investigate the storage capacity determined that the lattice constant can be expanded by increasing the size of LMGs and temperature while it is inversely proportional to the operating pressure. In addition, the fractional occupancy of small cavities by CH_4 is entirely related to the type of LMGs. [348]. By computing Quantum free-energy rates of diffusion of H_2 molecules at 8 to 200 K it was shown that at temperatures lower than 25 K, the quantum rate is greater than the classical rate whereas it inversely occurs at above 25 K [81]. Theoretically, MD simulations demonstrated that the guest-free sIII clathrate can overtake sII and sH clathrate and emerge at negative pressure e.g. -583 MPa and 0 K or -341 MPa and 300 K [349].

3.4 Hydrate guest role

Understanding the structural properties of clathrate hydrates such as metastable clathrate crystals, guest role and size, interstitial defects, structural configurations, and vibrational analysis can be worthwhile either to promote or prevent clathrate formation which has been highly sought after. The elucidation of these specifications has been to some extent uncovered via MD explorations. The anomalous shift in the stretching vibration frequencies of free and guest molecules in small and large cages is not the same. The dynamics and molecular environment of guest molecules can be reflected by the changes in molecular vibrations [350]. Also, the water-guest attraction regulates the nucleus pathway in which weak attraction

along with the poor molecule mixing in the interface layer hinders the nucleus from growing in the water phase. In such systems, along with the interface, the hydrate grows but develops toward the gas phase whereas this shift does not occur for the strong attraction [351]. To predict the ^{13}C NMR powder lineshapes of the guests, classical MD simulations were performed at the 77-250 K temperature range. A limited range of motion of C_2H_4 molecules in the cages at low temperature was observed while with increasing temperature, guest molecules gain greater rotational freedom [352]. Also, estimating the ^{13}C NMR lineshape of CO_2 at a low temperature is less accurate with experiments [353]. MD simulations showed that the thermal conductivities and speed of sound for CO_2 and Xe hydrates are lower than the empty lattice or CH_4 hydrate which points out the importance of host-guest coupling [260]. However, the overall nucleation mechanism for all guests was found to be similar and multiple competing channels form the nuclei. The size of guest molecules mostly determines the structure of the nuclei rather than ordering the stable or metastable hydrate crystals or the cage composition [236]. The stability of the hydrate nucleus in the presence of the solid surface to investigate the effect of its affinity indicated that the hydrate nucleus can be stabilized by the slab with a weak affinity for guest molecules which may be correlated with the ordered water structure on the solid surface [258]. As Figure 14 (left) shows, the free energy of the guest molecules directly corresponds to affinities. Figure 14 (right) exhibits the initial configuration in that grey plate, cyan balls, silver dots, and red sticks represent the solid slab, guest molecules, liquid water, and the largest hydrate cluster respectively. Based on this Figure, the decline of interaction among the guest molecules and the solid slab weakens the free energy for the guest molecules adsorbed on the slab which is nearly equivalent to that of guest molecules adsorbed on the hydrate nucleus surface for ε_{si} = 0.15 kcal·mol^{-1}. This demonstrates the existence of competitive adsorption behaviour among the slab and the hydrate which notably decreases the hydrate nucleus size, leading to the nucleus decomposition. Also, a stronger affinity slab has a shorter hydrate nucleation lifetime.

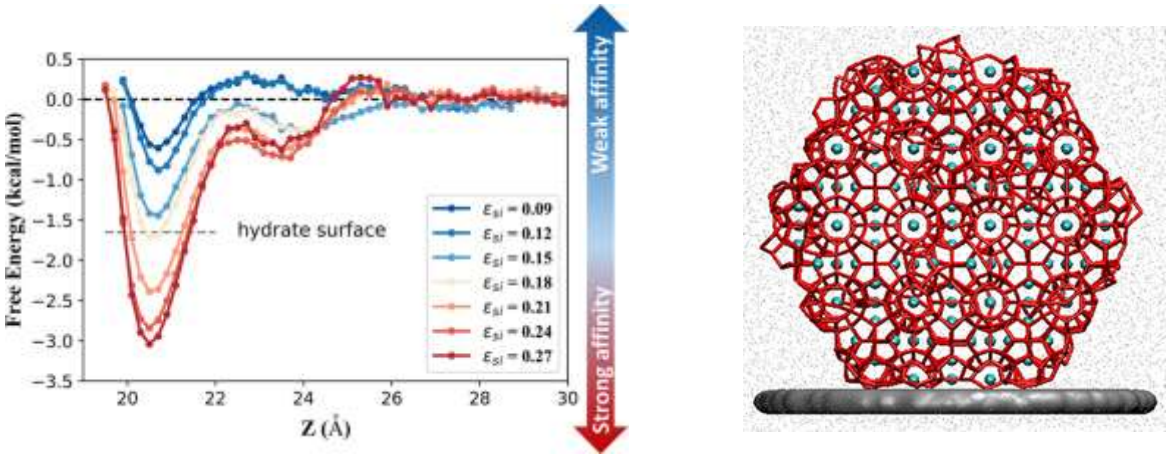

Figure 14: The effect of different guest molecule affinities (ε_{si} = 0.27–0.09 kcal·mol^{-1}) on the free energy of guest molecules adsorbed onto the slabs [258].

Although the experimental investigations provide important insights into the hydrate structural analysis and role of guest molecules, some details are not still well-understood whereas MD simulations can systematically be employed to explore such gaps. For example, the effects of guest molecules on hydrate growth showed that the attraction of guest-water molecules may control the nucleus growth rate whereas the size of guest molecules may probably determine the hydrate structure [351].

3.5 Thermo-physical and mechanical properties of gas hydrate

Understanding the mechanical characteristics is of importance for utilizing and predicting the stability of gas hydrate formation. By employing *ab initio* density functional theory (DFT) thermo-physical properties of CH_4 hydrate can be accurately calculated [215]. Structural, energetic, and mechanical properties of CO_2 hydrate by calculating DFT and MD methodology showed that although the cage distortions are mostly isotropic, a loss in the ideal symmetry of the empty structure is mainly due to the guest molecules [354]. MD indicates the surface tension and intermolecular active forces may decrease with increasing temperature and pressure in the system [355]. Moreover, simulating CH_4 hydrate under compression and tension clarified that the tensile stress is lower than maximum compressive stress under

the same conditions [49]. Tensile stress and strain rate of calcium silicate hydrate at 300 K demonstrated that the dynamic tensile of calcium silicate hydrate directly depends on water content but it is an inverse function of strain rates [356]. Also, the shear modulus of CO_2 and CH_4 hydrate directly and inversely depends on temperature [357]. According to the MD results of nucleation of CH_4 hydrate sandwiched by elastic silica, the nucleation was found to be dependent on the elasticity of silica in which the weak elastic provides a minimum induction time but in the case of extremely weak elastic, the process of nucleation due to the fluctuation of the layers cannot easily take place [358]. Through MD simulations of acoustic and elastic properties e.g. anisotropy factor, bulk modulus, shear modulus of CH_4, C_2H_6, C_3H_8, i-butane, and empty hydrates, it was found that the repulsive impact of the guest molecule upon tension and compression can weaken and strengthen the structure of hydrate lattice respectively. The sensitivity of the large cavity to pressure is also more than the small cavity, however, H-bond and O-H bond lengths exhibit the opposite behaviour [158]. MD CH_4 hydrate simulations of strain-stress, shear strain, and elastic moduli to investigate the ideal strength under shear deformation showed that CH_4 hydrate has no dominant slip system but displays brittle behaviours in terms of its strength [359]. By evaluating the hydrate elasticity and by analyzing the parameters e.g. binding energy, shear elastic constant, and anisotropy index, it was revealed that due to a cage-like structure, gas hydrate frameworks are very isotropic. The presence of highly symmetric proton configurations is one of the reasons for the higher anisotropy of ice *Ih* [360]. The relationship between grain size, mechanical instability, and fracture behaviour of polycrystalline and monocrystalline CH_4 hydrates highlighted that CH_4 hydrate is highly sensible to cage occupancy changes and environmental conditions. In monocrystalline CH_4 hydrate, dislocation-free brittle failure was observed which showed that upon depressurization process, the polycrystalline CH_4 hydrate can be destabilized by strain-induced [73]. The determination of mechanical properties of different gas hydrates indicated that under a uniaxial mechanical load, gas hydrate's stability

is critically affected by the polarity, shape, and size of the guest molecules [361]. According to MD insights, the impact of defects on the mechanical property of sI CH_4 hydrate was also found to be substantial. Additionally, considerable fluctuations for F_3 order parameters just before hydrate structure failure were observed. Also, at a deletion rate of 9%, the mechanical property was decreased [52]. Previously, to analyse the heterogeneous crystal growth of hydrate, a number of defects were observed. Typically, independent of the applied pressure and temperature, around 20% of hydrate cages were unoccupied while some large cages trapped two CH_4 molecules [59]. Explored Heterogeneous crystal growth of H_2S hydrate demonstrated that the growth rate of H_2S hydrate is higher than CH_4 hydrate, however, in the newly formed crystal of H_2S hydrate, a relatively low level of defects was observed [362]. Also, increased gas concentration reduces the induction time for H_2S hydrate nucleation while the homogenous nucleation process features the amorphous initial formation more specifically at high super-saturations [363]. Analysis of the dynamic and structural nature of water is also confined in the quasi-two-dimensional pores which is the main binding phase in the cement. It was shown that the defective silicate chains and the interlayer calcium can render a hydrophilic interaction among the C-S-H and confined water. In this regard, the dynamical behaviour of the confined water as a glassy material at an intermediate range up to 4.2 Å was evidenced [364]. To investigate the steady-state heterogeneous crystal growth during the sI crystal formation, an unexpected kind of structural defect (consisting of $5^{12}6^3$ cages) was previously confirmed. Additionally, an in-situ transformation of sI to sK was found to be possible albeit under prevailing operating conditions [58]. it was also revealed that guest-host H-bond leads to the formation of Bjerrum L-defects in the clathrate phase where 2 adjacent water molecules have no covalently bonded hydrogen atom between them. By conducting this simulation, it was determined that an activation barrier for the THF-water defect formation is about 8.3 kJ/mol [365]. NEMD simulations revealed that diffusion of released CH_4 from the hydrate surface during decomposition is not homogenous

and the solution phase does not necessarily remain isothermal [38]. The examination of the mechanical failure of monocrystalline CH_4 hydrate revealed that the failure may take place in two phases: gradual crack growth and quick crack propagation [91]. To investigate the mechanical properties of monocrystalline CH_4 hydrate and its intrinsic differences from ice, the impacts of guest occupancy, crystal-orientation temperature, and strain rate at 263 K and 10 MPa highlighted that although the influence of crystal orientation is not significant on monocrystalline CH_4 hydrate, mechanical strength greatly depends on temperature, strain rate, and large cage occupancy [89]. The mechanical stress–strain curves of CH_4 hydrate under three different strain rates and the directional deformation are presented in Figure 15.

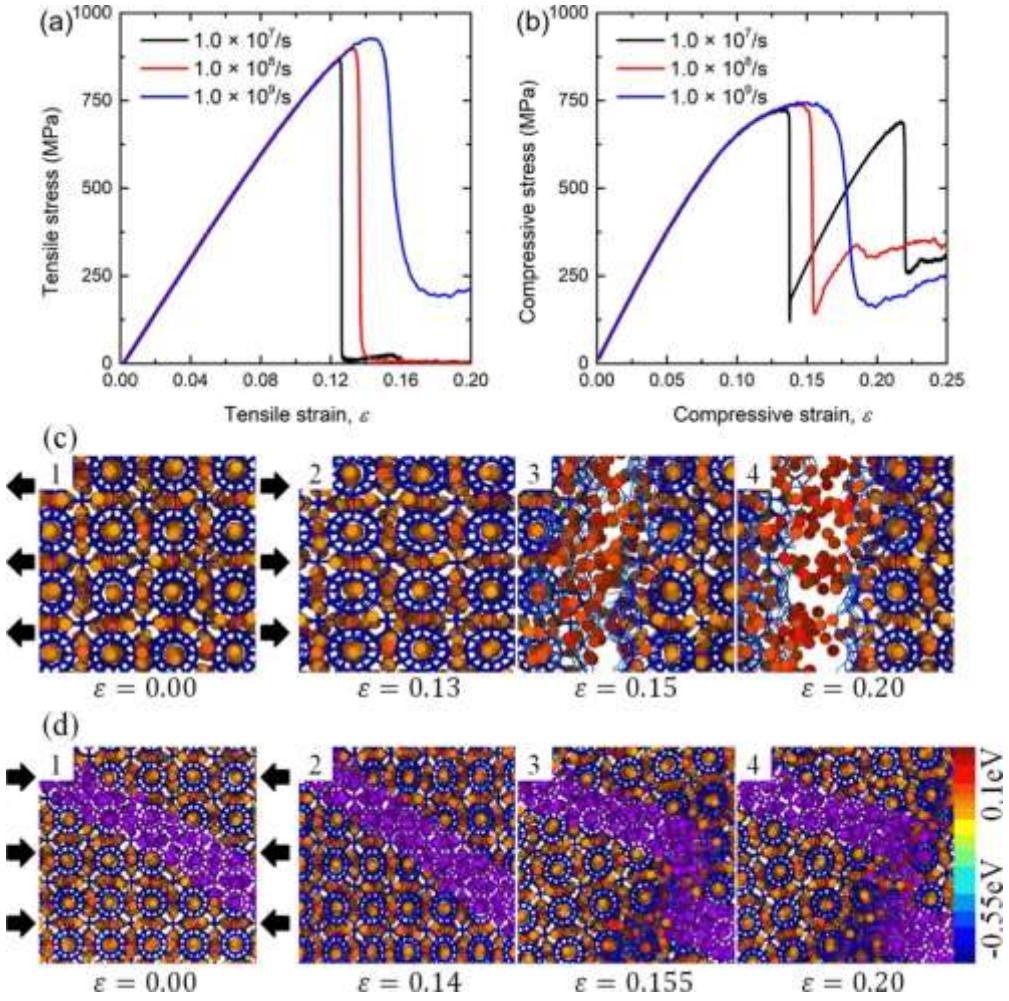

Figure 15: Mechanical properties of CH_4 hydrate for various engineering strain rates. (a) Tensile stress versus strain curves. (b) Compressive stress versus strain. (c) Tensile deformation test conditions. (d) Compressive deformation test conditions [89]. (The color of molecule particles is based on the potential energy. The purple molecules indicate the uniformly structural changes during deformation)

By evaluating the mechanics of CH_4 hydrate at the liquid water-hydrate interface, it was observed that in the region close to the interface, CH_4 molecules due to dense hydrogen-bonded water molecules cannot be soluble. However, the growth of local density and surface excess of CH_4 near the surface indicate anomalous CH_4 adsorption to the CH_4-water interface [366]. Previously, the free energies and thermal expansivity of clathrates showed that the large expansivity of xenon hydrate stems from guest molecules and a difference in oxygen atom arrangement between ice and hydrate plays a minor role [367]. By employing rigid geometry and adopting the non-polarizable model in NEMD simulations it was shown that except at low temperatures (50 K), although the estimated thermal conductivity values are relatively insensitive to the cage occupancy, a small number of defects (1%) in the water lattice can result in a large reduction (10%) in thermal conductivity [86]. The effect of electrostatics methods on the prediction of CH_4 hydrate thermal conductivity showed that the estimated thermal conductivities by non-periodic techniques would be more in agreement with the experiments, however, electrostatic treatments affect thermal conductivity [368]. Thermal conductivity may also depend on both rigidities of the framework and guest-host interactions but the lower thermal conductivity compared to ice *Ih* is because of differences in crystal structures [369]. Studying the mechanisms for thermal conduction of CH_4 hydrate revealed that the guest-host interactions and crystal structure can contribute to glasslike temperature dependence so that they can lower the hydrate thermal conductivity relative to ice *Ih* [370]. Based on MD analysis of the thermal conductivity of CH_4 hydrate in porous media, it was determined that with increasing temperature, CH_4 hydrate-SiO_2 thermal conductivity enhances more quickly near the freezing point. Also, at a certain temperature, smaller pore sizes have a larger effect on increasing hydrate thermal

conductivity which is several times less than the porous media [227]. Mechanisms for thermal conduction in H_2 hydrate demonstrated that dissimilar to CH_4, a single occupation of the small cavity by H_2 results in more harmonic energy transfer and less resonant scattering [371]. The thermal properties of sI CH_4 + LMGs hydrates also showed that at high-temperature ranges, guest molecules with strong host-guest interactions have more thermal expansion but increasing the size of LMGs subsequently decreases the $C_{P,}$, and C_V of hydrate [372]. A correction technique to determine isothermal expansion coefficients and lattice parameters at 287 K and 10-100 MPa highlighted that the isothermal expansion coefficient and specific heat capacity of C_3H_8 hydrate are somewhat higher than that in THF hydrate. Furthermore, by comparing C_3H_8 + CO_2 and C_3H_8 + CH_4 binary hydrates, it was revealed that the small cages occupied by CO_2 molecules dissimilar to CH_4 can result in increasing compressibility and expansion coefficient but decreasing the heat capacity [373]. According to structure-mechanical properties of CH_4/ Xe/ N_2/ H_2/ Ar + neohexene sH hydrates using *ab initio* atomic simulations, the type of help gas was identified as the main contributor to the shear, elastic and anisotropic characteristics of sH hydrate. Also, the brittleness of filled sH hydrate was found to be higher than empty sH hydrate which can be attributed to the role of guests inside cavities. However, wave velocities of ice *Ih* were determined less than sH hydrates [156]. Based on the simulated values of the lattice constants using anisotropic site-site potential models of the N_2+ neohexane hydrate, the same tendency as obtained by the powder X-ray diffraction was observed [374]. Moreover, studying the impact of help gas on the crystal lattice of Ar/ Kr/ CH_4+ neohexane (NH) at different temperatures determined that the order of their crystal lattice as CH_4 > Kr > Ar may be the evidence of the effects and importance of small guest molecular sizes [152]. It was also indicated that the lattice constants and system average volume for xenon hydrate in the presence of cyclopropane and propane are directly related to the guest molecular sizes and pressure [375]. Recently, the lattice expansion of CH_4 sII hydrate in the existence of linear and cyclic guest molecules (cyclobutanol and

butyraldehyde) with the identical formula of C_4H_8O was studied to figure out the effect of bonding characteristics on hydrate thermal expansion. Based on the results, less lattice expansion in the system consisting of cyclobutanol in comparison with butyraldehyde was observed but the promotion impact of cyclobutanol on hydrate equilibrium was found to be higher [376].

Simulation of the thin liquid film at the hydrate/ CH_4 gas interface showed that the thin liquid film makes substantial contributions to the interfacial properties [69]. The interfacial free energy, excess enthalpy, and stress at the crystal-liquid interface by employing a normal pressure-cross-sectional area (NP_NAT) ensemble elucidated that interfacial tension is directly and reversely proportional to temperature and pressure respectively [46]. Based on molecular analysis of the interfacial mechanics and thermodynamics at the interface of liquid water and natural gas, it was found that for the pressure range of less than 50 MPa, the increase of pressure and temperature reduces the interfacial tension [377]. Interfacial tension and CH_4 hydrate morphologies at the liquid water-hydrate interface showed that the nucleation may take place in the ranked order of film-shaped, cap-shaped, lens-shaped, and homogeneous [378]. By examination of the interfacial tension and behaviour of the single and mixture of CH_4, C_2H_6, and C_3H_6 hydrates, equilibrium molecular dynamics and hydrate formation at the water-gas interface were observed. At the interface, the surface adsorption of gas molecules enhances the gas local concentration but reduces the interfacial tension, however, both of these factors boost the formation of gas clathrate hydrate [222]. To determine the mechanical and key structural properties such as bulk modulus and equilibrium lattice volume for C_3H_8, $C_2H_6 + C_3H_8$, $CH_4 + C_3H_8$, and empty hydrates, it was determined that the equilibrium lattice volumes are directly proportional to the guest size in double hydrates which may experience the greater increase than pure hydrates [379]. Based on MD analysis of H_2 and D_2 molecular scape from the hydrate phase using the same force-field parameters at 150 to 195 K, it was also revealed that the stronger collisions between the cage and guest molecules may increase the

likelihood of cage distortion which results in the subsequent escape of D_2 molecules. Also, the leakage rates of H_2 were observed to be lower than those for D_2 [218]. In addition, the in-slab translational order parameters of the CH_4 hydrate surface in contact with the gas phase determined that the molecules of water in the adlayers and slab surfaces can be periodically arranged while the internal slabs can remain completely rigid [97].

3.6 Dynamical and vibrational behaviour

According to MD results, it was confirmed that the power spectra would be a reliable technique to evaluate the vibrational behaviour of guests in the hydrate phase [380]. Previously, the idea of a resonant scattering mechanism for the host-guest phonon interactions in clathrate hydrates was supported by MD simulations [381]. The dynamical behaviour of ice and sI clathrate hydrate showed that the phonon densities in both states are similar which represents the resemblance of their infrared spectra. Also, the phonon density enhancement of selective vibrational modes can be induced by guest species [34]. Phonon scattering off the rotational and vibrational motions of guests was also found to be responsible for the lower thermal conductivity of hydrates relative to ice [382]. According to the exploration of lattice vibrations in clathrate hydrates for Xe at 220 K, vibrational couplings lead to energy exchange between the guest vibrations and the host lattice which results in anomalous glasslike behaviour in the thermal conductivity [383]. Examining anomalous thermal conductivity of clathrate hydrates using EMD, and NEMD simulations revealed that the resonance scattering model is the most likely mechanism of anomalous temperature dependence and low thermal conductivity [384]. Evaluating energetic dynamical and H-bond vibrational properties in sI and sII hydrates demonstrated that H-bond energies are the largest in magnitude in structure I, followed by sII hydrate and then ice *Ih*. However, unlike ice and sII hydrate, energy transfer via H-bonds in sI occurs at higher frequencies [74]. MD calculations for the vibrational spectral band of molecular H_2 trapped in hydrate indicated that H_2 molecules in large cavities provide a

high-frequency peak than those in small cages [385]. With the combination of *ab initio* and classical MD simulations to analyse the host-guest H-bonding in alcohol clathrate hydrates it was found that due to the strong host-guest H-bonding, vibrational spectra of alcohol O–H bonds consistent with experimental Raman spectra display large frequency shifts. Also, conducting similar investigations of dynamical properties of H_2S revealed that a preferred orientation of the dipole-vector exists at 150 K whereas there is no preferred orientation at 300 K [386]. Interestingly, some alcohol molecules can fit into $5^{12}6^4$ cages of clathrate hydrates [387]. The mechanical and vibrational features of CH_4/ Xe/ CO_2+ neohexane sH hydrates showed that vibrational frequencies are dependent on interatomic distances of hydrate and pressure. Also, the relations between interatomic distances, H-bond strength, and vibrational frequency shifts, affected by guest-host interactions and guest type were previously certified [388]. Based on the stretching vibrations of sI CH_4 hydrate investigated with *ab initio* density functional theory, although the consistency between calculated vibrational frequencies and experiments was confirmed, the computed H-C stretching vibrations are less than in the free molecules [350]. In addition, *ab initio* results to investigate the vibrational spectra of sH CH_4 hydrate indicated that asymmetric and symmetric stretching vibrational frequencies of CH_4 molecules are higher in small cages of sH hydrate than in medium cavities, however, the H-C bond length in medium cavities is slightly longer [389]. Also, asymmetric and symmetric stretching vibrational frequencies of CH_4 molecules are higher in small cavities than in large ones of sI hydrate [390]. Based on the infrared spectra of sII C_3H_8, i-butane, $CH_4 + C_2H_6$, $CH_4 + C_3H_8$, and empty hydrates using DFT, it was determined that the calculated vibrational frequencies of the guest and host molecules can give comparable results to experimental data which can be useful to detect the presence of gas hydrates [391]. Analysing the properties of multiple occupied N_2 clathrate hydrates showed that there is a large vibrational host-guest coupling for both double and single occupancies, however, the frequency range is broader in the former case [392]. To evaluate the mobility of water and

CO_2 molecules in the hydrate phase, it was elucidated that negligible composition change leads to significant impacts on the mobility of CO_2 molecules. For example, altering 3% cage occupancy may result in two orders of magnitude change in the diffusion coefficient [393]. Molecular H_2 mobility within the sII clathrate at 200-265 K demonstrated that on the time scale of the simulations, H_2 molecular mobility in the small cavities is not substantial but can be more clathrate stable with the presence of THF [394]. By analysing apparent high mobility and transport of interstitial H_2O defects in CH_4 hydrate crystal it was concluded that H_2O molecules are somewhat high mobile entities within a gas hydrate. Also, the presence of empty cavities facilitates the pathways for the H_2O molecular transportation between them [395]. In addition, the hydration shell nucleation of guest molecules becomes more ordered with increasing the concentration of guest molecules, resulting in a decline of entropy and guest mobility [396]. The results of first-principles DFT and MD to determine the thermal properties of gas hydrates at very low temperatures confirmed the negative thermal expansion which is similar to the ice [397]. The structural and dynamical properties of CO_2, CH_4, and Xe hydrates indicated that by elevating the temperature, the lattice expansion of CO_2 hydrate is larger than that in Xe and CH_4 hydrates. Also, the thermal conductivities of both Xe and CO_2 are less than that in CH_4 or even empty lattice [398]. With respect to the analysis of structural and energetic properties of the sI and sII CO hydrate it was revealed that increasing the content of CO molecules in the large cages can stabilize the sII but destabilize sI hydrate [399]. Using the rotational autocorrelation function (RACF) to study the host and guest rotational dynamics, it was highlighted that altering the rotational motion of both water and guest molecules affect the proportion of them in mixed CO_2+CH_4 hydrate [400]. Dynamical and energetic properties of H_2+THF hydrate through EMD simulations determined that the van der Waals component with the surrounding water molecules in the constituent cavities is the largest contribution to the interaction energy of both guests [401]. Using first-principles DFT to study the vibrational, structural, and mechanical properties of

THF and THF+Xe hydrates, it was found that compared to THF hydrate, THF+Xe hydrate has a larger OH stretching frequency, lattice volume, hydrogen bond length but lower Poisson ratio, density, compressional wave velocity, and hydrogen bond stretching frequency [402].

3.7 Coexistence of phases

The phase equilibrium of clathrate hydrates more specifically those at thermodynamically difficult to conduct the experiments in a laboratory can be studied using MD simulations. For example, the thermodynamic stability of sII neon hydrate at 480 MPa and 260 K with employing MD simulations was confirmed [403]. Previously, by employing MDs, a new phase between equilibrium conditions of sT′ and C_0-II structures for H_2 hydrate was explored which helped to clarify the experimental puzzle of H_2 hydrates [116]. In addition, at ambient temperature and 3-130 GPa, the phase diagram of the C_2 structure of H_2 hydrate was determined [216]. However, the results of MD to determine the three-phase coexistence of H_2 hydrate at 90-400 MPa were found to underestimate the experiments by approximately 25 K [404]. The MD predictions of the three-phase coexistence of binary CH_4+CO_2 hydrates at 40, 100, and 200 MPa compared to experimental data indicated that the deviation of simulations up to 100 MPa is not significant [405]. MD insights into the stability of CO hydrate at 17.3 MPa and 243 K revealed that CO tends to form sI rather than sII clathrate, however, with increasing pressure and temperature to 10 MPa and 252 K, it would be more prone to generate sII clathrate hydrate [406]. In addition, *ab initio* intermolecular potentials at the MP2 level to calculate energy surfaces of CH_4-H_2O and CO_2-H_2O showed that the angle-dependent approach improves the prediction of the CO_2 and CH_4 hydrates phase equilibrium [407]. MD simulation of three-phase equilibrium suggested that compared to NPT simulation, NVT has two benefits: first, there is no need to control the pressure. Second, NVT reduces the number of time steps in simulations. Therefore, it is more suitable to study the phase coexistence of gas hydrates [75]. Moreover,

the equilibrium condition can be reached more accurately when the temperature and total energy become constant [408].

3.8 Gas exchange phenomenon

Evidence suggests the gas exchange occurs via a transient co-occupation of CO_2 and CH_4 in cages [409,410]. Both MD simulations as well as Raman spectroscopic confirmed that the process of CO_2/CH_4 replacement is the breakup of the cage, the scape of CH_4, and cage occupation by CO_2 molecules [411]. It was also elucidated that during gas exchange phenomena, replacement takes place at both small and large cages of CH_4 hydrate without changing the structure and with the partial collapse in which the hydrate surface is partially melted so that the interface becomes active [120]. MD evidence indicated that the increase of temperature from 250 to 270 K accelerates the kinetics of the CO_2/CH_4 replacement by at least 1.5 times, also, a swap of the guest molecules without a breakup of cages was confirmed [410]. Previously, for CO_2 capture and storage analysis, Gibbs free energy calculations for CO_2 clathrate hydrates in the presence of H_2S, CH_4, N_2, and SO_2 were performed. Based on the results, the negative values of ΔG for SO_2 and H_2S impurities compared to CO_2 showed more stability in the hydrate phase. Although at lower concentrations, these impurities act as promoters, large amounts of them decline the CO_2 capture and storage capacity [412]. According to the CH_4+CO_2 hydrate formation, the concentration of CO_2 plays a key role in the kinetics of CH_4+CO_2 hydrate formation. However, increasing CO_2 concentration in the aqueous phase cannot give faster growth [413]. It was also revealed that during the gas replacement process, CO_2 molecules in mixed bubbles mostly surround the CH_4 molecules so that they influence the process of gas exchange specifically at the initial stage [414]. MD investigations of the replacement or co-growth of CO_2 and CH_4 hydrates indicated that CH_4 hydrate in the presence of CO_2 gas is more stable than with CO_2 solution. It was also estimated that nearly 20% of the dissociated CH_4 hydrates can be replaced by CO_2 and most likely CO_2+CH_4 mixed hydrates can be formed [220].

Additionally, the guest behaviour in a porous environment would be dissimilar. MD exploration of the transport properties of CH_4 and CO_2 hydrates in Na-montmorillonite clay determined that increasing CH_4 and CO_2 molecules in Na-montmorillonite interlayers probably result in a decrease in their self-diffusion coefficients [200]. Also, the formation and dissociation of CH_4 hydrate in the clay pore with fatty acids showed that the existence of fatty acids slightly accelerates the breakdown of CH_4 hydrate in the heterogeneous sediment [228]. Moreover, the amorphous layer formation was detected as a barrier against mass transfer which results in a slower rate of CO_2/CH_4 replacement because as time proceeds, the CO_2 amorphous layer forms on the CH_4 hydrate surfaces [119].

Another barrier is that since CH_4 relative to CO_2 possesses a smaller size, it can be more stable in small cages [415]. Also, N_2 guests can be used as a carrier gas because it does not compete directly with CO_2 during CH_4 substitution. In addition, the substitution of CH_4 in the small cavities with N_2 has positive free energy [416]. The effects of N_2 on the process of CO_2/CH_4 replacement showed that the addition of N_2 aids CO_2 penetrate into all CH_4 hydrate cages on a broader scale. However, this diffusion is sensitive to the ratio of CO_2 to N_2 [221]. The CH_4 replacement by flue gas in the hydrate phase in the presence of SO_2, H_2S, N_2O/ NO, and CS_2 revealed that N_2O, SO_2, and CS_2 molecules tend to occupy the large cavities of sII and sI hydrates while NO, and H_2S have no preference to occupy small or large cavities. It was also confirmed that CS_2, N_2O, H_2S, and SO_2 can replace CH_4 in the hydrate phase and help the process of gas exchange [417].

3.9 Memory effect phenomenon

Another feature of gas hydrate is the observation of a memory effect. In this phenomenon, the resulting solution from the decomposed hydrate is able to form a hydrate more readily with a shorter induction time than a fresh solution. Since a number of studies to test a memory effect have failed to observe this

phenomenon, it may be concluded that the memory effect does occur for just specific hydrate systems. Generally, the most popular model for the memory effect is the residual structure hypothesis which assumes the dissociation of gas hydrates leads to the formation of some ‘‘hydrate melt”. Therefore, residual structures that retain some structural features of the hydrate phase would persist in the liquid water phase for a long time after the decomposition. For example, guest molecules with associated pentagonal rings of hydrogen-bonded water molecules provide nucleation sites for the second formation of gas hydrate when they cooled again [7]. MD simulations of CH_4 hydrate pointed out that the lifetime of a hydrogen bond in water is of the order of picoseconds [418]. It was also assumed that the freezing of a bulk hydrate-forming solution occurs similarly to the freezing of bulk water in which the nucleation is mostly heterogeneous and rarely homogeneous in bulk solution [419]. MD investigations of the properties of melting temperature considering the memory effect suggested that the coordination atoms of oxygen in water are an important factor in the memory effect but water molecules near the interface of water-CH_4 have fewer memory properties [40]. Moreover, MD modelling of two-step nucleation and memory effect in CH_4 hydrate clarified that the areas locally richer by CH_4 molecules enhance the apparent nucleation rate more readily. Also, the memory of the crystal for fast re-crystallization was found to be insignificant [4].

3.10 Self-preservation phenomenon

Self-preservation would be an advantageous property for the transportation and storage of gas hydrates. Quasi-harmonic lattice dynamics (QLD) model considering guest-guest interactions of multiple H_2 occupancies to predict self-preservation and the thermodynamic properties of sII H_2 hydrate specified that the pressure in the H_2 hydrate is more than that in the ice phase but the hydrogen bonds between the ice and hydrate do not allow hydrate to be destroyed, so that, the hydrate phase under heating remains stable [420]. The self-preservation mechanism using the combination of the NVT and NVE method for

CH_4 hydrate also proved that the coupling of heat and mass transfer resistances is the driving mechanism for self-preservation impact [55]. According to MD simulations, the water self-diffusion coefficient can be changed by altering the temperature and guest concentration [57]. Based on the calculated order parameter, it was found that the order parameter value for ice, hydrate and liquid water phases by partially heating is different but it can be changed at the interfaces of the phases [54]. Through MD exploration of the self-preservation of hydrate decomposition using NVT/E to represent different levels of heat transfer resistance, it was observed that heat transfer resistance facilitates the formation of the solid-like layer which inhibits further hydrate dissociation. Also, the increase in pressure and particularly the decrease in temperature enhances self-preservation [55]. Moreover using MD algorithms, the number and type of cavities in the amorphous and clathrate (sI, sII, HS-I) coexist with ice during CH_4 hydrate self-preservation can be monitored [421]. Recently, the sources of the THF hydrate anomalous preservation surrounded by CP hydrate were evaluated outside the stability conditions. The melting temperature of uncoated THF hydrate was determined to be 270 K whereas THF hydrate encapsulated with CP hydrate could not be dissociated up to 290 K. This phenomenon also indicates the transformation of the THF hydrate from heterogeneous to homogeneous mechanism. As Figure 16 (a) shows, the potential energy of the coated THF hydrate for the 50 ns at 280 K can remain stable. Figure 16 (b) indicates the partial breakup of coting layers of THF hydrate at 290 K which results in the liquid layer formation on top of the hydrate phase. With increasing temperature to 300 K, the potential energy suddenly elevates due to the dissociation of all CP hydrate followed by the breakdown of THF hydrate as the inner layer [422].

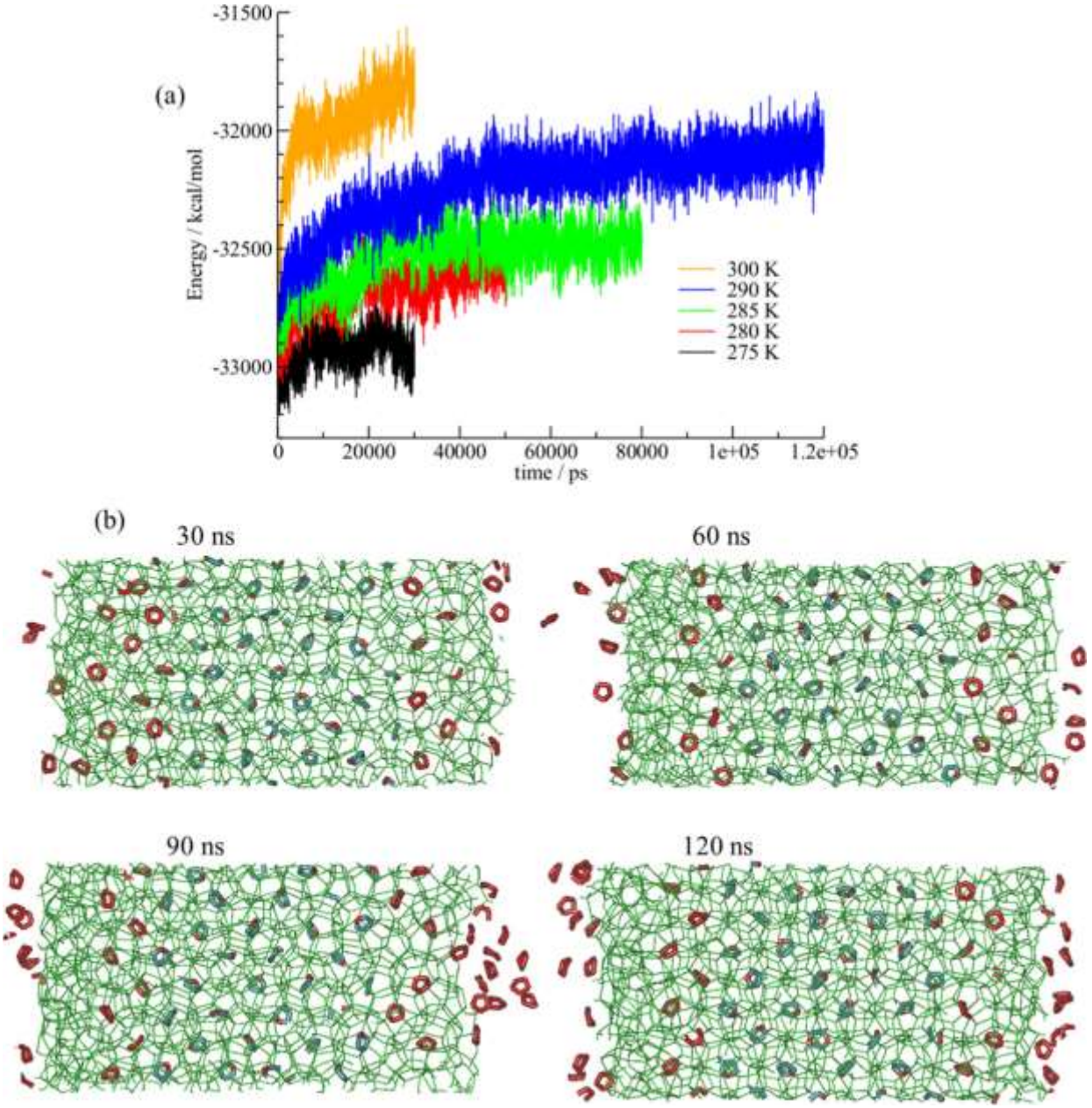

Figure 16: (a), Time evolution of the potential energy of THF hydrate coated by CP hydrate at different temperatures; (b) Snapshots of THF–CP hydrate decomposition at 290 K [422]

In the self-preservation phenomenon, the effects of H-bonds are also critical. In this regard, the influence of host-guest H-bond on the properties of H_2S/ Xe + pinacolone/ MTBE sH hydrates showed that MD simulation results are consistent with the observations of X-ray crystallographic at the temperature range

from 100 K to 250 K [423]. Based on MD simulations of the halogen bonding in BrCl, mixed Cl_2+Br_2, Cl_2, and Br_2 clathrate hydrates, the short and strong interactions between water molecules and bromine atoms in the sI clathrate hydrates were observed [424]. In addition, halogen bonding in Cl_2 and Br_2 clathrate hydrates studied via both MD simulations and DFT showed that the obtained halogen-water distances were compatible with values observed in X-ray diffraction [425]. The anomalous halogen bonding interactions between Cl_2 and Br_2 with water indicated that a combination of the dihalogen interaction with oxygen lone electron pairs may result in the halogen bonding non-bonded interactions between water in the clathrate and guest molecules [426]. To explore the hydrogen bonding in binary sI hydrate at 183-263 K, it was found that although gas molecules in the small cavity do not themselves form hydrogen bonds with water, the THF molecules affect the occurrence of hydrogen bonds. Also, nearest neighbour guest-guest interactions were found to influence the stability and structure of the clathrate network [427]. Hydrogen bonding study of pure and binary CO_2+THF hydrates indicated that a small percentage of hydrogen bond formation between water and THF occurs, however, it cannot be seen through single-crystal X-ray diffraction at low temperatures. Interestingly, the presence of hydrogen bonding guests can increase CO_2 migration and boosts the hydrate formation kinetics [428]. MD simulations of the role of the medium and small cage guests on the hydrogen bonding of the large cage guests with the hydrate framework water molecules exhibited that the presence of CH_3F enhances the H-bonding probability of the TBME with the water molecules [429]. Exploring the hydrogen bonding in binary sI hydrate at 100-250 K revealed that ethanol molecules by forming a long-lived proton- accepting and donating hydrogen bonds with water molecules, support the general cage integrity of clathrate hydrate [430]. The hydroxyl groups of inhibitors e.g. ethanol/ 1-propanol/ 2-propanol may act as both proton donors and proton acceptors. Also, the probability of H-bond between hydroxyl atoms with water molecules was found to be considerable [226]. By conducting the MD exploration of the microscopic

properties of the HFC-41/ CH_4+ pinacolone hydrate, although the anisotropic expansion of the sH hydrate lattice for sH HFC-41+pinacolone hydrate was not observed, weak H-bonding of the water and pinacolone molecules was detected [224]. Recently, hydrogen bonding analysis for CH_4/ HFC-32 +N-methylpiperidine (NMP) hydrate determined that for HFC-32+NMP sH hydrate which was more stable than CH_4+NMP sH hydrate, NMP molecules with water form H-bonds whereas similar hydrogen bonding for CH_4+NMP system was not observed [431].

4 Proportions of MD gas hydrate investigations and future research guidelines

Figure 17 exhibits the proportion of different MD studies that have been conducted on gas hydrates in the literature. As is shown, semiclathrate hydrates possess the least share of these investigations whereas over half of MD studies have been performed on pure gas hydrates. It should be kept in mind that to perceive fundamental microscopic characteristics of gas hydrates, most MD studies have been performed on CH_4 hydrate, therefore that is why its percentage is near one-third of the total explorations. In addition, the proportions of insight into the specifications of other pure, binary, and mixed gas hydrates, the effects of minerals, thermodynamic/ kinetic promoters, and inhibitors have been reasonably close together.

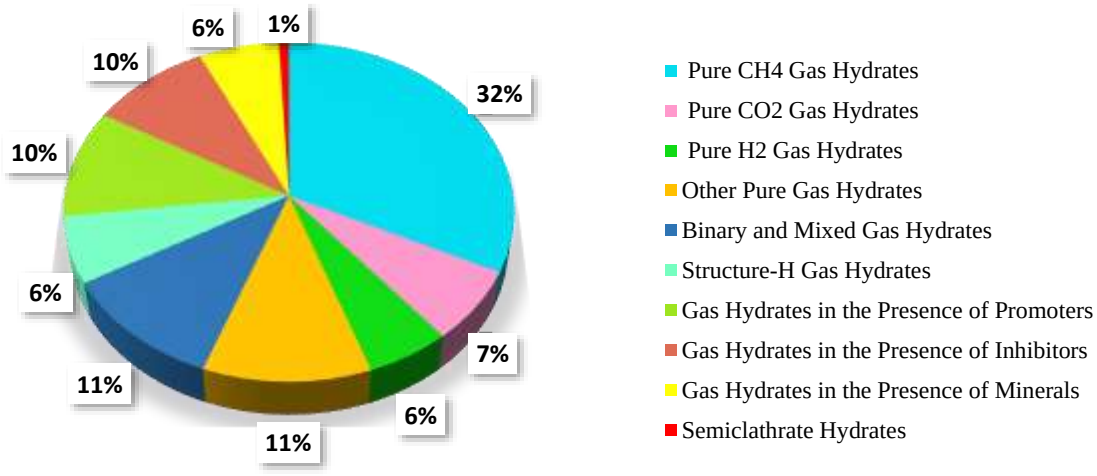

Figure 17: The proportion of MD simulation studies on gas hydrates.

In this work, different phenomena and properties of gas hydrates were overviewed. The summary list of MD computational studies conducted on clathrate (sI/II/H) hydrates ranging from pure/binary/mixed components, or in the presence of promoters/ inhibitors/ minerals is presented in Table 2.

Table 2: Investigated phenomena for various hydrate systems using MD simulations.

	Component	Dynamical and Nucleation/ aggregation	Growth	Dissociation	Thermo-physical properties	Mechanical properties	Thermodynamic / Kinetic properties	Morphology/ structural analysis (stabilization)	Heat and mass transfer properties	Memory effect	Self-preservation	Coexistence of phases/ Phase equilibrium	Cage occupancy/ Storage capacity	Ref.
Pure hydrates	CH_4	✱	✱	✱	✱	✱	✱	✱	✱	✱	✱	✱	✱	[4,23,38–46,49,26,50–59,27,60–64,66–70,32,71–80,33,82,84,86,88–94,34,95–100,108,113,117,213,35,214,215,234,235,237,244,245,253–255,36,256,257,261,290,291,297,298,304,318,355,37,366,368–370,378,380,421,432]
	H_2	✱	✱	✱	✱	✱		✱	✱	✱			✱	✱	[40,115,420,116,216,218,294,307,331,385,404]
	CO_2	✱	✱	✱	✱	✱	✱	✱	✱	✱			✱	✱	[25,212,221,247,328,361,428]
	C_2H_4, C_2H_6, C_3H_8	✱	✱	✱	✱	✱		✱	✱	✱			✱	✱	[21,111,219,262,295,302,303,352]
	Acid gas (H_2S, CO, CS, CS_2, SO_2, N_2O)	✱	✱	✱	✱		✱	✱	✱	✱				✱	[210,240,353,361–363,386,399,406]
	Noble gas (Ar, Kr, Xe, Ne, N_2)	✱	✱	✱	✱	✱	✱	✱	✱	✱			✱	✱	[163,299,398,403,339,340,367,381,383,384,392,396]
	Liquid hydrocarbon (EO, CP, THF, THP, C_3H_9NO, C_2H_4O, CH_2O, $C_3H_6O_2$, C_3H_8O)	✱	✱	✱	✱	✱		✱	✱	✱		✱		✱	[106,110,232,233,248,250,263,365,382,397]
Gas hydrates + KHP/THP	CH_4/ H_2/ Xe + THP (C_3H_8/ THF/ TBME/ C_2H_6 /TMO/ EO/ FA/ CB/ CP/ ISA/ TBAB/ SF_6/ Asphaltene)	✱	✱	✱	✱	✱	✱	✱	✱	✱		✱	✱	✱	[109,131,269–271,300,308,330,333,334,336,337,132,347,372,375,387,394,401,402,141,142,168,208,252,267,268]
	CH_4/ H_2/ N_2 + KHP (SDS/ CAPB/ SWCNT/ Protein/ lecithin)		✱	✱		✱		✱	✱	✱	✱		✱	✱	[140,185,266,301]
Gas hydrates + KHI/THI	CH_4 + C_2H_6 / C_3H_8/ C_4H_{10} + THI (Salt: NaCl/ NH_4Cl / KCl/ $CaCl_2$)/ (Alcohol: (methanol/ Ethanol/ 1-Propanol/ 2-Propanol/ Glycerol)	✱	✱	✱	✱	✱		✱	✱	✱			✱	✱	[166,169,277,281,311–315,327,170–172,182,225,226,275,276]
	CH_4+ KHI (Na-MMT/LHA/ Amino acids/ PVPs/ PVCap/ PDMAEMA/ PEO / VIMA/ AFPs)		✱	✱	✱	✱		✱		✱				✱	[167,173,183,184,279,280,174–181]

Mixed gas hydrates	CH_4+ C_2H_6/ C_3H_8/ Acid gas (H_2S/ CO NO/ N_2O/ SO_2/ CS_2)	❋	❋	❋	❋	❋	❋	❋	❋	❋		❋	❋	[102,124,417,125,222,242,243, 373,377,408,412]
	H_2 + CH_4/ C_2H_6/ C_3H_8			❋	❋	❋				❋			❋	[251,265,296,338]
	Cl_2 + BrCl/ Br_2/ NH_3	❋				❋		❋						[309,422,424–426,429]
sH hydrates	H_2/ CH_4/ N_2/ Ar/ Kr/ Xe/ H_2S + LMGs	❋	❋	❋	❋	❋		❋	❋	❋		❋	❋	[150,152,346,374,423,156,160, 161,223,224,310,341,345]
Hydrate + minerals	CH_4 + NMP/ SiO_2/ Clay/ Graphite / Kaolinite	❋	❋	❋	❋	❋	❋	❋	❋	❋		❋		[29,196,292,293,356,358,364,4 31,197,203,227,228,283–286]

The performed MD frameworks to analyse the phenomena and characteristics associated with hydrate-based applications either for gas separation or utilization can complete or at least support the experimental measurements. Despite a number of MD simulations of gas hydrates reported in the literature, conducting MD simulations to investigate unexplored gas hydrate characteristics can also complete the present findings at the macroscopic level. Hence, we aim to highlight some suggestions for future research below:

- Additional MD investigations on the combined effects of various inhibitors and promoters such as KHI+THI and KHP+THP on clathrate hydrates to identify the relationship between hydrate phenomena and the presence of additives can be performed. These simulations may help to comprehend the characteristics connected to the performance parameters of hydrate-based gas separation, CO_2 hydrate utilization, or other hydrate-relevant applications.
- More MD simulations to understand some gas hydrate phenomena such as memory effect and self-preservation at different environmental or operating conditions need to be carried out.
- In spite of several experimental suggestions to utilize the semiclathrate hydrates in different processes of hydrate-based applications e.g. secondary refrigeration and air conditioning aims, the least proportion of MD simulations is for this type of gas hydrates. Therefore, a manifold of

MD explorations to reveal the molecular mechanisms of semiclathrate hydrate promoters can be conducted.

- Only a few studies focused on clathrate hydrate structural transitions from sI to sII or sH and the coexistence of the phases based on the guest molecular sizes, shapes, and concentrations at the molecular scale. Hence, simulations considering different thermophysical properties during the process of structural transitions need to be performed.
- Heterogeneous nucleation MD simulations with fast mass transfer in the hydrate formation, and analyzing the role of nanobubbles during the nucleation phase can be considered for further research.
- To date, although some MD simulations in porous media have been performed, studying the systems simultaneously including mixed minerals e.g. kaolinite, quartz, montmorillonite, and kaolinite can help to assess the effects of these components on gas hydrate phenomena.
- In order to evaluate the influences of permeability and wettability on hydrate-bearing sediments, more MD studies should be carried out.
- Discrepancies between MD simulations and experimental outcomes in terms of consistency with the real condition can be assessed by providing simulations of the phenomena at larger scales. Therefore, a better understanding of the mutual relationship among mechanisms can be achieved.

Nomenclature

HBGS	Hydrate-Based Gas Separation	NPE	Nonyl Phenol Ethoxylates
HBCC	Hydrate-Based Carbon Capture	LAE	Lauryl Alcohol Ethoxylates
NGH	Natural Gas Hydrate	SDS	Sodium Dodecyl Sulfate
InSAR	Interferometric Synthetic Aperture Radar	SL	Sulfonated Lignin
MRI	Magnetic Resonance Imaging	SHS	Sodium Hexadecyl Sulfate

^{13}CNMR	Carbon-13 Nuclear Magnetic Resonance	STS	Sodium Tetradecyl Sulfate
COC	Cyclic Organic Compounds	SDBS	Sodium Dodecyl Benzene Sulfonate
CN	Coordination Number	DMSO	Di-Methyl Sulf-Oxide
GHSZ	Gas Hydrate Stability Zone	TMS	Tetra-Methylene Sulfone
CSMHYD	Colorado School of Mines Hydrate	SWNT	Single-Walled carbon Nano-Tube
T/KHI	Thermodynamic/Kinetic Hydrate Inhibitor	MWCNT	Multi-Walled Carbon Nano-Tube
T/KHP	Thermodynamic/Kinetic Hydrate Promoter	Na-MMT	Sodium Mont-Morillonite
LMGs	Large Molecule Guests	SW-CNTs	Single-Walled Carbon Nano-Tubes
AIMD	*Ab Initio* Molecular Dynamics	SAMs	Self-Assembled Monolayers
TMO	Tri-Methylene-Oxide	TMS	Tetra-Methylene Sulfone
FA	FormAldehyde	EO	Ethylene Oxide
CB	CycloButane	LHA	Leonardite Humic Acid
MWCNT	Multi-Walled Carbon Nano-Tube	ACF	Auto-Correlation of the Fluctuations
THT	Tetrahydrothiophene	AOP	Angular Order Parameter
THF	TetraHydroFuran	APDF	Angular probability distribution function
PMF	Potential of Mean Force	CGMC	Grand Canonical Monte Carlo
OACF	Orientation Auto-Correlation Function	DFT	Density Functional Theory
QLD	Quasi-harmonic Lattice Dynamics	DWC	Dodecahedral Water Cluster
TCF	Time Correlation Function	FSICA	Face-Saturated Incomplete Cage Analysis
VACF	Velocity Auto-Correlation Function	HCACF	Flux AutoCorrelation Function
RDF	Radial Displacement Function	MCG-OP	Mutually Coordinated Guest Order Parameter
RACF	Rotational Auto-Correlation Function	MCG	Mutually Coordinated Guest
RPMD	Ring Polymer Molecular Dynamics	MSD	Mean Square Displacement
RMSF	Root Mean Square Fluctuation	NEMD	Non-Equilibrium Molecular Dynamics
RPMD	Ring Polymer Molecular Dynamics	MFPT	Mean First-Passage Time

Conflict of interest

The authors declare no conflicts of interest.

Acknowledgment

The first author would like to thank Curtin University Malaysia for providing Curtin Malaysia Postgraduate Scholarship (CMPRS) and necessary resources and financial support for this work. Also, we would like to thank Dr. Saman Alavi for their valuable suggestions and comments on this work.

Reference

[1] Sloan ED, Koh CA. Clathrate hydrates of natural gases. 3rd Ed. CRC Press, Taylor & Francis Group, Boca Raton: 2008.

[2] Suginaka T, Sakamoto H, Iino K, Sakakibara Y, Ohmura R. Phase equilibrium for ionic semiclathrate hydrate formed with CO2, CH4, or N2 plus tetrabutylphosphonium bromide. Fluid Phase Equilib 2013;344:108–11. https://doi.org/10.1016/j.fluid.2013.01.018.

[3] Sakamoto J, Hashimoto S, Tsuda T, Sugahara T, Inoue Y, Ohgaki K. Thermodynamic and Raman spectroscopic studies on hydrogen+tetra-n-butyl ammonium fluoride semi-clathrate hydrates. Chem Eng Sci 2008;63:5789–94. https://doi.org/10.1016/j.ces.2008.08.026.

[4] Liang S, Kusalik PG. Explorations of gas hydrate crystal growth by molecular simulations. Chem Phys Lett 2010;494:123–33. https://doi.org/10.1016/j.cplett.2010.05.088.

[5] English NJ, Macelroy JMD. Perspectives on molecular simulation of clathrate hydrates: Progress, prospects and challenges. Chem Eng Sci 2015;121:133–56. https://doi.org/10.1016/j.ces.2014.07.047.

[6] English NJ, Waldron CJ. Perspectives on external electric fields in molecular simulation: Progress, prospects and challenges. Phys Chem Chem Phys 2015;17:12407–40. https://doi.org/10.1039/c5cp00629e.

[7] Ripmeester JA, Alavi S. Some current challenges in clathrate hydrate science: Nucleation,

decomposition and the memory effect. Curr Opin Solid State Mater Sci 2016;20:344–51. https://doi.org/10.1016/j.cossms.2016.03.005.

[8] Alavi S, Ripmeester JA. Simulations of hydrogen gas in clathrate hydrates. Mol Simul 2017;43:808–20. https://doi.org/10.1080/08927022.2017.1295456.

[9] Sinehbaghizadeh S, Saptoro A, Mohammadi AH. CO2 hydrate properties and applications: A state of the art. Prog Energy Combust Sci 2022;93:101026. https://doi.org/10.1016/j.pecs.2022.101026.

[10] Sokhan V. P. and Tildesley D. J. The free surface of water: molecular orientation, surface potential and nonlinear susceptibility. Mol Phys 1997;92:625–40. https://doi.org/10.1080/002689797169916.

[11] Stoddard SD, Ford J. Numerical experiments on the stochastic behavior of a Lennard-Jones gas system. Phys Rev A 1973;8:1504–12. https://doi.org/10.1103/PhysRevA.8.1504.

[12] Rapaport DC. The Art of Molecular dynamics simulation. Cambridge University Press; 2004. https://doi.org/10.1017/CBO9780511816581.

[13] Orsi M. Molecular dynamics simulation of humic substances. Chem Biol Technol Agric 2014;1:10. https://doi.org/10.1186/s40538-014-0010-4.

[14] Alavi S., Ripmeester J. Molecular simulations fundamentals and practice. vol. 1. 2020. https://doi.org/10.1002/9783527699452.

[15] Kohn W, Sham LJ. Self-consistent equations including exchange and correlation effects. Phys Rev 1965;140:1133–8. https://doi.org/10.1103/PhysRev.140.A1133.

[16] Tan H, Li Y, Zhang SB, Duan W. Effect of Hartree–Fock pseudopotentials on local density

functional theory calculations. Phys Chem Chem Phys 2018;20:18844–9. https://doi.org/10.1039/C8CP00990B.

[17] Duan X-M, Song G-L, Li Z-H, Wang X-J, Chen G-H, Fan K-N. Accurate prediction of heat of formation by combining Hartree–Fock/density functional theory calculation with linear regression correction approach. J Chem Phys 2004;121:7086–95. https://doi.org/10.1063/1.1786582.

[18] Neese F, Wennmohs F, Hansen A, Becker U. Efficient, approximate and parallel Hartree–Fock and hybrid DFT calculations. A 'chain-of-spheres'' algorithm for the Hartree–Fock exchange.' Chem Phys 2009;356:98–109. https://doi.org/10.1016/j.chemphys.2008.10.036.

[19] Adjiman CS, Sahinidis N V, Vlachos DG, Bakshi B, Maravelias CT, Georgakis C. Process systems engineering perspective on the design of materials and molecules. Ind Eng Chem Res 2021:acs.iecr.0c05399. https://doi.org/10.1021/acs.iecr.0c05399.

[20] Papadimitriou NI, Tsimpanogiannis IN, Economou IG, Stubos AK. Monte Carlo simulations of the separation of a binary gas mixture (CH4 + CO2) using hydrates. Phys Chem Chem Phys 2018;20:28026–38. https://doi.org/10.1039/C8CP02050G.

[21] Tanaka H. The thermodynamic stability of clathrate hydrate. III. Accommodation of nonspherical propane and ethane molecules. J Chem Phys 1994;101:10833–42. https://doi.org/10.1063/1.467832.

[22] Qiu N, Bai X, Sun N, Yu X, Yang L, Li Y, et al. Grand Canonical Monte Carlo simulations on phase equilibria of methane, carbon dioxide, and their mixture hydrates. J Phys Chem B 2018;122:9724–37. https://doi.org/10.1021/acs.jpcb.8b04551.

[23] Brumby PE, Yuhara D, Wu DT, Sum AK, Yasuoka K. Cage occupancy of methane hydrates from Gibbs ensemble Monte Carlo simulations. Fluid Phase Equilib 2016;413:242–8. https://doi.org/10.1016/j.fluid.2015.10.005.

[24] Radhakrishnan R, Trout BL. A new approach for studying nucleation phenomena using molecular simulations: Application to CO2 hydrate clathrates. J Chem Phys 2002;117:1786–96. https://doi.org/10.1063/1.1485962.

[25] Ferdows M, Ota M. Molecular simulation study for CO2 clathrate hydrate. Chem Eng Technol 2005;28:168–73. https://doi.org/10.1002/ceat.200407056.

[26] Taylor CE, Link DD, English N. Methane hydrate research at NETL: Research to make methane production from hydrates a reality. J Pet Sci Eng 2007;56:186–91. https://doi.org/10.1016/j.petrol.2005.08.006.

[27] Jin D, Coasne B. Molecular simulation of the phase diagram of methane hydrate: Free energy calculations, direct coexistence method, and hyperparallel tempering. Langmuir 2017;33:11217–30. https://doi.org/10.1021/acs.langmuir.7b02238.

[28] Trinh TT, Waage MH, van Erp TS, Kjelstrup S. Low barriers for hydrogen diffusion in sII clathrate. Phys Chem Chem Phys 2015;17:13808–12. https://doi.org/10.1039/C5CP01713K.

[29] Nath Chakraborty S, Gelb LD. A monte carlo simulation study of methane clathrate hydrates confined in slit-shaped pores. J Phys Chem B 2012;116:2183–97. https://doi.org/10.1021/jp205241n.

[30] Kirchner MT, Boese R, Billups WE, Norman LR. Gas hydrate single-crystal structure analyses. J Am Chem Soc 2004;126:9407–12. https://doi.org/10.1021/ja049247c.

[31] Takeuchi F, Hiratsuka M, Ohmura R, Alavi S, Sum AK, Yasuoka K. Water proton configurations in structures I, II, and H clathrate hydrate unit cells. J Chem Phys 2013;138:124504. https://doi.org/10.1063/1.4795499.

[32] Izadkhah S. Molecular insights into structural properties around the threshold of gas hydrate formation. Pet Sci Technol 2017;34:1964–71. https://doi.org/10.1080/10916466.2016.1235047.

[33] Varini N, English NJ, Trott CR. Molecular dynamics simulations of clathrate hydrates on specialised hardware platforms. Energies 2012;5:3526–33. https://doi.org/10.3390/en5093526.

[34] Tse JS, Klein ML, McDonald IR. Molecular dynamics studies of ice Ic and the structure I clathrate hydrate of methane. J Phys Chem 1983;87:4198–203. https://doi.org/10.1021/j100244a044.

[35] Rodger PM. Stability of gas hydrates. J Phys Chem 1990;94:6080–9. https://doi.org/10.1021/j100378a082.

[36] Hawtin RW, Quigley D, Rodger PM. Gas hydrate nucleation and cage formation at a water/methane interface. Phys Chem Chem Phys 2008;10:4853. https://doi.org/10.1039/b807455k.

[37] Guo G, Zhang Y, Liu C, Li K. Using the face-saturated incomplete cage analysis to quantify the cage compositions and cage linking structures of amorphous phase hydrates. Phys Chem Chem Phys 2011;13:12048. https://doi.org/10.1039/c1cp20070d.

[38] Bagherzadeh SA, Englezos P, Alavi S, Ripmeester J. Molecular simulation of non-equilibrium methane hydrate decomposition process. J Chem Thermodyn 2012;44:13–9. https://doi.org/10.1016/j.jct.2011.08.021.

[39] Conde MM, Vega C. Note: A simple correlation to locate the three phase coexistence line in methane-hydrate simulations. J Chem Phys 2013;138:14–6. https://doi.org/10.1063/1.4790647.

[40] Li Q, Liu C, Chen X. Molecular characteristics of dissociated water with memory effect from methane hydrates. Int J Mod Phys B 2014;28:1450062. https://doi.org/10.1142/S0217979214500623.

[41] Baghel VS, Kumar R, Roy S. Heat transfer calculations for decomposition of structure I methane hydrates by molecular dynamics simulation. J Phys Chem C 2013;117:12172–82. https://doi.org/10.1021/jp4023772.

[42] Baez L, Clancy P. Computer simulation of the crystal growth and dissolution of natural gas hydrates. Ann N Y Acad Sci 1994;715:177–86. https://doi.org/10.1111/j.1749-6632.1994.tb38833.x.

[43] Alavi S, Ripmeester JA. Nonequilibrium adiabatic molecular dynamics simulations of methane clathrate hydrate decomposition. J Chem Phys 2010;132:144703. https://doi.org/10.1063/1.3382341.

[44] English NJ, Macelroy JMD. Structural and dynamical properties of methane clathrate hydrates. J Comput Chem 2003;24:1569–81. https://doi.org/10.1002/jcc.10303.

[45] Li J, Wang Z. Fluctuation–dissipation analysis of nonequilibrium thermal transport at the hydrate dissociation interface. Phys Chem Chem Phys 2019;21:23492–500. https://doi.org/10.1039/C9CP04780H.

[46] Mirzaeifard S, Servio P, Rey AD. Multiscale modeling and simulation of water and methane hydrate crystal interface. Cryst Growth Des 2019;19:5142–51.

https://doi.org/10.1021/acs.cgd.9b00578.

[47] Jorgensen WL. Revised TIPS for simulations of liquid water and aqueous solutions. J Chem Phys 1982;77:4156–63. https://doi.org/10.1063/1.444325.

[48] Ning FL, Glavatskiy K, Ji Z, Kjelstrup S, H. Vlugt TJ. Compressibility, thermal expansion coefficient and heat capacity of CH4 and CO2 hydrate mixtures using molecular dynamics simulations. Phys Chem Chem Phys 2015;17:2869–83. https://doi.org/10.1039/C4CP04212C.

[49] Wang Q, Tang Q, Tian S. Molecular dynamics simulation of sI methane hydrate under compression and tension. Open Chem 2020;18:69–76. https://doi.org/10.1515/chem-2020-0008.

[50] English NJ, Macelroy JMD. Structural and dynamical properties of methane clathrate hydrates. J Comput Chem 2003;24:1569–81. https://doi.org/10.1002/jcc.10303.

[51] English NJ, MacElroy JMD. Theoretical studies of the kinetics of methane hydrate crystallization in external electromagnetic fields. J Chem Phys 2004;120:10247–56. https://doi.org/10.1063/1.1730092.

[52] Cai S, Tang Q, Tian S, Lu Y, Gao X. Molecular simulation study on the microscopic structure and mechanical property of defect-containing sI methane hydrate. Int J Mol Sci 2019;20:2305. https://doi.org/10.3390/ijms20092305.

[53] Melgar D, Ghaani MR, Lauricella M, O'Brien GS, English NJ. Acoustic-propagation properties of methane clathrate hydrates from non-equilibrium molecular dynamics. J Chem Phys 2019;151:144505. https://doi.org/10.1063/1.5121712.

[54] Li Q, Tang Q, Peng T, Zhang X, Liu C, Shi X. Molecular characteristics of H2O in hydrate/ice/liquid water mixture. Int J Mod Phys B 2015;29:1550185.

https://doi.org/10.1142/S0217979215501854.

[55] Bai D, Zhang D, Zhang X, Chen G. Origin of self-preservation effect for hydrate decomposition: Coupling of mass and heat transfer resistances. Sci Rep 2015;5:14599. https://doi.org/10.1038/srep14599.

[56] English N. Massively-parallel molecular dynamics simulation of clathrate hydrates on blue gene platforms. Energies 2013;6:3072–81. https://doi.org/10.3390/en6063072.

[57] Zhang J, Piana S, Freij-Ayoub R, Rivero M, Choi SK. Molecular dynamics study of methane in water: diffusion and structure. Mol Simul 2006;32:1279–86. https://doi.org/10.1080/08927020601039598.

[58] Vatamanu J, Kusalik PG. Unusual crystalline and polycrystalline structures in methane hydrates. J Am Chem Soc 2006;128:15588–9. https://doi.org/10.1021/ja066515t.

[59] Vatamanu J, Kusalik PG. Heterogeneous crystal growth of methane hydrate on its sII [001] Ccystallographic face. J Phys Chem B 2008;112:2399–404. https://doi.org/10.1021/jp077583k.

[60] Smirnov GS, Stegailov V V. Melting and superheating of sI methane hydrate: Molecular dynamics study. J Chem Phys 2012;136:44523. https://doi.org/10.1063/1.3679860.

[61] Docherty H, Galindo A, Vega C, Sanz E. A potential model for methane in water describing correctly the solubility of the gas and the properties of the methane hydrate. J Chem Phys 2006;125:74510. https://doi.org/10.1063/1.2335450.

[62] Guo G-J, Rodger PM. Solubility of aqueous methane under metastable conditions: Implications for gas hydrate nucleation. J Phys Chem B 2013;117:6498–504. https://doi.org/10.1021/jp3117215.

[63] Yagasaki T, Matsumoto M, Andoh Y, Okazaki S, Tanaka H. Effect of bubble formation on the dissociation of methane hydrate in water: A molecular dynamics study. J Phys Chem B 2014;118:1900–6. https://doi.org/10.1021/jp412692d.

[64] Liang S, Yi L, Liang D. Molecular insights into the homogeneous melting of methane hydrates. J Phys Chem C 2014;118:28542–7. https://doi.org/10.1021/jp511362s.

[65] Nguyen NN, Nguyen A V, Steel KM, Dang LX, Galib M. Interfacial gas enrichment at hydrophobic surfaces and the origin of promotion of gas hydrate formation by hydrophobic solid particles. J Phys Chem C 2017;121:3830–40. https://doi.org/10.1021/acs.jpcc.6b07136.

[66] Walsh M, Beckham G, Koh C, Sloan ED, Wu D, Sum A. Methane hydrate nucleation rates from molecular dynamics simulations: Effects of aqueous methane concentration, interfacial curvature, and system size. J Phys Chem C 2011;115:21241–8. https://doi.org/10.1021/jp206483q.

[67] Barnes BC, Knott BC, Beckham GT, Wu DT, Sum AK. Reaction coordinate of incipient methane clathrate hydrate nucleation. J Phys Chem B 2014;118:13236–43. https://doi.org/10.1021/jp507959q.

[68] Jiménez-Ángeles F, Firoozabadi A. Nucleation of methane hydrates at moderate subcooling by molecular dynamics simulations. J Phys Chem C 2014;118:11310–8. https://doi.org/10.1021/jp5002012.

[69] Jiménez-Ángeles F, Firoozabadi A. Induced charge density and thin liquid film at hydrate/methane gas interfaces. J Phys Chem C 2014;118:26041–8. https://doi.org/10.1021/jp507160s.

[70] Yuhara D, Barnes BC, Suh D, Knott BC, Beckham GT, Yasuoka K, et al. Nucleation rate analysis of methane hydrate from molecular dynamics simulations. Faraday Discuss 2015;179:463–74. https://doi.org/10.1039/C4FD00219A.

[71] Xu T, Lang X, Fan S, Wang Y, Chen J. The effect of electric fields in methane hydrate growth and dissociation: A molecular dynamics simulation. Comput Theor Chem 2019;1149:57–68. https://doi.org/10.1016/j.comptc.2018.12.018.

[72] Bagherzadeh SA, Alavi S, Ripmeester J, Englezos P. Formation of methane nano-bubbles during hydrate decomposition and their effect on hydrate growth. J Chem Phys 2015;142:214701. https://doi.org/10.1063/1.4920971.

[73] Wu J, Ning F, Trinh TT, Kjelstrup S, Vlugt TJH, He J, et al. Mechanical instability of monocrystalline and polycrystalline methane hydrates. Nat Commun 2015;6:8743. https://doi.org/10.1038/ncomms9743.

[74] Chakraborty SN, English NJ. Hydrogen-bond vibrational and energetic dynamical properties in sI and sII clathrate hydrates and in ice Ih: Molecular dynamics insights. J Chem Phys 2015;143:154504. https://doi.org/10.1063/1.4932681.

[75] Yuhara D, Brumby PE, Wu DT, Sum AK, Yasuoka K. Analysis of three-phase equilibrium conditions for methane hydrate by isometric-isothermal molecular dynamics simulations. J Chem Phys 2018;148:184501. https://doi.org/10.1063/1.5016609.

[76] Luis DP, Herrera-Hernández EC, Saint-Martin H. A theoretical study of the dissociation of the sI methane hydrate induced by an external electric field. J Chem Phys 2015;143:204503. https://doi.org/10.1063/1.4936214.

[77] Walsh MR, Koh CA, Sloan ED, Sum AK, Wu DT. Microsecond simulations of spontaneous methane hydrate nucleation and growth. Science (80-) 2009;326:1095–8. https://doi.org/10.1126/science.1174010.

[78] Walsh MR, Rainey JD, Lafond PG, Park D-H, Beckham GT, Jones MD, et al. The cages, dynamics, and structuring of incipient methane clathrate hydrates. Phys Chem Chem Phys 2011;13:19951. https://doi.org/10.1039/c1cp21899a.

[79] English NJ, Johnson JK, Taylor CE. Molecular-dynamics simulations of methane hydrate dissociation. J Chem Phys 2005;123:244503. https://doi.org/10.1063/1.2138697.

[80] Rosenbaum EJ, English NJ, Johnson JK, Shaw DW, Warzinski RP. Thermal conductivity of methane hydrate from experiment and molecular simulation. J Phys Chem B 2007;111:13194–205. https://doi.org/10.1021/jp074419o.

[81] Cendagorta JR, Powers A, Hele TJH, Marsalek O, Bačić Z, Tuckerman ME. Competing quantum effects in the free energy profiles and diffusion rates of hydrogen and deuterium molecules through clathrate hydrates. Phys Chem Chem Phys 2016;18:32169–77. https://doi.org/10.1039/C6CP05968F.

[82] Ding LY, Geng CY, Zhao YH, Wen H. Molecular dynamics simulation on the dissociation process of methane hydrates. Mol Simul 2007;33:1005–16. https://doi.org/10.1080/08927020701528524.

[83] Chialvo AA, Houssa M, Cummings PT. Molecular dynamics study of the structure and thermophysical properties of model sI clathrate hydrates. J Phys Chem B 2002;106:442–51. https://doi.org/10.1021/jp012735b.

[84] Jiang H, Jordan KD, Taylor CE. Molecular dynamics simulations of methane hydrate using polarizable force fields. J Phys Chem B 2007;111:6486–92. https://doi.org/10.1021/jp068505k.

[85] Costandy J, Michalis VK, Tsimpanogiannis IN, Stubos AK, Economou IG. Molecular dynamics simulations of pure methane and carbon dioxide hydrates: lattice constants and derivative properties. Mol Phys 2016;114:2672–87. https://doi.org/10.1080/00268976.2016.1241442.

[86] Jiang H, Myshakin EM, Jordan KD, Warzinski RP. Molecular dynamics simulations of the thermal conductivity of methane hydrate. J Phys Chem B 2008;112:10207–16. https://doi.org/10.1021/jp802942v.

[87] Molinero V, Moore EB. Water modeled as an intermediate element between carbon and silicon. J Phys Chem B 2009;113:4008–16. https://doi.org/10.1021/jp805227c.

[88] Lauricella M, Ciccotti G, English NJ, Peters B, Meloni S. Mechanisms and nucleation rate of methane hydrate by dynamical nonequilibrium molecular dynamics. J Phys Chem C 2017;121:24223–34. https://doi.org/10.1021/acs.jpcc.7b05754.

[89] Cao P, Wu J, Zhang Z, Fang B, Ning F. Mechanical properties of methane hydrate: Intrinsic differences from ice. J Phys Chem C 2018;122:29081–93. https://doi.org/10.1021/acs.jpcc.8b06002.

[90] Bi Y, Li T. Probing methane hydrate nucleation through the forward flux sampling method. J Phys Chem B 2014;118:13324–32. https://doi.org/10.1021/jp503000u.

[91] Sveinsson HA, Malthe-Sørenssen A. Molecular-scale thermally activated fractures in methane hydrates: a molecular dynamics study. Phys Chem Chem Phys 2019;21:13539–44. https://doi.org/10.1039/C9CP01337G.

[92] Knott BC, Molinero V, Doherty MF, Peters B. Homogeneous nucleation of methane hydrates: Unrealistic under realistic conditions. J Am Chem Soc 2012;134:19544–7. https://doi.org/10.1021/ja309117d.

[93] Nguyen AH, Jacobson LC, Molinero V. Structure of the clathrate/solution interface and mechanism of cross-nucleation of clathrate hydrates. J Phys Chem C 2012;116:19828–38. https://doi.org/10.1021/jp305468s.

[94] English NJ, Lauricella M, Meloni S. Massively parallel molecular dynamics simulation of formation of clathrate-hydrate precursors at planar water-methane interfaces: Insights into heterogeneous nucleation. J Chem Phys 2014;140:204714. https://doi.org/10.1063/1.4879777.

[95] Bi Y, Porras A, Li T. Free energy landscape and molecular pathways of gas hydrate nucleation. J Chem Phys 2016;145:211909. https://doi.org/10.1063/1.4961241.

[96] Lauricella M, Meloni S, English NJ, Peters B, Ciccotti G. Methane clathrate hydrate nucleation mechanism by advanced molecular simulations. J Phys Chem C 2014;118:22847–57. https://doi.org/10.1021/jp5052479.

[97] Chihaia V, Adams S, Kuhs WF. Molecular dynamics simulations of properties of a (001) methane clathrate hydrate surface. Chem Phys 2005;317:208–25. https://doi.org/10.1016/j.chemphys.2005.05.024.

[98] Zhang J, Pan Z. Effect of potential energy on the formation of methane hydrate. J Pet Sci Eng 2011;76:148–54. https://doi.org/10.1016/j.petrol.2011.01.004.

[99] Waldron CJ, Lauricella M, English NJ. Structural and dynamical properties of methane clathrate hydrates from molecular dynamics: Comparison of atomistic and more coarse-grained potential

models. Fluid Phase Equilib 2016;413:235–41. https://doi.org/10.1016/j.fluid.2015.12.030.

[100] Jacobson LC, Molinero V. A methane−water model for coarse-grained simulations of solutions and clathrate hydrates. J Phys Chem B 2010;114:7302–11. https://doi.org/10.1021/jp1013576.

[101] Burnham CJ, English NJ. Study of clathrate hydrates via equilibrium molecular-dynamics simulation employing polarisable and non-polarisable, rigid and flexible water models. J Chem Phys 2016;144:164503. https://doi.org/10.1063/1.4947039.

[102] Plattner N, Bandi T, Doll JD, Freeman DL, Meuwly M. MD simulations using distributed multipole electrostatics: Structural and spectroscopic properties of CO and methane containing clathrates. Mol Phys 2008;106:1675–84. https://doi.org/10.1080/00268970802314394.

[103] Míguez JM, Conde MM, Torré J, Blas FJ, Piñeiro MM, Vega C. Molecular dynamics simulation of CO2 hydrates : Prediction of three phase coexistence line Molecular dynamics simulation of CO 2 hydrates : Prediction of three phase coexistence line 2015;124505. https://doi.org/10.1063/1.4916119.

[104] Alavi S, Ripmeester JA, Klug DD. Molecular dynamics study of the stability of methane structure H clathrate hydrates Molecular dynamics study of the stability of methane structure H clathrate hydrates 2007;124708. https://doi.org/10.1063/1.2710261.

[105] Jiao L, Wang Z, Li J, Zhao P, Wan R. Stability and dissociation studies of CO2 hydrate under different systems using molecular dynamic simulations. J Mol Liq 2021;338:116788. https://doi.org/10.1016/j.molliq.2021.116788.

[106] Mohammadi-Manesh H, Ghafari H, Alavi S. Molecular dynamics study of guest–host hydrogen bonding in ethylene oxide, trimethylene oxide, and formaldehyde structure I clathrate hydrates. J

Phys Chem C 2017;121:8832–40. https://doi.org/10.1021/acs.jpcc.7b00218.

[107] Iwai Y, Nakamura H, Arai Y, Shimoyama Y. Analysis of dissociation process for gas hydrates by molecular dynamics simulation. Mol Simul 2010;36:246–53. https://doi.org/10.1080/08927020903307529.

[108] Michalis VK, Costandy J, Tsimpanogiannis IN, Stubos AK, Economou IG. Prediction of the phase equilibria of methane hydrates using the direct phase coexistence methodology. J Chem Phys 2015;142:44501. https://doi.org/10.1063/1.4905572.

[109] Veesam SK, Punnathanam SN. Computation of the dissociation temperature of TBAB semiclathrate in an aqueous solution using molecular simulations. J Phys Chem B 2020;124:9195–203. https://doi.org/10.1021/acs.jpcb.0c05238.

[110] Udachin K, Alavi S, Ripmeester JA. Communication: Single crystal x-ray diffraction observation of hydrogen bonding between 1-propanol and water in a structure II clathrate hydrate. J Chem Phys 2011;134:65–8. https://doi.org/10.1063/1.3574393.

[111] Wilson DT, Barnes BC, Wu DT, Sum AK. Molecular dynamics simulations of the formation of ethane clathrate hydrates. Fluid Phase Equilib 2016;413:229–34. https://doi.org/10.1016/j.fluid.2015.12.001.

[112] Sarupria S, Debenedetti PG. Molecular dynamics study of carbon dioxide hydrate dissociation. J Phys Chem A 2011;115:6102–11. https://doi.org/10.1021/jp110868t.

[113] Li J, Liang Z, Wang Z, Bao W. Molecular dynamics simulation of decomposition of methane hydrate and interfacial characteristics in nanostructure region. Int J Thermophys 2020;41:13. https://doi.org/10.1007/s10765-019-2591-4.

[114] Tung Y, Chen L-J, Chen Y, Lin S. Growth of structure I carbon dioxide hydrate from molecular dynamics simulations. J Phys Chem C 2011;115:7504–15. https://doi.org/10.1021/jp112205x.

[115] Smirnov G, Stegailov V. Anomalous diffusion of guest molecules in hydrogen gas hydrates. High Temp 2015;53:829–36. https://doi.org/10.1134/S0018151X15060188.

[116] Smirnov GS, Stegailov V V. Toward determination of the new hydrogen hydrate clathrate structures. J Phys Chem Lett 2013;4:3560–4. https://doi.org/10.1021/jz401669d.

[117] Zhang Z, Liu C-JJ, Walsh MR, Guo G-JJ. Effects of ensembles on methane hydrate nucleation kinetics. Phys Chem Chem Phys 2016;18:15602–8. https://doi.org/10.1039/C6CP02171A.

[118] Sizova A, Sizov V, Brodskaya E. Molecular dynamics simulation of the stability of spherical nanoclusters of methane and carbon dioxide hydrates. Colloid J 2020;82:180–7. https://doi.org/10.1134/S1061933X2002012X.

[119] Bai D, Zhang X, Chen G, Wang W. Replacement mechanism of methane hydrate with carbon dioxide from microsecond molecular dynamics simulations. Energy Environ Sci 2012;5:7033. https://doi.org/10.1039/c2ee21189k.

[120] Iwai Y, Nakamura H, Hirata M. Molecular dynamics simulation of replacement of methane hydrate with carbon dioxide. Mol Simul 2012;38:481–90. https://doi.org/10.1080/08927022.2011.647817.

[121] Xu C-G, Cai J, Yu Y-S, Chen Z-Y, Li X-S. Research on micro-mechanism and efficiency of CH4 exploitation via CH4-CO2 replacement from natural gas hydrates. Fuel 2018;216:255–65. https://doi.org/10.1016/j.fuel.2017.12.022.

[122] Klapproth A, Piltz RO, Kennedy SJ, Kozielski KA. Kinetics of sII and mixed sI/sII, gas hydrate

growth for a methane/propane mixture using neutron diffraction. J Phys Chem C 2019;123:2703–15. https://doi.org/10.1021/acs.jpcc.8b06693.

[123] Yang Y, Narayanan Nair AK, Sun S. Molecular dynamics simulation study of carbon dioxide, methane, and their mixture in the presence of brine. J Phys Chem B 2017;121:9688–98. https://doi.org/10.1021/acs.jpcb.7b08118.

[124] Zhang Z, Guo G-J, Wu N, Kusalik PG. Molecular insights into guest and composition dependence of mixed hydrate nucleation. J Phys Chem C 2020;124:25078–86. https://doi.org/10.1021/acs.jpcc.0c07375.

[125] Hall KW, Carpendale S, Kusalik PG. Evidence from mixed hydrate nucleation for a funnel model of crystallization. Proc Natl Acad Sci 2016;113:12041–6. https://doi.org/10.1073/pnas.1610437113.

[126] Buch V, Devlin JP, Monreal IA, Jagoda-Cwiklik B, Uras-Aytemiz N, Cwiklik L. Clathrate hydrates with hydrogen-bonding guests. Phys Chem Chem Phys 2009;11:10245. https://doi.org/10.1039/b911600c.

[127] Chapoy A, Anderson R, Tohidi B. Low-Pressure Molecular Hydrogen Storage in Semi-clathrate Hydrates of Quaternary Ammonium Compounds. J Am Chem Soc 2007;129:746–7. https://doi.org/10.1021/ja066883x.

[128] Strobel TA, Hester KC, Koh CA, Sum AK, Sloan ED. Properties of the clathrates of hydrogen and developments in their applicability for hydrogen storage. Chem Phys Lett 2009;478:97–109. https://doi.org/10.1016/j.cplett.2009.07.030.

[129] Lee BR, Sa J-H, Hong SY, Lee JD, Lee K-H, Seo Y, et al. Guest–Guest interactions and co-

occupation by distinct guests in the metastable state of clathrate hydrates. J Phys Chem C 2019;123:3811–6. https://doi.org/10.1021/acs.jpcc.8b08629.

[130] Sinehbaghizadeh S, Saptoro A, Amjad-Iranagh S, Tze Tiong AN, Mohammadi AH. Molecular dynamics simulation studies on the stability and dissociation of clathrate hydrates of single and double greenhouse gases. Energy & Fuels 2022;36:8323–39. https://doi.org/10.1021/acs.energyfuels.2c01396.

[131] Hasegawa T, Brumby PE, Yasuoka K, Sum AK. Mechanism for H2 diffusion in sII hydrates by molecular dynamics simulations. J Chem Phys 2020;153:054706. https://doi.org/10.1063/5.0017505.

[132] Tian H, Zhang Z. Revealing the growth of H2 + THF binary hydrate through molecular simulations. Energy & Fuels 2020;34:15004–10. https://doi.org/10.1021/acs.energyfuels.0c03096.

[133] Castillo-Borja F, Bravo-Sánchez UI, Vázquez-Román R, Díaz-Ovalle CO. Biogas purification via sII hydrates in the presence of THF and DMSO solutions using MD simulations. J Mol Liq 2020;297:111904. https://doi.org/10.1016/j.molliq.2019.111904.

[134] Torré J-P, Ricaurte M, Dicharry C, Broseta D. CO2 enclathration in the presence of water-soluble hydrate promoters: Hydrate phase equilibria and kinetic studies in quiescent conditions. Chem Eng Sci 2012;82:1–13. https://doi.org/10.1016/j.ces.2012.07.025.

[135] Albertí M, Pirani F, Laganaì A. Carbon dioxide clathrate hydrates: Selective role of intermolecular interactions and action of the SDS catalyst. J Phys Chem A 2013;117:6991–7000. https://doi.org/10.1021/jp3126158.

[136] Zhang L, Sun L, Lu Y, Kuang Y, Ling Z, Yang L, et al. Molecular dynamics simulation and in-situ MRI observation of organic exclusion during CO2 hydrate growth. Chem Phys Lett 2021;764:138287. https://doi.org/10.1016/j.cplett.2020.138287.

[137] Lim LH V, Lloren AV, Lamorena RB. The effect of urea in the nucleation process of CO2 clathrate hydrates. J Mol Liq 2014;194:245–50. https://doi.org/10.1016/j.molliq.2014.03.003.

[138] Wang P-W, Wu DT, Lin S-T. Promotion mechanism for the growth of CO2 hydrate with urea using molecular dynamics simulations. Chem Commun 2021. https://doi.org/10.1039/D0CC06165D.

[139] Sinehbaghizadeh S, Saptoro A, Naeiji P, Tiong ANT, Mohammadi AH. Insights into the synergistic effects of metal particles (Ag, Cu, and Fe) and urea on CO2 clathrate hydrate growth using molecular dynamics simulations. Chem Eng Sci 2022;264:118194. https://doi.org/10.1016/j.ces.2022.118194.

[140] Hande V, Choudhary N, Chakrabarty S, Kumar R. Morphology and dynamics of self-assembled structures in mixed surfactant systems (SDS + CAPB) in the context of methane hydrate growth. J Mol Liq 2020;319:114296. https://doi.org/10.1016/j.molliq.2020.114296.

[141] Wang L, Jiang G, Zhang X. Modeling and molecular simulation of natural gas hydrate stabilizers. Eur J Remote Sens 2020:1–12. https://doi.org/10.1080/22797254.2020.1738901.

[142] Ghaani MR, Allen C, Skvortsov T, English NJ. Engineering peptides to catalyze and control stabilization of gas hydrates: Learning from nature. J Phys Chem Lett 2020;11:5068–75. https://doi.org/10.1021/acs.jpclett.0c01224.

[143] Liu N, Zhu H, Zhou J, Yang L, Liu D. Molecular dynamics simulations on formation of CO2

hydrate in the presence of metal particles. J Mol Liq 2021;331:115793. https://doi.org/10.1016/j.molliq.2021.115793.

[144] Kuznetsova T, Jensen B, Kvamme B, Sjøblom S. Water-wetting surfaces as hydrate promoters during transport of carbon dioxide with impurities. Phys Chem Chem Phys 2015;17:12683–97. https://doi.org/10.1039/C5CP00660K.

[145] Sinehbaghizadeh S, Javanmardi J, Mohammadi AH. Phase stability conditions of clathrate hydrates in the (methane + 3-methyl-1-butanol + water), (methane + 3,3-dimethyl-2-butanone + water) and (methane + 2,3-dimethyl-2-butene + water) systems: Experimental measurements and thermodynamic modeling. J Chem Thermodyn 2018;125:64–70. https://doi.org/10.1016/j.jct.2018.05.006.

[146] Sinehbaghizadeh S, Javanmardi J, Roosta A, Mohammadi AH. A fugacity approach for prediction of phase equilibria of methane clathrate hydrate in structure H. Phys Chem Res 2017;5:465–81. https://doi.org/10.22036/pcr.2017.69958.1334.

[147] Sinehbaghizadeh S, Roosta A, Rezaei N, Ghiasi MM, Javanmardi J, Zendehboudi S. Evaluation of phase equilibrium conditions of clathrate hydrates using connectionist modeling strategies. Fuel 2019;255:115649. https://doi.org/10.1016/j.fuel.2019.115649.

[148] Sinehbaghizadeh S, Javanmardi J, Roosta A, Mohammadi AH. Estimation of the dissociation conditions and storage capacities of various sH clathrate hydrate systems using effective deterministic frameworks. Fuel 2019;247:272–86. https://doi.org/10.1016/j.fuel.2019.01.189.

[149] Jokar SM, Wood DA, Sinehbaghizadeh S, Parvasi P, Javanmardi J. Transformation of associated natural gas into valuable products to avoid gas wastage in the form of flaring. J Nat Gas Sci Eng 2021:104078. https://doi.org/10.1016/j.jngse.2021.104078.

[150] Liu J, Yan YY, Chen G, Hou J, Yan YY, Liu H, et al. Prediction of efficient promoter molecules of sH hydrogen hydrate: An ab initio study. Chem Phys 2019;516:15–21. https://doi.org/10.1016/j.chemphys.2018.08.032.

[151] Zhang Z, Kusalik PG, Guo G-J. Might a 2,2-Dimethylbutane Molecule Serve as a Site to Promote Gas Hydrate Nucleation? J Phys Chem C 2019;123:20579–86. https://doi.org/10.1021/acs.jpcc.9b04518.

[152] Murayama K, Takeya S, Alavi S, Ohmura R. Anisotropic lattice expansion of structure H clathrate hydrates induced by help guest: Experiments and molecular dynamics simulations. J Phys Chem C 2014;118:21323–30. https://doi.org/10.1021/jp5058786.

[153] Tezuka K, Murayama K, Takeya S, Alavi S, Ohmura R. Effect of guest size and conformation on crystal structure and stability of structure H clathrate hydrates: Experimental and molecular dynamics simulation studies. J Phys Chem C 2013;117:10473–82. https://doi.org/10.1021/jp4005899.

[154] Imasato K, Murayama K, Takeya S, Alavi S, Ohmura R. Effect of nitrogen atom substitution in cyclic guests on properties of structure H clathrate hydrates. Can J Chem 2015;93:906–12. https://doi.org/10.1139/cjc-2014-0553.

[155] Huo H, Liu Y, Zheng Z, Zhao J, Jin C, Lv T. Mechanical and thermal properties of methane clathrate hydrates as an alternative energy resource. J Renew Sustain Energy 2011;3:63110. https://doi.org/10.1063/1.3670410.

[156] Daghash SM, Servio P, Rey AD. Elastic properties and anisotropic behavior of structure-H (sH) gas hydrate from first principles. Chem Eng Sci 2020;227:115948. https://doi.org/10.1016/j.ces.2020.115948.

[157] Jendi ZM, Rey AD, Servio P. Ab initio DFT study of structural and mechanical properties of methane and carbon dioxide hydrates. Mol Simul 2015;41:572–9. https://doi.org/10.1080/08927022.2014.899698.

[158] Vlasic TM, Servio PD, Rey AD. Effect of guest size on the mechanical properties and molecular structure of gas hydrates from first-principles. Cryst Growth Des 2017;17:6407–16. https://doi.org/10.1021/acs.cgd.7b01072.

[159] Erfan-Niya H, Modarress H. Molecular dynamics simulation of structure H clathrate-hydrates of binary guest molecules. J Nat Gas Chem 2011;20:577–84. https://doi.org/10.1016/S1003-9953(10)60242-3.

[160] Reshadi P, Modarress H, Dabir B, Amjad-iranagh S. Molecular dynamics simulation for studying the stability of structure H clathrate-hydrates of argon and large guest molecules. J Dispers Sci Technol 2018;0:1–10. https://doi.org/10.1080/01932691.2018.1446145.

[161] Daghash SM, Servio P, Rey AD. Structural properties of sH hydrate: a DFT study of anisotropy and equation of state. Mol Simul 2019;45:1524–37. https://doi.org/10.1080/08927022.2019.1660326.

[162] Okano Y, Yasuoka K. Free-energy calculation of structure-H hydrates. J Chem Phys 2006;124:24510. https://doi.org/10.1063/1.2150430.

[163] Tanaka H, Kiyohara K. The thermodynamic stability of clathrate hydrate. II. Simultaneous occupation of larger and smaller cages. J Chem Phys 1993;98:8110–8. https://doi.org/10.1063/1.464567.

[164] Kelland MA. History of the development of low dosage hydrate inhibitors. Energy & Fuels

2006;20:825–47. https://doi.org/10.1021/ef050427x.

[165] Gao S. Hydrate risk management at high watercuts with anti-agglomerant hydrate inhibitors. Energy & Fuels 2009;23:2118–21. https://doi.org/10.1021/ef8009876.

[166] Mehrabian H, Bellucci MA, Walsh MR, Trout BL. Effect of salt on antiagglomerant surface adsorption in natural gas hydrates. J Phys Chem C 2018;122:12839–49. https://doi.org/10.1021/acs.jpcc.8b03154.

[167] Naullage PM, Bertolazzo AA, Molinero V. How do surfactants control the agglomeration of clathrate hydrates? ACS Cent Sci 2019;5:428–39. https://doi.org/10.1021/acscentsci.8b00755.

[168] Zi M, Chen D, Wu G. Molecular dynamics simulation of methane hydrate formation on metal surface with oil. Chem Eng Sci 2018;191:253–61. https://doi.org/10.1016/j.ces.2018.06.070.

[169] Yagasaki T, Matsumoto M, Tanaka H. Effects of thermodynamic inhibitors on the dissociation of methane hydrate: a molecular dynamics study. Phys Chem Chem Phys 2015;17:32347–57. https://doi.org/10.1039/C5CP03008K.

[170] Storr MT, Taylor PC, Monfort J-P, Rodger PM. Kinetic inhibitor of hydrate crystallization. J Am Chem Soc 2004;126:1569–76. https://doi.org/10.1021/ja035243g.

[171] Gómez Gualdrón DA, Balbuena PB. Classical molecular dynamics of clathrate−methane−water kinetic inhibitor composite systems. J Phys Chem C 2007;111:15554–64. https://doi.org/10.1021/jp071959c.

[172] Kvamme B, Selvåg J, Saeidi N, Kuznetsova T. Methanol as a hydrate inhibitor and hydrate activator. Phys Chem Chem Phys 2018;20:21968–87. https://doi.org/10.1039/C8CP02447B.

[173] Bagherzadeh A, Alavi S, Ripmeester JA, Englezos P. Why ice-binding type I antifreeze protein

acts as a gas hydrate crystal inhibitor. Phys Chem Chem Phys 2015;17:9984–90. https://doi.org/10.1039/C4CP05003G.

[174] Maddah M, Maddah M, Peyvandi K. Investigation on structural properties of winter flounder antifreeze protein in interaction with clathrate hydrate by molecular dynamics simulation. J Chem Thermodyn 2021;152:106267. https://doi.org/10.1016/j.jct.2020.106267.

[175] Maddah M, Maddah M, Peyvandi K. The influence of a type III antifreeze protein and its mutants on methane hydrate adsorption–inhibition: a molecular dynamics simulation study. Phys Chem Chem Phys 2019;21:21836–46. https://doi.org/10.1039/C9CP03833G.

[176] Anderson BJ, Tester JW, Borghi GP, Trout BL. Properties of inhibitors of methane hydrate formation via molecular dynamics simulations. J Am Chem Soc 2005;127:17852–62. https://doi.org/10.1021/ja0554965.

[177] Yagasaki T, Matsumoto M, Tanaka H. Adsorption of kinetic hydrate inhibitors on growing surfaces: A molecular dynamics study. J Phys Chem B 2018;122:3396–406. https://doi.org/10.1021/acs.jpcb.7b10356.

[178] Maddah M, Maddah M, Peyvandi K. Molecular dynamics simulation of methane hydrate formation in presence and absence of amino acid inhibitors. J Mol Liq 2018;269:721–32. https://doi.org/10.1016/j.molliq.2018.08.108.

[179] Oluwunmi PA, Finney AR, Rodger PM. Molecular dynamics screening for new kinetic inhibitors of methane hydrate. Can J Chem 2015;93:1043–9. https://doi.org/10.1139/cjc-2015-0003.

[180] Moon C, Hawtin RW, Rodger PM. Nucleation and control of clathrate hydrates: insights from

simulation. Faraday Discuss 2007;136:367. https://doi.org/10.1039/b618194p.

[181] Zhang J, Hawtin RW, Yang Y, Nakagava E, Rivero M, Choi SK, et al. Molecular dynamics study of methane hydrate formation at a water/methane interface. J Phys Chem B 2008;112:10608–18. https://doi.org/10.1021/jp076904p.

[182] Kvamme B, Kuznetsova T, Aasoldsen K. Molecular dynamics simulations for selection of kinetic hydrate inhibitors. J Mol Graph Model 2005;23:524–36. https://doi.org/10.1016/j.jmgm.2005.04.001.

[183] Xu J, Li L, Liu J, Wang X, Yan Y, Zhang J. The molecular mechanism of the inhibition effects of PVCaps on the growth of sI hydrate: an unstable adsorption mechanism. Phys Chem Chem Phys 2018;20:8326–32. https://doi.org/10.1039/C8CP00010G.

[184] Yagasaki T, Matsumoto M, Tanaka H. Adsorption mechanism of inhibitor and guest molecules on the surface of gas hydrates. J Am Chem Soc 2015;137:12079–85. https://doi.org/10.1021/jacs.5b07417.

[185] Li S, Lv R, Wu Y, Huang F, Zhang X, Yue T. Size, aggregation, and oxidization-dependent perturbation of methane hydrate by graphene nanosheets revealed by molecular dynamics simulations. J Phys Chem C 2019:acs.jpcc.9b02659. https://doi.org/10.1021/acs.jpcc.9b02659.

[186] Yeon S-H, Seol J, Koh D-Y, Seo Y, Park K-P, Huh D-G, et al. Abnormal methane occupancy of natural gas hydrates in deep sea floor sediments. Energy Environ Sci 2011;4:421–4. https://doi.org/10.1039/C0EE00355G.

[187] Seo Y, Seol J, Yeon S-H, Koh D-Y, Cha M, Kang S-P, et al. Structural, mineralogical, and rheological properties of methane hydrates in smectite clays. J Chem Eng Data 2009;54:1284–

91. https://doi.org/10.1021/je800833y.

[188] Myshakin EM, Saidi WA, Romanov VN, Cygan RT, Jordan KD. Molecular dynamics simulations of carbon dioxide intercalation in hydrated Na-montmorillonite. J Phys Chem C 2013;117:11028–39. https://doi.org/10.1021/jp312589s.

[189] Yan L, Chen G, Pang W, Liu J. Experimental and modeling study on hydrate formation in wet activated carbon. J Phys Chem B 2005;109:6025–30. https://doi.org/10.1021/jp045679y.

[190] Kim D, Ahn Y-H, Kim S-J, Lee JY, Lee J, Seo Y, et al. Gas hydrate in crystalline-swelled clay: The effect of pore dimension on hydrate formation and phase equilibria. J Phys Chem C 2015;119:22148–53. https://doi.org/10.1021/acs.jpcc.5b03229.

[191] Kim D, Lee H. Phase behavior of gas hydrates in nanoporous materials: Review. Korean J Chem Eng 2016;33:1977–88. https://doi.org/10.1007/s11814-016-0064-z.

[192] Cuadrado-Collados C, Fauth F, Such-Basañez I, Martínez-Escandell M, Silvestre-Albero J. Methane hydrate formation in the confined nanospace of activated carbons in seawater environment. Microporous Mesoporous Mater 2018;255:220–5. https://doi.org/10.1016/j.micromeso.2017.07.047.

[193] Borchardt L, Nickel W, Casco M, Senkovska I, Bon V, Wallacher D, et al. Illuminating solid gas storage in confined spaces – methane hydrate formation in porous model carbons. Phys Chem Chem Phys 2016;18:20607–14. https://doi.org/10.1039/C6CP03993F.

[194] Casco ME, Jordá JL, Rey F, Fauth F, Martinez-Escandell M, Rodríguez-Reinoso F, et al. High-performance of gas hydrates in confined nanospace for reversible CH4 /CO2 storage. Chem - A Eur J 2016;22:10028–35. https://doi.org/10.1002/chem.201600958.

[195] Casco ME, Silvestre-Albero J, Ramírez-Cuesta AJ, Rey F, Jordá JL, Bansode A, et al. Methane hydrate formation in confined nanospace can surpass nature. Nat Commun 2015;6:6432. https://doi.org/10.1038/ncomms7432.

[196] Yu K Bin, Yazaydin AO. Does confinement enable methane hydrate growth at low pressures? Insights from molecular dynamics simulations. J Phys Chem C 2020;124:11015–22. https://doi.org/10.1021/acs.jpcc.0c02246.

[197] Cox SJ, Taylor DJF, Youngs TGA, Soper AK, Totton TS, Chapman RG, et al. Formation of methane hydrate in the presence of natural and synthetic nanoparticles. J Am Chem Soc 2018;140:3277–84. https://doi.org/10.1021/jacs.7b12050.

[198] Park T, Kyung D, Lee W. Effect of organic matter on CO2 hydrate phase equilibrium in phyllosilicate suspensions. Environ Sci Technol 2014;48:6597–603. https://doi.org/10.1021/es405099z.

[199] Cygan RT, Guggenheim S, Koster van Groos AF. Molecular models for the intercalation of methane hydrate complexes in montmorillonite clay. J Phys Chem B 2004;108:15141–9. https://doi.org/10.1021/jp037900x.

[200] Kadoura A, Narayanan Nair AK, Sun S. Molecular dynamics simulations of carbon dioxide, methane, and their mixture in montmorillonite clay hydrates. J Phys Chem C 2016;120:12517–29. https://doi.org/10.1021/acs.jpcc.6b02748.

[201] Bagherzadeh SA, Englezos P, Alavi S, Ripmeester JA. Influence of hydrated silica surfaces on interfacial water in the presence of clathrate hydrate forming gases. J Phys Chem C 2012;116:24907–15. https://doi.org/10.1021/jp305529d.

[202] Cai T, Johnson JK, Wu Y, Chen X. Toward understanding the kinetics of CO2 capture on sodium carbonate. ACS Appl Mater Interfaces 2019;11:9033–41. https://doi.org/10.1021/acsami.8b20000.

[203] Hou D, Zhang Q, Xu X, Zhang J, Li W, Wang P. Insights on ions migration in the nanometer channel of calcium silicate hydrate under external electric field. Electrochim Acta 2019;320:134637. https://doi.org/10.1016/j.electacta.2019.134637.

[204] Tzirakis F, Stringari P, von Solms N, Coquelet C, Kontogeorgis G. Hydrate equilibrium data for the CO2 + N2 system with the use of tetra-n-butylammonium bromide (TBAB), cyclopentane (CP) and their mixture. Fluid Phase Equilib 2016;408:240–7. https://doi.org/10.1016/j.fluid.2015.09.021.

[205] Sun Q, Guo X, Liu A, Liu B, Huo Y, Chen G. Experimental Study on the Separation of CH4 and N2 via Hydrate Formation in TBAB Solution. Ind Eng Chem Res 2011;50:2284–8. https://doi.org/10.1021/ie101726f.

[206] Liao Z, Guo X, Zhao Y, Wang Y, Sun Q, Liu A, et al. Experimental and modeling study on phase equilibria of semiclathrate hydrates of Tetra-n-butyl Ammonium Bromide + CH4 , CO2, N2 , or gas mixtures. Ind Eng Chem Res 2013;52:18440–6. https://doi.org/10.1021/ie402903m.

[207] Muromachi S, Hashimoto H, Maekawa T, Takeya S, Yamamoto Y. Phase equilibrium and characterization of ionic clathrate hydrates formed with tetra- n -butylammonium bromide and nitrogen gas. Fluid Phase Equilib 2016;413:249–53. https://doi.org/10.1016/j.fluid.2015.09.002.

[208] Muromachi S, Udachin KA, Alavi S, Ohmura R, Ripmeester JA. Selective occupancy of methane by cage symmetry in TBAB ionic clathrate hydrate. Chem Commun 2016;52:5621–4. https://doi.org/10.1039/C6CC00264A.

[209] Muromachi S, Udachin A, Shin K, Alavi S MI, Ohmura R, Ripmeester J . Guest-induced symmetry lowering of an ionic clathrate material for carbon capture. Chem Commun 2014;50:11476–9. https://doi.org/10.1039/C4CC02111H.

[210] Liang S, Kusalik PG. Nucleation of gas hydrates within constant energy systems. J Phys Chem B 2013;117:1403–10. https://doi.org/10.1021/jp308395x.

[211] English NJ, Clarke ET. Molecular dynamics study of CO2 hydrate dissociation: Fluctuation-dissipation and non-equilibrium analysis. J Chem Phys 2013;139:94701. https://doi.org/10.1063/1.4819269.

[212] Arjun A, Bolhuis PG. Molecular understanding of homogeneous nucleation of CO2 hydrates using transition path sampling. J Phys Chem B 2021;125:338–49. https://doi.org/10.1021/acs.jpcb.0c09915.

[213] Naeiji P, Varaminian F, Rahmati M. The kinetic modeling of methane hydrate growth by using molecular dynamic simulations. Int J Heat Mass Transf 2019;142:118356. https://doi.org/10.1016/j.ijheatmasstransfer.2019.07.006.

[214] Nguyen AH, Koc MA, Shepherd TD, Molinero V. Structure of the ice–clathrate interface. J Phys Chem C 2015;119:4104–17. https://doi.org/10.1021/jp511749q.

[215] Jendi ZM, Servio P, Rey AD. Ab initio modelling of methane hydrate thermophysical properties. Phys Chem Chem Phys 2016;18:10320–8. https://doi.org/10.1039/C5CP06530E.

[216] Zhang J, Kuo J, Iitaka T. First principles molecular dynamics study of filled ice hydrogen hydrate. J Chem Phys 2012;137:84505. https://doi.org/10.1063/1.4746776.

[217] Krishnan Y, Ghaani MR, Desmedt A, English NJ. Hydrogen inter-cage hopping and cage

occupancies inside hydrogen hydrate: Molecular-dynamics analysis. Appl Sci 2020;11:282. https://doi.org/10.3390/app11010282.

[218] Krishnan Y, Ghaani MR, English NJ. Hydrogen and deuterium molecular escape from clathrate hydrates: “Leaky” microsecond-molecular-dynamics predictions. J Phys Chem C 2021;125:8430–9. https://doi.org/10.1021/acs.jpcc.1c00987.

[219] Alavi S, Ohmura R. Understanding decomposition and encapsulation energies of structure I and II clathrate hydrates. J Chem Phys 2016;145:154708. https://doi.org/10.1063/1.4964673.

[220] Wu G, Tian L, Chen D, Niu M, Ji H. CO2 and CH4 hydrates: Replacement or co-growth? J Phys Chem C 2019;123:13401–9. https://doi.org/10.1021/acs.jpcc.9b00579.

[221] Matsui H, Jia J, Tsuji T, Liang Y, Masuda Y. Microsecond simulation study on the replacement of methane in methane hydrate by carbon dioxide, nitrogen, and carbon dioxide – nitrogen mixtures. Fuel 2019:116640. https://doi.org/10.1016/j.fuel.2019.116640.

[222] Naeiji P, Woo TK, Alavi S, Varaminian F, Ohmura R. Interfacial properties of hydrocarbon/water systems predicted by molecular dynamic simulations. J Chem Phys 2019;150:114703. https://doi.org/10.1063/1.5078739.

[223] Wang Y, Yin K, Lang X, Fan S, Li G, Yu C, et al. Hydrogen storage in sH binary hydrate: Insights from molecular dynamics simulation. Int J Hydrogen Energy 2021;46:15748–60. https://doi.org/10.1016/j.ijhydene.2021.02.112.

[224] Kondo Y, Alavi S, Takeya S, Ohmura R. Characterization of the clathrate hydrate formed with fluoromethane and pinacolone: The thermodynamic stability and volumetric behavior of the structure H binary hydrate. J Phys Chem B 2021;125:328–37.

https://doi.org/10.1021/acs.jpcb.0c09818.

[225] Xu J, Gu T, Sun Z, Li X, Wang X. Molecular dynamics study on the dissociation of methane hydrate via inorganic salts. Mol Phys 2016;114:34–43. https://doi.org/10.1080/00268976.2015.1081708.

[226] Alavi S, Takeya S, Ohmura R, Woo TK, Ripmeester JA. Hydrogen-bonding alcohol-water interactions in binary ethanol, 1-propanol, and 2-propanol+methane structure II clathrate hydrates. J Chem Phys 2010;133:74505. https://doi.org/10.1063/1.3469776.

[227] Guo P, Pan Y-K, Li L-L, Tang B. Molecular dynamics simulation of decomposition and thermal conductivity of methane hydrate in porous media. Chinese Phys B 2017;26:73101. https://doi.org/10.1088/1674-1056/26/7/073101.

[228] Ji H, Chen D, Zhao C, Wu G. Molecular dynamics simulation of methane hydrate formation and dissociation in the clay pores with fatty acids. J Phys Chem C 2018;122:1318–25. https://doi.org/10.1021/acs.jpcc.7b08808.

[229] Ripmeester JA, Alavi S. Molecular simulations of methane hydrate nucleation. Chem Phys Chem 2010;11:978–80. https://doi.org/10.1002/cphc.201000024.

[230] Christiansen RL, Sloan ED. Mechanisms and kinetics of hydrate formation. Ann N Y Acad Sci 1994;715:283–305. https://doi.org/10.1111/j.1749-6632.1994.tb38841.x.

[231] Sloan ED, Fleyfel F. A molecular mechanism for gas hydrate nucleation from ice. AIChE J 1991;37:1281–92. https://doi.org/10.1002/aic.690370902.

[232] DeFever RS, Sarupria S. Nucleation mechanism of clathrate hydrates of water-soluble guest molecules. J Chem Phys 2017;147:204503. https://doi.org/10.1063/1.4996132.

[233] Defever RS, Sarupria S. Surface chemistry effects on heterogeneous clathrate hydrate nucleation : A molecular dynamics study. J Chem Thermodyn 2017. https://doi.org/10.1016/j.jct.2017.08.021.

[234] Zhang Z, Walsh MR, Guo G-JJ. Microcanonical molecular simulations of methane hydrate nucleation and growth: evidence that direct nucleation to sI hydrate is among the multiple nucleation pathways. Phys Chem Chem Phys 2015;17:8870–6. https://doi.org/10.1039/C5CP00098J.

[235] Barnes BC, Beckham GT, Wu DT, Sum AK. Two-component order parameter for quantifying clathrate hydrate nucleation and growth. J Chem Phys 2014;140:164506. https://doi.org/10.1063/1.4871898.

[236] Jacobson LC, Hujo W, Molinero V. Nucleation pathways of clathrate hydrates: Effect of guest size and solubility. J Phys Chem B 2010;114:13796–807. https://doi.org/10.1021/jp107269q.

[237] Tung Y-T, Chen L-J, Chen Y-P, Lin S-T. The growth of structure I methane hydrate from molecular dynamics simulations. J Phys Chem B 2010;114:10804–13. https://doi.org/10.1021/jp102874s.

[238] Bai D, Chen G, Zhang X, Wang W. Microsecond molecular dynamics simulations of the kinetic pathways of gas hydrate formation from solid surfaces. Langmuir 2011;27:5961–7. https://doi.org/10.1021/la105088b.

[239] Jacobson LC, Hujo W, Molinero V. Amorphous precursors in the nucleation of clathrate hydrates. J Am Chem Soc 2010;132:11806–11. https://doi.org/10.1021/ja1051445.

[240] Lauricella M, Meloni S, Liang S, English NJ, Kusalik PG, Ciccotti G. Clathrate structure-type

recognition: Application to hydrate nucleation and crystallisation. J Chem Phys 2015;142:244503. https://doi.org/10.1063/1.4922696.

[241] Sarupria S, Debenedetti PG. Homogeneous nucleation of methane hydrate in microsecond molecular dynamics simulations. J Phys Chem Lett 2012;3:2942–7. https://doi.org/10.1021/jz3012113.

[242] Hall KW, Zhang Z, Kusalik PG. Unraveling mixed hydrate formation: Microscopic insights into early stage behavior. J Phys Chem B 2016;120:13218–23. https://doi.org/10.1021/acs.jpcb.6b11961.

[243] Hall KW, Zhang Z, Burnham CJ, Guo G-J, Carpendale S, English NJ. Does local structure bias how a crystal nucleus evolves? J Phys Chem Lett 2018;9:6991–8. https://doi.org/10.1021/acs.jpclett.8b03115.

[244] Pirzadeh P, Kusalik PG. Molecular insights into clathrate hydrate nucleation at an ice–solution interface. J Am Chem Soc 2013;135:7278–87. https://doi.org/10.1021/ja400521e.

[245] Moon C, Taylor PC, Rodger PM. Molecular dynamics study of gas hydrate formation. J Am Chem Soc 2003;125:4706–7. https://doi.org/10.1021/ja028537v.

[246] He Z, Gupta KM, Linga P, Jiang J. Molecular insights into the nucleation and growth of CH4 and CO2 mixed hydrates from microsecond simulations. J Phys Chem C 2016;120:25225–36. https://doi.org/10.1021/acs.jpcc.6b07780.

[247] He Z, Linga P, Jiang J. What are the key factors governing the nucleation of CO2 hydrate? Phys Chem Chem Phys 2017;19:15657–61. https://doi.org/10.1039/C7CP01350G.

[248] Carvalho PH, Mace A, Bull CL, Funnell NP, Tulk CA, Häussermann U. Elucidation of the

pressure induced amorphization of tetrahydrofuran clathrate hydrate 2019;204506. https://doi.org/10.1063/1.5083958.

[249] Bai D, Chen G, Zhang X, Wang W. Nucleation of the CO2 hydrate from three-phase contact lines. Langmuir 2012;28:7730–6. https://doi.org/10.1021/la300647s.

[250] Jacobson LC, Hujo W, Molinero V. Thermodynamic stability and growth of guest-free clathrate hydrates: A low-density crystal phase of water. J Phys Chem B 2009;113:10298–307. https://doi.org/10.1021/jp903439a.

[251] Zhang Z, Kusalik P, Guo G. Molecular insight into the growth of hydrogen and methane binary hydrates. J Phys Chem C 2018;122:7771–8. https://doi.org/10.1021/acs.jpcc.8b00842.

[252] Phan A, Schlösser H, Striolo A. Molecular mechanisms by which tetrahydrofuran affects CO2 hydrate growth: Implications for carbon storage. Chem Eng J 2021:129423. https://doi.org/10.1016/j.cej.2021.129423.

[253] Vatamanu J, Kusalik PG. Molecular insights into the heterogeneous crystal growth of sI methane hydrate. J Phys Chem B 2006;110:15896–904. https://doi.org/10.1021/jp061684l.

[254] Małolepsza E, Keyes T. Pathways through equilibrated states with coexisting phases for gas hydrate formation. J Phys Chem B 2015;119:15857–65. https://doi.org/10.1021/acs.jpcb.5b06832.

[255] Naeiji P, Varaminian F, Rahmati M. Comparison of the thermodynamic, structural and dynamical properties of methane/water and methane/water/hydrate systems using molecular dynamic simulations. J Nat Gas Sci Eng 2017. https://doi.org/10.1016/j.jngse.2017.04.010.

[256] Guo G, Zhang Y, Liu H. Effect of methane adsorption on the lifetime of a dodecahedral water

cluster immersed in liquid water: A molecular dynamics study on the hydrate nucleation mechanisms. J Phys Chem C 2007;111:2595–606. https://doi.org/10.1021/jp064271t.

[257] Guo G-J, Li M, Zhang Y-G, Wu C-H. Why can water cages adsorb aqueous methane? A potential of mean force calculation on hydrate nucleation mechanisms. Phys Chem Chem Phys 2009;11:10427. https://doi.org/10.1039/b913898f.

[258] Ma R, Zhong H, Li L, Zhong J, Yan Y, Zhang J, et al. Molecular insights into the effect of a solid surface on the stability of a hydrate nucleus. J Phys Chem C 2020;124:2664–71. https://doi.org/10.1021/acs.jpcc.9b09704.

[259] Nguyen AH, Molinero V. Cross-nucleation between clathrate hydrate polymorphs: Assessing the role of stability, growth rate, and structure matching. J Chem Phys 2014;140:84506. https://doi.org/10.1063/1.4866143.

[260] Burnham CJ, English NJ. Communication: Librational dynamics in water, sI and sII clathrate hydrates, and ice Ih: Molecular-dynamics insights. J Chem Phys 2016;144:51101. https://doi.org/10.1063/1.4941330.

[261] Zhang Z, Guo G-JJ. The effects of ice on methane hydrate nucleation: a microcanonical molecular dynamics study. Phys Chem Chem Phys 2017;19:19496–505. https://doi.org/10.1039/C7CP03649C.

[262] Jiménez-Ángeles F, Firoozabadi A. Enhanced hydrate nucleation near the limit of stability. J Phys Chem C 2015;119:8798–804. https://doi.org/10.1021/acs.jpcc.5b01869.

[263] Yagasaki T, Matsumoto M, Tanaka H. Formation of clathrate hydrates of water-soluble guest molecules. J Phys Chem C 2016;120:21512–21. https://doi.org/10.1021/acs.jpcc.6b06498.

[264] Forester TR, McDonald IR, Klein ML. Intermolecular potentials and the properties of liquid and solid hydrogen sulphide. Chem Phys 1989;129:225–34. https://doi.org/10.1016/0301-0104(89)80008-4.

[265] Zhao W, Bai J, Francisco JS, Zeng XC. Formation of CO2 hydrates within single-walled carbon nanotubes at ambient pressure: CO2 capture and selective separation of a CO2/H2 mixture in water. J Phys Chem C 2018;122:7951–8. https://doi.org/10.1021/acs.jpcc.7b12700.

[266] Zhao W, Wang L, Bai J, Francisco JS, Zeng XC. Spontaneous formation of one-dimensional hydrogen gas hydrate in carbon nanotubes. J Am Chem Soc 2014;136:10661–8. https://doi.org/10.1021/ja5041539.

[267] Wu J, Chen L, Chen Y, Lin S. methane + tetrahydrofuran mixed guest hydrate. Phys Chem Chem Phys 2016. https://doi.org/10.1039/C5CP06419H.

[268] Hu P, Wu G, Zi M, Li L, Chen D. Effects of modified metal surface on the formation of methane hydrate. Fuel 2019;255:115720. https://doi.org/10.1016/j.fuel.2019.115720.

[269] Bhattacharjee G, Choudhary N, Kumar A, Chakrabarty S, Kumar R. Effect of the amino acid l-histidine on methane hydrate growth kinetics. J Nat Gas Sci Eng 2016;35:1453–62. https://doi.org/10.1016/j.jngse.2016.05.052.

[270] Albertí M, Costantini A, Laganá A, Pirani F. Are micelles needed to form methane hydrates in sodium dodecyl sulfate solutions? J Phys Chem B 2012;116:4220–7. https://doi.org/10.1021/jp301124z.

[271] Min J, Kang DW, Lee W, Lee JW. Molecular dynamics simulations of hydrophobic nanoparticle effects on gas hydrate formation. J Phys Chem C 2020;124:4162–71.

https://doi.org/10.1021/acs.jpcc.9b11459.

[272] Mahmoodi MH, Manteghian M, Naeiji P. Study the effect of Ag nanoparticles on the kinetics of CO2 hydrate growth by molecular dynamics simulation. J Mol Liq 2021;343:117668. https://doi.org/10.1016/j.molliq.2021.117668.

[273] Susilo R, Alavi S, Lang S, Ripmeester J, Englezos P. Interactions between structure H hydrate formers and water molecules. J Phys Chem C 2008;112:9106–13. https://doi.org/10.1021/jp8006848.

[274] Yi L, Liang D, Zhou X, Li D, Wang J. Molecular dynamics simulations of carbon dioxide hydrate growth in electrolyte solutions of NaCl and MgCl2. Mol Phys 2014;112:3127–37. https://doi.org/10.1080/00268976.2014.932454.

[275] Tung Y, Chen L-J, Chen Y, Lin S. Molecular dynamics study on the growth of structure I methane hydrate in aqueous solution of sodium chloride. J Phys Chem B 2012;116:14115–25. https://doi.org/10.1021/jp308224v.

[276] Choudhary N, Kushwaha OS, Bhattacharjee G, Chakrabarty S, Kumar R. Macro and molecular level insights on gas hydrate growth in the presence of hofmeister salts. Ind Eng Chem Res 2020;59:20591–600. https://doi.org/10.1021/acs.iecr.0c04389.

[277] Choudhary N, Kushwaha OS, Bhattacharjee G, Chakrabarty S, Kumar R. Molecular dynamics simulation and experimental study on the growth of methane hydrate in presence of methanol and sodium chloride. Energy Procedia 2017;105:5026–33. https://doi.org/10.1016/j.egypro.2017.03.1008.

[278] Makiya T, Murakami T, Takeya S, Sum AK, Alavi S, Ohmura R. Synthesis and characterization

of clathrate hydrates containing carbon dioxide and ethanol. Phys Chem Chem Phys 2010;12:9927. https://doi.org/10.1039/c002187c.

[279] Ji H, Wu G, Zi M, Chen D. Microsecond molecular dynamics simulation of methane hydrate formation in humic-acid-amended sodium montmorillonite. Energy & Fuels 2016;30:7206–13. https://doi.org/10.1021/acs.energyfuels.6b01544.

[280] Cheng L, Liao K, Li Z, Cui J, Liu B, Li F, et al. The invalidation mechanism of kinetic hydrate inhibitors under high subcooling conditions. Chem Eng Sci 2019;207:305–16. https://doi.org/10.1016/j.ces.2019.06.032.

[281] Bai D, Wu Z, Lin C, Zhou D. The effect of aqueous NaCl solution on methane hydrate nucleation and growth. Fluid Phase Equilib 2019;487:76–82. https://doi.org/10.1016/j.fluid.2019.01.008.

[282] Bai D, Chen G, Zhang X, Sum AK, Wang W. How properties of solid surfaces modulate the nucleation of gas hydrate. Sci Rep 2015;5:12747. https://doi.org/10.1038/srep12747.

[283] He Z, Linga P, Jiang J. CH4 hydrate formation between silica and graphite surfaces: Insights from microsecond molecular dynamics simulations. Langmuir 2017;33:11956–67. https://doi.org/10.1021/acs.langmuir.7b02711.

[284] Yan K-F, Li X-S, Chen Z-Y, Xia Z-M, Xu C-G, Zhang Z. Molecular dynamics simulation of the crystal nucleation and growth behavior of methane hydrate in the presence of the surface and nanopores of porous sediment. Langmuir 2016;32:7975–84. https://doi.org/10.1021/acs.langmuir.6b01601.

[285] Li Y, Chen M, Liu C, Song H, Yuan P, Zhang B, et al. Effects of layer-charge distribution of 2:1

clay minerals on methane hydrate formation: A molecular dynamics simulation study. Langmuir 2020;36:3323–35. https://doi.org/10.1021/acs.langmuir.0c00183.

[286] Park S-H, Sposito G. Do montmorillonite surfaces promote methane hydrate formation? monte carlo and molecular dynamics simulations. J Phys Chem B 2003;107:2281–90. https://doi.org/10.1021/jp021427q.

[287] Kyung D, Lim H-K, Kim H, Lee W. CO2 hydrate nucleation kinetics enhanced by an organo-mineral complex formed at the montmorillonite–water interface. Environ Sci Technol 2015;49:1197–205. https://doi.org/10.1021/es504450x.

[288] Kvamme B, Graue A, Buanes T, Kuznetsova T, Ersland G. Storage of CO2 in natural gas hydrate reservoirs and the effect of hydrate as an extra sealing in cold aquifers. Int J Greenh Gas Control 2007;1:236–46. https://doi.org/10.1016/S1750-5836(06)00002-8.

[289] Das S, Baghel VS, Roy S, Kumar R. A molecular dynamics study of model SI clathrate hydrates: the effect of guest size and guest–water interaction on decomposition kinetics. Phys Chem Chem Phys 2015;17:9509–18. https://doi.org/10.1039/C5CP00678C.

[290] Yasuoka K, Murakoshi S. Molecular dynamics simulation of dissociation process for methane hydrate. Ann N Y Acad Sci 2006;912:678–84. https://doi.org/10.1111/j.1749-6632.2000.tb06823.x.

[291] English NJ, Phelan GM. Molecular dynamics study of thermal-driven methane hydrate dissociation. J Chem Phys 2009;131:74704. https://doi.org/10.1063/1.3211089.

[292] Fang B, Ning F, Ou W, Wang D, Zhang Z, Yu Y, et al. The dynamic behavior of gas hydrate dissociation by heating in tight sandy reservoirs: A molecular dynamics simulation study. Fuel

2019;258:116106. https://doi.org/10.1016/j.fuel.2019.116106.

[293] Bagherzadeh SA, Englezos P, Alavi S, Ripmeester JA. Molecular modeling of the dissociation of methane hydrate in contact with a silica surface. J Phys Chem B 2012;116:3188–97. https://doi.org/10.1021/jp2086544.

[294] English NJ, Ghaani MR. Hybrid versus global thermostatting in molecular-dynamics simulation of methane-hydrate crystallisation. Chinese J Chem Eng 2019;27:2180–8. https://doi.org/10.1016/j.cjche.2019.02.034.

[295] Ghaani MR, English NJ. Molecular-dynamics study of propane-hydrate dissociation: Fluctuation-dissipation and non-equilibrium analysis. J Chem Phys 2018;114504. https://doi.org/10.1063/1.5018192.

[296] Ghaani MR, English NJ. Hydrogen-/propane-hydrate decomposition: thermodynamic and kinetic analysis. Mol Phys 2019;117:2434–42. https://doi.org/10.1080/00268976.2019.1567845.

[297] Waldron CJ, English NJ. Global-density fluctuations in methane clathrate hydrates in externally applied electromagnetic fields. J Chem Phys 2017;147:24506. https://doi.org/10.1063/1.4990029.

[298] Waldron CJ, English NJ. System-density fluctuations and electro-dissociation of methane clathrate hydrates in externally-applied static electric fields. J Chem Thermodyn 2018;117:68–80. https://doi.org/10.1016/j.jct.2017.08.016.

[299] Krishnan Y, Ghaani MR, English NJ. Electric-field control of neon uptake and release to and from clathrate hydrates. J Phys Chem C 2019;123:27554–60. https://doi.org/10.1021/acs.jpcc.9b07257.

[300] Ghaani MR, English NJ, Allen CCR. Magnetic-field manipulation of naturally occurring microbial chiral peptides to regulate gas-hydrate formation. J Phys Chem Lett 2020;11:9079–85. https://doi.org/10.1021/acs.jpclett.0c02347.

[301] Li J, Lu H, Zhou X. Electric field triggered release of gas from a quasi-one-dimensional hydrate in the carbon nanotube. Nanoscale 2020;12:12801–8. https://doi.org/10.1039/D0NR01113D.

[302] Ghaani MR, English NJ. Molecular dynamics study of propane hydrate dissociation: Nonequilibrium analysis in externally applied electric fields. J Phys Chem C 2018;122:7504–15. https://doi.org/10.1021/acs.jpcc.7b12238.

[303] Ghaani MR, English NJ. Non-equilibrium molecular-dynamics study of electromagnetic-field-induced propane-hydrate dissociation. J Chem Phys 2018;149:124702. https://doi.org/10.1063/1.5029457.

[304] Bagherzadeh SA, Alavi S, Ripmeester JA, Englezos P. Evolution of methane during gas hydrate dissociation. Fluid Phase Equilib 2013;358:114–20. https://doi.org/10.1016/j.fluid.2013.08.017.

[305] Kondori J, James L, Zendehboudi S. Molecular scale modeling approach to evaluate stability and dissociation of methane and carbon dioxide hydrates. J Mol Liq 2020;297:111503. https://doi.org/10.1016/j.molliq.2019.111503.

[306] Zhang Z, Kusalik PG, Guo G-J, Ning F, Wu N. Insight on the stability of polycrystalline natural gas hydrates by molecular dynamics simulations. Fuel 2021;289:119946. https://doi.org/10.1016/j.fuel.2020.119946.

[307] Liu Y, Zhao J, Xu J. Dissociation mechanism of carbon dioxide hydrate by molecular dynamic simulation and ab initio calculation. Comput Theor Chem 2012;991:165–73.

https://doi.org/10.1016/j.comptc.2012.04.016.

[308] Geng C-Y, Han Q-Z, Wen H, Dai Z-Y, Song C-H. Molecular dynamics simulation on the decomposition of type SII hydrogen hydrate and the performance of tetrahydrofuran as a stabiliser. Mol Simul 2010;36:474–83. https://doi.org/10.1080/08927021003664041.

[309] Alavi S, Shin K, Ripmeester JA. Molecular dynamics simulations of hydrogen bonding in clathrate hydrates with ammonia and methanol guest molecules. J Chem Eng Data 2015;60:389–97. https://doi.org/10.1021/je5006517.

[310] Reshadi P, Modarress H, Dabir B, Amjad-Iranagh S. A study on dissociation of sII krypton hydrate and the effect of hydrocarbon guest molecules as stabilizer by molecular dynamics simulation. Phase Transitions 2017;90:1128–42. https://doi.org/10.1080/01411594.2017.1309404.

[311] Yagasaki T, Matsumoto M, Andoh Y, Okazaki S, Tanaka H. Dissociation of methane hydrate in aqueous NaCl solutions. J Phys Chem B 2014;118:11797–804. https://doi.org/10.1021/jp507978u.

[312] Dai C, Hu Y, Wu Y, Zhao M, Yue T. Effects of structural properties of alcohol molecules on decomposition of natural gas hydrates: A molecular dynamics study. Fuel 2020;268:117322. https://doi.org/10.1016/j.fuel.2020.117322.

[313] Sun X, Zhou G, Zhu J, Wu H, Lu G, Bai D. Molecular dynamics simulation of methane hydrate decomposition in the presence of alcohol additives. ChemPhysChem 2019;20:2553–65. https://doi.org/10.1002/cphc.201900742.

[314] Kondori J, Zendehboudi S, James L. Molecular dynamic simulations to evaluate dissociation of

hydrate structure II in the presence of inhibitors : A mechanistic study. Chem Eng Res Des 2019;149:81–94. https://doi.org/10.1016/j.cherd.2019.05.048.

[315] Li K, Shi R, Huang Y, Tang L, Cao X, Su Y, et al. Dissociation mechanism of propane hydrate with methanol additive: A molecular dynamics simulation. Comput Theor Chem 2018;1123:79–86. https://doi.org/10.1016/j.comptc.2017.11.011.

[316] Srivastava HK, Sastry GN. Viability of clathrate hydrates as CO2 capturing agents: A theoretical study. J Phys Chem A 2011;115:7633–7. https://doi.org/10.1021/jp203599g.

[317] Velaga SC, Anderson BJ. Carbon dioxide hydrate phase equilibrium and cage occupancy calculations using Ab initio intermolecular potentials. J Phys Chem B 2014;118:577–89. https://doi.org/10.1021/jp410306v.

[318] Myshakin EM, Jiang H, Warzinski RP, Jordan KD. Molecular dynamics simulations of methane hydrate decomposition. J Phys Chem A 2009;113:1913–21. https://doi.org/10.1021/jp807208z.

[319] Burnham CJ, English NJ. Free-energy calculations of the intercage hopping barriers of hydrogen molecules in clathrate hydrates. J Phys Chem C 2016;120:16561–7. https://doi.org/10.1021/acs.jpcc.6b06524.

[320] Burnham CJ, Futera Z, English NJ. Quantum and classical inter-cage hopping of hydrogen molecules in clathrate hydrate: temperature and cage-occupation effects. Phys Chem Chem Phys 2017;19:717–28. https://doi.org/10.1039/c6cp06531g.

[321] Burnham CJ, Futera Z, English NJ. Study of hydrogen-molecule guests in type II clathrate hydrates using a force-matched potential model parameterised from ab initio molecular dynamics. J Chem Phys 2018;148:102323. https://doi.org/10.1063/1.4999909.

[322] Brumby PE, Yuhara D, Hasegawa T, Wu DT, Sum AK, Yasuoka K. Cage occupancies, lattice constants, and guest chemical potentials for structure II hydrogen clathrate hydrate from Gibbs ensemble Monte Carlo simulations. J Chem Phys 2019;150:134503. https://doi.org/10.1063/1.5084785.

[323] Lu Q, He X, Hu W, Chen X, Liu J. Stability, vibrations, and diffusion of hydrogen gas in clathrate hydrates: Insights from Ab initio calculations on condensed-phase crystalline structures. J Phys Chem C 2019;123:12052–61. https://doi.org/10.1021/acs.jpcc.8b11586.

[324] Mondal S, Ghosh S, Chattaraj PK. A molecular dynamics study on sI hydrogen hydrate. J Mol Model 2013;19:2785–90. https://doi.org/10.1007/s00894-012-1625-7.

[325] Liu J, Yan Y, Zhang J, Xu J, Chen G, Hou J. Theoretical investigation of storage capacity of hydrocarbon gas in sH hydrate. Chem Phys 2019;525:110393. https://doi.org/10.1016/j.chemphys.2019.110393.

[326] Sun ZZ, Wang H, Yao J, Bongole K, Zhu X, Liu L, et al. Effect of cage-specific occupancy on the dissociation rate of a three-phase coexistence methane hydrate system: A molecular dynamics simulation study. J Nat Gas Sci Eng 2018;55:235–42. https://doi.org/10.1016/j.jngse.2018.05.004.

[327] Kondori J, Zendehboudi S, James L. New insights into methane hydrate dissociation: Utilization of molecular dynamics strategy. Fuel 2019;249:264–76. https://doi.org/10.1016/j.fuel.2019.02.125.

[328] Matsuo M, Takii Y, Matsumoto M, Tanaka H. On the occupancy of carbon dioxide clathrate hydrates: Grandcanonical monte carlo simulations. J Phys Soc Japan 2012;81:SA027. https://doi.org/10.1143/JPSJS.81SA.SA027.

[329] English NJ, Burnham CJ. Intra-cage structure, vibrations and tetrahedral-site hopping of H2 and D2 in doubly-occupied 51264 cages in sII clathrate hydrates from path-integral and classical molecular dynamics. Appl Sci 2020;11:54. https://doi.org/10.3390/app11010054.

[330] Song B, Nguyen AH, Molinero V. Can guest occupancy in binary clathrate hydrates be tuned through control of the growth temperature? J Phys Chem C 2014;118:23022–31. https://doi.org/10.1021/jp504852k.

[331] Alavi S, Ripmeester JA, Klug DD. Molecular-dynamics study of structure II hydrogen clathrates. J Chem Phys 2005;123:24507. https://doi.org/10.1063/1.1953577.

[332] Alavi S, Ripmeester JA. Migration of hydrogen radicals through clathrate hydrate cages. Chem Phys Lett 2009;479:234–7. https://doi.org/10.1016/j.cplett.2009.08.044.

[333] Cao H, English NJ, MacElroy JMD. Diffusive hydrogen inter-cage migration in hydrogen and hydrogen-tetrahydrofuran clathrate hydrates. J Chem Phys 2013;138:0–10. https://doi.org/10.1063/1.4793468.

[334] Gorman PD, English NJ, MacElroy JMD. Dynamical cage behaviour and hydrogen migration in hydrogen and hydrogen-tetrahydrofuran clathrate hydrates. J Chem Phys 2012;136:44506. https://doi.org/10.1063/1.3677188.

[335] Liu Y, Chen C, Hu W, Li W, Dong B, Qin Y. Molecular dynamics simulation studies of gas hydrate growth with impingement. Chem Eng J 2021;426:130705. https://doi.org/10.1016/j.cej.2021.130705.

[336] Alavi S, Ripmeester JA, Klug DD. Molecular-dynamics simulations of binary structure II hydrogen and tetrahydrofurane clathrates. J Chem Phys 2006;124:14704.

https://doi.org/10.1063/1.2141506.

[337] Tsimpanogiannis IN, Economou IG, Stubos AK. A practical methodology to estimate the H2 storage capacity of pure and binary hydrates based on monte carlo simulations. J Chem Eng Data 2020;65:1289–99. https://doi.org/10.1021/acs.jced.9b00707.

[338] Ghaani MR, Takeya S, English NJ. Hydrogen storage in propane-hydrate: Theoretical and experimental study. Appl Sci 2020;10:8962. https://doi.org/10.3390/app10248962.

[339] Tanaka H, Nakatsuka T, Koga K. On the thermodynamic stability of clathrate hydrates IV: Double occupancy of cages. J Chem Phys 2004;121:5488–93. https://doi.org/10.1063/1.1782471.

[340] Papadimitriou NI, Tsimpanogiannis IN, Economou IG, Stubos AK. Influence of combining rules on the cavity occupancy of clathrate hydrates by Monte Carlo simulations. Mol Phys 2014;112:2258–74. https://doi.org/10.1080/00268976.2014.902136.

[341] Papadimitriou NI, Tsimpanogiannis IN, Peters CJ, Papaioannou AT, Stubos AK. Hydrogen storage in sH hydrates: A monte carlo study. J Phys Chem B 2008;112:14206–11. https://doi.org/10.1021/jp805906c.

[342] Alavi S, Woo TK. How much carbon dioxide can be stored in the structure H clathrate hydrates?: A molecular dynamics study. J Chem Phys 2007;126:44703. https://doi.org/10.1063/1.2424936.

[343] Gharebeiglou M, Izadkhah S. Molecular dynamics simulation study on the structure II clathrate-hydrates of methane + cyclic organic compounds 2016;6466. https://doi.org/10.1080/10916466.2016.1194860.

[344] Susilo R, Alavi S, Ripmeester JA, Englezos P. Molecular dynamics study of structure H clathrate hydrates of methane and large guest molecules. J Chem Phys 2008;128:194505. https://doi.org/10.1063/1.2908074.

[345] Alavi S, Ripmeester JA, Klug DD. Molecular dynamics simulations of binary structure H hydrogen and methyl-tert-butylether clathrate hydrates. J Chem Phys 2006;124:204707. https://doi.org/10.1063/1.2199850.

[346] Grim RG, Barnes BC, Lafond PG, Kockelmann WA, Keen DA, Soper AK, et al. Observation of interstitial molecular hydrogen in clathrate hydrates. Angew Chemie Int Ed 2014;53:10710–3. https://doi.org/10.1002/anie.201406546.

[347] Susilo R, Alavi S, Ripmeester J, Englezos P. Tuning methane content in gas hydrates via thermodynamic modeling and molecular dynamics simulation. Fluid Phase Equilib 2008;263:6–17. https://doi.org/10.1016/j.fluid.2007.09.015.

[348] Erfan-Niya H, Modarress H, Zaminpayma E. Computational study on the structure II clathrate hydrate of methane and large guest molecules. J Incl Phenom Macrocycl Chem 2011;70:227–39. https://doi.org/10.1007/s10847-010-9899-9.

[349] Huang Y, Zhu C, Wang L, Cao X, Su Y, Jiang X, et al. A new phase diagram of water under negative pressure: The rise of the lowest-density clathrate s-III. Sci Adv 2016;2:e1501010. https://doi.org/10.1126/sciadv.1501010.

[350] Tse JS. Vibrations of methane in structure I clathrate hydrate—an ab initio density functional molecular dynamics study. J Supramol Chem 2002;2:429–33. https://doi.org/10.1016/S1472-7862(03)00053-4.

[351] Bai D, Liu B, Chen G, Zhang X, Wang W. Role of guest molecules on the hydrate growth at vapor-liquid interfaces. AIChE J 2013;59:2621–9. https://doi.org/10.1002/aic.14011.

[352] Mohammadi-Manesh H, Alavi S, Woo TK, Najafi B. Computational prediction of temperature dependence of 13C NMR lineshapes of planar molecules in structure I clathrate hydrates. J Iran Chem Soc 2013;10:659–67. https://doi.org/10.1007/s13738-012-0198-9.

[353] Mohammadi-Manesh H, Alavi S, Woo TK, Najafi B. Molecular dynamics simulation of NMR powder lineshapes of linear guests in structure I clathrate hydrates. Phys Chem Chem Phys 2011;13:2367–77. https://doi.org/10.1039/C0CP01920H.

[354] Izquierdo-Ruiz F, Otero-de-la-Roza A, Contreras-García J, Prieto-Ballesteros O, Recio JM. Effects of the CO2 guest molecule on the sI clathrate hydrate structure. Materials (Basel) 2016;9:777. https://doi.org/10.3390/ma9090777.

[355] Naeiji P, Varaminian F, Rahmati M. Thermodynamic and structural properties of methane/water systems at the threshold of hydrate formation predicted by molecular dynamic simulations. J Nat Gas Sci Eng 2016. https://doi.org/10.1016/j.jngse.2016.03.044.

[356] Zhou J, Liang Y. Effect of water on the dynamic tensile mechanical properties of calcium silicate hydrate: Based on molecular dynamics simulation. Materials (Basel) 2019;12:2837. https://doi.org/10.3390/ma12172837.

[357] Jia J, Liang Y, Tsuji T, Murata S, Matsuoka T. Elasticity and stability of clathrate hydrate: Role of guest molecule motions. Sci Rep 2017;7:1290. https://doi.org/10.1038/s41598-017-01369-0.

[358] Hou J, Bai D, Zhou W. Methane hydrate nucleation within elastic confined spaces: Suitable spacing and elasticity can accelerate the nucleation. Langmuir 2018;34:10889–96.

https://doi.org/10.1021/acs.langmuir.8b02387.

[359] Jendi ZM, Servio P, Rey AD. Ideal strength of methane hydrate and ice Ih from first-principles. Cryst Growth Des 2015;15:5301–9. https://doi.org/10.1021/acs.cgd.5b00829.

[360] Gudkovskikh S V, Kirov M V. Proton disorder and elasticity of hexagonal ice and gas hydrates. J Mol Model 2019;25:32. https://doi.org/10.1007/s00894-018-3919-x.

[361] Shi Q, Cao P, Han Z, Ning F, Gong H, Xin Y, et al. Role of guest molecules in the mechanical properties of clathrate hydrates. Cryst Growth Des 2018;18:6729–41. https://doi.org/10.1021/acs.cgd.8b01017.

[362] Liang S, Kusalik PG. Crystal growth simulations of H2S hydrate. J Phys Chem B 2010;114:9563–71. https://doi.org/10.1021/jp102584d.

[363] Liang S, Kusalik PG. Exploring nucleation of H2S hydrates. Chem Sci 2011;2:1286. https://doi.org/10.1039/c1sc00021g.

[364] Youssef M, Pellenq RJ-M, Yildiz B. Glassy nature of water in an ultraconfining disordered material: The case of calcium−silicate−hydrate. J Am Chem Soc 2011;133:2499–510. https://doi.org/10.1021/ja107003a.

[365] Alavi S, Susilo R, Ripmeester JA. Linking microscopic guest properties to macroscopic observables in clathrate hydrates: Guest-host hydrogen bonding. J Chem Phys 2009;130:174501. https://doi.org/10.1063/1.3124187.

[366] Mirzaeifard S, Servio P, Rey AD. Molecular dynamics characterization of temperature and pressure effects on the water-methane interface. Colloids Interface Sci Commun 2018;24:75–81. https://doi.org/10.1016/j.colcom.2018.04.004.

[367] Tanaka H, Tamai Y, Koga K. Large thermal expansivity of clathrate hydrates. J Phys Chem B 1997;101:6560–5. https://doi.org/10.1021/jp970511g.

[368] English NJ. Effect of electrostatics techniques on the estimation of thermal conductivity via equilibrium molecular dynamics simulation: Application to methane hydrate. Mol Phys 2008;106:1887–98. https://doi.org/10.1080/00268970802360348.

[369] English NJ, Tse JS. Mechanisms for thermal conduction in methane hydrate. Phys Rev Lett 2009;103:15901. https://doi.org/10.1103/PhysRevLett.103.015901.

[370] English NJ, Tse JS, Carey DJ. Mechanisms for thermal conduction in various polymorphs of methane hydrate. Phys Rev B 2009;80:134306. https://doi.org/10.1103/PhysRevB.80.134306.

[371] English N, Gorman P, MacElroy J. Mechanisms for thermal conduction in hydrogen hydrate. J Chem Phys 2012;136:44501. https://doi.org/10.1063/1.3677189.

[372] Ghafari H, Mohammadi-Manesh H. The thermal properties of binary structure sI clathrate hydrate from molecular dynamics simulation. Mol Simul 2019;45:614–22. https://doi.org/10.1080/08927022.2019.1572142.

[373] Fang B, Ning F, Cao P, Peng L, Wu J, Zhang Z, et al. Modeling thermodynamic properties of propane or tetrahydrofuran mixed with carbon dioxide or methane in structure-II clathrate hydrates. J Phys Chem C 2017;121:23911–25. https://doi.org/10.1021/acs.jpcc.7b06623.

[374] Arai Y, Takeya S, Alavi S, Yamauchi Y, Ohmura R. Effect of nonspherical encapsulated guests on the volumetric behavior of structure H clathrate hydrates. J Phys Chem C 2018;122:27631–9. https://doi.org/10.1021/acs.jpcc.8b09923.

[375] Erfan Niya H, Modarress H, Zaminpayma E. Molecular dynamics simulation of structure II

clathrate hydrates of xenon and large hydrocarbon guest molecules. J Clust Sci 2011;22:11–30. https://doi.org/10.1007/s10876-011-0358-6.

[376] Min J, Ahn Y, Baek S, Shin K, Cha M, Lee JW. Effects of large guest molecular structure on thermal expansion. J Phys Chem C 2019;123:20705–14. https://doi.org/10.1021/acs.jpcc.9b04125.

[377] Mirzaeifard S, Servio P, Rey AD. Molecular dynamics characterization of the water-methane, ethane, and propane gas mixture interfaces. Chem Eng Sci 2019;208:114769. https://doi.org/10.1016/j.ces.2019.01.051.

[378] Mirzaeifard S, Servio P, Rey AD. Characterization of nucleation of methane hydrate crystals: Interfacial theory and molecular simulation. J Colloid Interface Sci 2019;557:556–67. https://doi.org/10.1016/j.jcis.2019.09.056.

[379] Vlasic TM, Servio P, Rey AD. Atomistic modeling of structure II gas hydrate mechanics: Compressibility and equations of state. AIP Adv 2016;6:85317. https://doi.org/10.1063/1.4961728.

[380] Greathouse JA, Cygan RT, Simmons BA. Vibrational spectra of methane clathrate hydrates from molecular dynamics simulation. J Phys Chem B 2006;110:6428–31. https://doi.org/10.1021/jp060471t.

[381] Baumert J, Gutt C, Shpakov VP, Tse JS, Krisch M, Müller M, et al. Lattice dynamics of methane and xenon hydrate: Observation of symmetry-avoided crossing by experiment and theory. Phys Rev B 2003;68:174301. https://doi.org/10.1103/PhysRevB.68.174301.

[382] Tse JS, Klein ML, McDonald IR. Computer simulation studies of the structure I clathrate

hydrates of methane, tetrafluoromethane, cyclopropane, and ethylene oxide. J Chem Phys 1984;81:6146–53. https://doi.org/10.1063/1.447569.

[383] Tse JS, Shpakov VP, Murashov V V, Belosludov VR. The low frequency vibrations in clathrate hydrates. J Chem Phys 1997;107:9271–4. https://doi.org/10.1063/1.475218.

[384] Inoue R, Tanaka H, Nakanishi K. Molecular dynamics simulation study of the anomalous thermal conductivity of clathrate hydrates. J Chem Phys 1996;104:9569–77. https://doi.org/10.1063/1.471705.

[385] Futera Z, Celli M, del Rosso L, Burnham CJ, Ulivi L, English NJ. Vibrational modes of hydrogen hydrates: A first-principles molecular dynamics and raman spectra study. J Phys Chem C 2017;121:3690–6. https://doi.org/10.1021/acs.jpcc.6b11029.

[386] English NJ, Tse JS. Dynamical properties of hydrogen sulphide motion in its clathrate hydrate from Ab initio and classical isobaric−isothermal molecular dynamics. J Phys Chem A 2011;115:6226–32. https://doi.org/10.1021/jp111485w.

[387] Hiratsuka M, Ohmura R, Sum AK, Alavi S, Yasuoka K. A molecular dynamics study of guest–host hydrogen bonding in alcohol clathrate hydrates. Phys Chem Chem Phys 2015;17:12639–47. https://doi.org/10.1039/C4CP05732E.

[388] Daghash SM, Servio P, Rey AD. From infrared spectra to macroscopic mechanical properties of sH gas hydrates through atomistic calculations. Molecules 2020;25:5568. https://doi.org/10.3390/molecules25235568.

[389] Hiratsuka M, Ohmura R, Sum AK, Yasuoka K. Vibrational modes of methane in the structure H clathrate hydrate from ab initio molecular dynamics simulation. J Chem Phys 2012;137:144306.

https://doi.org/10.1063/1.4757914.

[390] Hiratsuka M, Ohmura R, Sum AK, Yasuoka K. Molecular vibrations of methane molecules in the structure I clathrate hydrate from ab initio molecular dynamics simulation. J Chem Phys 2012;136:44508. https://doi.org/10.1063/1.3677231.

[391] Vlasic TM, Servio PD, Rey AD. Infrared spectra of gas hydrates from first-principles. J Phys Chem B 2019;123:936–47. https://doi.org/10.1021/acs.jpcb.8b10223.

[392] Van Klaveren EP, Michels JPJ, Schouten JA, Klug DD, Tse JS. Computer simulations of the dynamics of doubly occupied N2 clathrate hydrates. J Chem Phys 2002;117:6637–45. https://doi.org/10.1063/1.1502645.

[393] Jendi ZM, Servio P, Rey AD. Molecular mobility in carbon dioxide hydrates. Mol Syst Des Eng 2017;2:500–6. https://doi.org/10.1039/C7ME00041C.

[394] Frankcombe TJ, Kroes G-J. Molecular dynamics simulations of type-sII hydrogen clathrate hydrate close to equilibrium conditions. J Phys Chem C 2007;111:13044–52. https://doi.org/10.1021/jp071006e.

[395] Liang S, Kusalik PG. The mobility of water molecules through gas hydrates. J Am Chem Soc 2011;133:1870–6. https://doi.org/10.1021/ja108434h.

[396] Zhang Z, Kusalik P, Guo G-J. Bridging solution properties to gas hydrate nucleation through guest dynamics. Phys Chem Chem Phys 2018;20:24535–8. https://doi.org/10.1039/C8CP04466J.

[397] Mathews SL, Servio PD, Rey AD. Heat capacity, thermal expansion coefficient, and grüneisen parameter of CH4, CO2, and C2H6 hydrates and ice Ih via density functional theory and phonon calculations. Cryst Growth Des 2020;20:5947–55. https://doi.org/10.1021/acs.cgd.0c00630.

[398] Jiang H, Jordan KD. Comparison of the properties of xenon, methane, and carbon dioxide hydrates from equilibrium and nonequilibrium molecular dynamics simulations. J Phys Chem C 2010;114:5555–64. https://doi.org/10.1021/jp9063406.

[399] Pétuya C, Martin-Gondre L, Aurel P, Damay F, Desmedt A. Unraveling the metastability of the SI and SII carbon monoxide hydrate with a combined DFT-neutron diffraction investigation. J Chem Phys 2019;150:184705. https://doi.org/10.1063/1.5093202.

[400] Cladek BR, Everett SM, Mcdonnell MT, Tucker MG, Ke DJ, Rawn CJ. Molecular rotational dynamics in mixed CH4−CO2 hydrates: insights from molecular dynamics simulations 2019. https://doi.org/10.1021/acs.jpcc.9b06242.

[401] Gorman PD, English NJ, MacElroy JMD. Dynamical and energetic properties of hydrogen and hydrogen–tetrahydrofuran clathrate hydrates. Phys Chem Chem Phys 2011;13:19780. https://doi.org/10.1039/c1cp21882d.

[402] Vlasic TM, Servio PD, Rey AD. THF hydrates as model systems for natural gas hydrates: Comparing their mechanical and vibrational properties. Ind Eng Chem Res 2019;58:16588–96. https://doi.org/10.1021/acs.iecr.9b02698.

[403] Yu X, Zhu J, Du S, Xu H, Vogel SC, Han J, et al. Crystal structure and encapsulation dynamics of ice II-structured neon hydrate. Proc Natl Acad Sci 2014;111:10456–61. https://doi.org/10.1073/pnas.1410690111.

[404] Luis DP, Romero-Ramirez IE, González-Calderón A, López-Lemus J. The coexistence temperature of hydrogen clathrates: A molecular dynamics study. J Chem Phys 2018;148:114503. https://doi.org/10.1063/1.5017854.

[405] Michalis VK, Tsimpanogiannis IN, Stubos AK, Economou IG. Direct phase coexistence molecular dynamics study of the phase equilibria of the ternary methane–carbon dioxide–water hydrate system. Phys Chem Chem Phys 2016;18:23538–48. https://doi.org/10.1039/C6CP04647A.

[406] Zhu J, Du S, Yu X, Zhang J, Xu H, Vogel SC, et al. Encapsulation kinetics and dynamics of carbon monoxide in clathrate hydrate. Nat Commun 2014;5:4128. https://doi.org/10.1038/ncomms5128.

[407] Sun R, Duan Z. Prediction of CH4 and CO2 hydrate phase equilibrium and cage occupancy from ab initio intermolecular potentials. Geochim Cosmochim Acta 2005;69:4411–24. https://doi.org/10.1016/j.gca.2005.05.012.

[408] Erfan-Niya H, Modarress H, Zaminpayma E. Molecular dynamics study on the structure I clathrate-hydrate of methane+ethane mixture. Energy Convers Manag 2011;52:523–31. https://doi.org/10.1016/j.enconman.2010.07.027.

[409] Tung Y-T, Chen L-J, Chen Y-P, Lin S-T. In situ methane recovery and carbon dioxide sequestration in methane hydrates: A molecular dynamics simulation study. J Phys Chem B 2011;115:15295–302. https://doi.org/10.1021/jp2088675.

[410] Zhang K, Qin G. Mechanistic and kinetic study of CO2-CH4 exchange process in methane hydrates using molecular dynamics simulation. Soc Pet Eng - SPE Eur Featur 81st EAGE Conf Exhib 2019 2019:1–15. https://doi.org/10.2118/195457-MS.

[411] Qi Y, Ota M, Zhang H. Molecular dynamics simulation of replacement of CH4 in hydrate with CO2. Energy Convers Manag 2011;52:2682–7. https://doi.org/10.1016/j.enconman.2011.01.020.

[412] Nohra M, Woo TK, Alavi S, Ripmeester JA. Molecular dynamics Gibbs free energy calculations for CO2 capture and storage in structure I clathrate hydrates in the presence of SO2, CH4, N2, and H2S impurities. J Chem Thermodyn 2012;44:5–12. https://doi.org/10.1016/j.jct.2011.08.025.

[413] Nakate P, Ghosh B, Das S, Roy S, Kumar R. Molecular dynamics study on growth of carbon dioxide and methane hydrate from a seed crystal. Chinese J Chem Eng 2019;27:2074–80. https://doi.org/10.1016/j.cjche.2019.02.006.

[414] Liu Y, Zhao L, Deng S, Bai D. Evolution of bubbles in decomposition and replacement process of methane hydrate. Mol Simul 2017;7022:1–13. https://doi.org/10.1080/08927022.2017.1359745.

[415] Geng C, Wen H, Zhou H. Molecular simulation of the potential of methane reoccupation during the replacement of methane hydrate by CO2. J Phys Chem A 2009;113:5463–9. https://doi.org/10.1021/jp811474m.

[416] Dornan P, Alavi S, Woo TK. Free energies of carbon dioxide sequestration and methane recovery in clathrate hydrates. J Chem Phys 2007;127:124510. https://doi.org/10.1063/1.2769634.

[417] Qiu N, Bai X, Xu J, Sun N, Francisco JS, Yang M, et al. Adsorption behaviors and phase equilibria for clathrate hydrates of sulfur and nitrogen containing small molecules. J Phys Chem C 2019;123:2691–702. https://doi.org/10.1021/acs.jpcc.8b05962.

[418] Buchanan P, Soper AK, Thompson H, Westacott RE, Creek JL, Hobson G, et al. Search for memory effects in methane hydrate: Structure of water before hydrate formation and after hydrate decomposition. J Chem Phys 2005;123:164507. https://doi.org/10.1063/1.2074927.

[419] Yagasaki T, Matsumoto M, Andoh Y, Okazaki S, Tanaka H. Effect of bubble formation on the dissociation of methane hydrate in water: A molecular dynamics study. J Phys Chem B 2014;118:1900–6. https://doi.org/10.1021/jp412692d.

[420] Belosudov R V, Bozhko YY, Zhdanov RK, Subbotin OS, Kawazoe Y, Belosludov VR. Hydrogen hydrates: Equation of state and self-preservation effect. Fluid Phase Equilib 2016;413:220–8. https://doi.org/10.1016/j.fluid.2015.11.031.

[421] Nguyen AH, Molinero V. Identification of clathrate hydrates, hexagonal ice, cubic ice, and liquid water in simulations: the CHILL+ algorithm. J Phys Chem B 2015;119:9369–76. https://doi.org/10.1021/jp510289t.

[422] Naeiji P, Woo TK, Alavi S, Ripmeester JA. Molecular dynamic simulations of clathrate hydrate anomalous preservation: The effect of coating clathrate hydrate phases. J Phys Chem C 2019;123:28715–25. https://doi.org/10.1021/acs.jpcc.9b07769.

[423] Alavi S, Udachin K, Ripmeester JA. Effect of guest-host hydrogen bonding on the structures and properties of clathrate hydrates. Chem - A Eur J 2010;16:1017–25. https://doi.org/10.1002/chem.200902351.

[424] Dureckova H, Woo TK, Alavi S, Ripmeester JA. Molecular dynamics simulation of halogen bonding in Cl2, BrCl, and mixed Cl2/Br2 clathrate hydrates. Can J Chem 2015;93:864–73. https://doi.org/10.1139/cjc-2014-0593.

[425] Dureckova H, Woo TK, Alavi S. Molecular simulations and density functional theory calculations of bromine in clathrate hydrate phases. J Chem Phys 2016;144:44501. https://doi.org/10.1063/1.4940321.

[426] Dureckova H, Woo TK, Udachin KA, Ripmeester JA, Alavi S. The anomalous halogen bonding interactions between chlorine and bromine with water in clathrate hydrates. Faraday Discuss 2017;203:61–77. https://doi.org/10.1039/C7FD00064B.

[427] Alavi S, Ripmeester JA. Effect of small cage guests on hydrogen bonding of tetrahydrofuran in binary structure II clathrate hydrates. J Chem Phys 2012;137:54712. https://doi.org/10.1063/1.4739928.

[428] Moudrakovski IL, Udachin KA, Alavi S, Ratcliffe CI, Ripmeester JA. Facilitating guest transport in clathrate hydrates by tuning guest-host interactions. J Chem Phys 2015;142:74705. https://doi.org/10.1063/1.4907720.

[429] Trueba AT, Kroon MC, Peters CJ, Moudrakovski IL, Ratcliffe CI, Alavi S, et al. Inter-cage dynamics in structure I, II, and H fluoromethane hydrates as studied by NMR and molecular dynamics simulations. J Chem Phys 2014;140:0–11. https://doi.org/10.1063/1.4874636.

[430] Alavi S, Ohmura R, Ripmeester JA. A molecular dynamics study of ethanol–water hydrogen bonding in binary structure I clathrate hydrate with CO2. J Chem Phys 2011;134:54702. https://doi.org/10.1063/1.3548868.

[431] Kondo Y, Alavi S, Murayama K, Ruiz A, Takeya S, Ohmura R. Effect of help-guest size and hydrogen bonding on the stability of N-methylpiperidine structure H clathrate hydrate. J Phys Chem C 2020;124:5978–86. https://doi.org/10.1021/acs.jpcc.9b11910.

[432] English NJ, Tse JS. Pressure-induced amorphization of methane hydrate. Phys Rev B 2012;86:104109. https://doi.org/10.1103/PhysRevB.86.104109.